Understanding and manipulating coalescence in dense emulsions

Huanhuan Feng

Thesis committee

Promotors

Emeritus Prof. Dr M.A. Cohen Stuart
Professor of Physical Chemistry and Colloid Science
Wageningen University

Prof. Dr J. van der Gucht
Professor of Physical Chemistry and Colloid Science
Wageningen University

Co-promotor

Dr J.H.B. Sprakel
Assistant professor, Laboratory for Physical Chemistry and Colloid Science
Wageningen University

Other members

Prof. Dr AH Velders,Wageningen Unversity
Prof. Dr J. Keddie, University of Surrey, Guildford, United Kingdom
Dr J. Snoeijer, University of Twente, Enschede, The Netherlands
Prof. P. Geurink, Akzo Nobel, Sassenheim, The Netherlands

This research was conducted under the auspices of the Graduate School VLAG (Advanced studies in Food Technology, Agrobiotechnology, Nutrition and Health Sciences).

Understanding and manipulating coalescence in dense emulsions

Huanhuan Feng

Thesis

submitted in fulfillment of the requirements for the degree of doctor

at Wageningen University

by the authority of the Rector Magnificus

Prof. Dr. M. J. Kropff

in the presence of the

Thesis Committee appointed by the Academic Board

to be defended in pubic

on Monday 9 December 2013

at 4 p.m. in the Aula

Huanhuan Feng
Understanding and manipulating of coalescence in dense emulsions
114 pages.

PhD thesis, Wageningen University, Wageningen, NL (2013)

ISBN:978-94-6173-737-3

Contents

Chapter 1

Introduction

1.1 Motivation

Coatings are found everywhere; they are applied to practically all visible and invisible surfaces. Their applications range from everyday surfaces, found in your house, car and furniture, to high-tech surfaces such as those found in military weapons, stealth aircrafts, submarines, airplanes, etc. The reasons for applying coatings also varies widely, ranging from very general protection against corrosion, weathering or fouling, to adding or removing some specific properties, or can even be just for aesthetic reasons such as to provide color or gloss.

Due to their widespread application, the coating industry is economically significant on both local and global markets; in 2012 the market for paints and coatings was valued at 111.2 billion US dollars, and is projected to grow to 116.9 billion in 2013. The total market value is expected to reach 141 billion US dollars in 2018 after increasing at a five-year compound annual growth rate of 3.8 %[1].

Coating systems can be categorized into several major segments based on their properties and composition:

- Solvent-borne coatings: the solvent usually is a volatile, apolar organic solvent.
- Waterborne coatings: the main solvent consists of water.
- High solids coatings: Higher concentration of solid materials(in organic solvent); this helps to reduce the VOC (volatile organic compound) content.
- Powder coatings: dry power which is applied as a coating and typically annealed with a heating process.

The market segment for waterborne coatings is expected to reach $31.1 billion in 2013 and nearly $40.1 billion in 2018; clearly there is a large market share increase for waterborne coatings with an expected average annual increase of 5.2% (Figure 1.1). While solvent-borne coatings still occupy a significant share, there is no doubt that waterborne coating systems are still on the rise. Solvent-borne coatings still exhibit better performance than waterborne coatings in terms of durability, leveling, gloss and resistivity; however, they bring a serious threat to environments and consumers. Large quantities of hazardous substances are released into the air during the drying of solvent-based coatings. Industry has already made a rapid shift from solvent-based to water-based systems in the decorative coating market. However, for high performance coatings, such as those on cars, airplanes, buildings and structures, water-borne coatings cannot yet deliver the same durability and

properties. Ultimately, the desire is to replace all solvent-borne coatings with other, less VOC containing coating technologies.

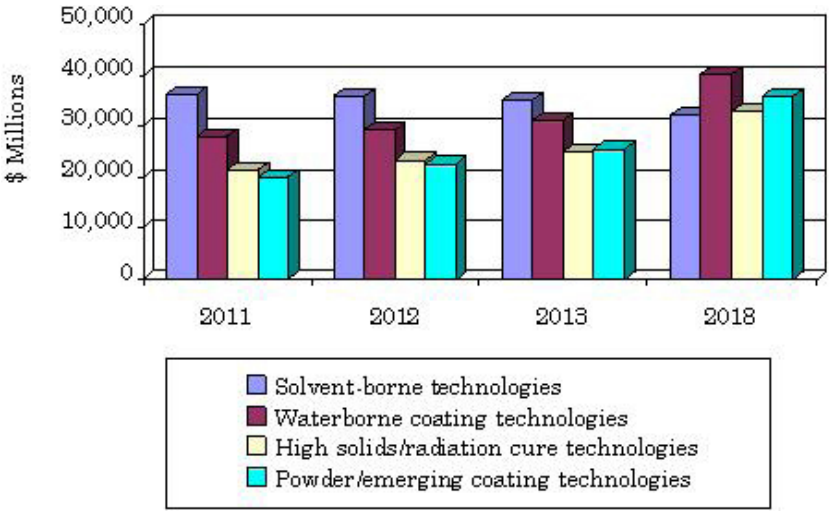

Figure 1.1 The market for paints and coatings in different segments from 2011-2018[1].

Waterborne coatings are multiphase systems. The two major components are water, the dispersing fluid, and the resin which will form the continuous phase in the final film. Because the resin is (and must be) insoluble in water, it is dispersed in the continuous water phase in the form of colloidal particles or droplets with the help of an emulsifier. Pigment particles can be present as a third colloidal phase, dispersed in the water or in the resin. When a water-borne paint dries, it should form a homogeneous and smooth resin film, in which any pigment particles should be homogeneously embedded. If this criterion can be effectively met with waterborne coatings, and thereby become competitive with solvent-based coatings in terms of performance, they will most certainly achieve a much larger market share.

To achieve a homogeneous film of the resin, from its initial dispersed state, the paint formulation must undergo a phase inversion process during the drying of the paint film. It is exactly this process, the phase inversion from a resin-in-water suspension and/or emulsion, to a continuous film of resin, without any embedded water, that is the main theme of this thesis. In recent years it has become accepted that this process is crucial in determining the final film properties; at the same time, it is one of the processes in coating science that remains the least understood. The reason for this is the complexity of the

problem; a wide variety of chemical and physical aspects come into play during the drying and phase inversion of a paint film. This is highlighted in the research map shown in Figure 1.2. The large complexity of the problem forces one to simplify the problem to begin developing a basic understanding of phase inversion. The aspects we investigated in this thesis are highlighted in Figure 1.2.

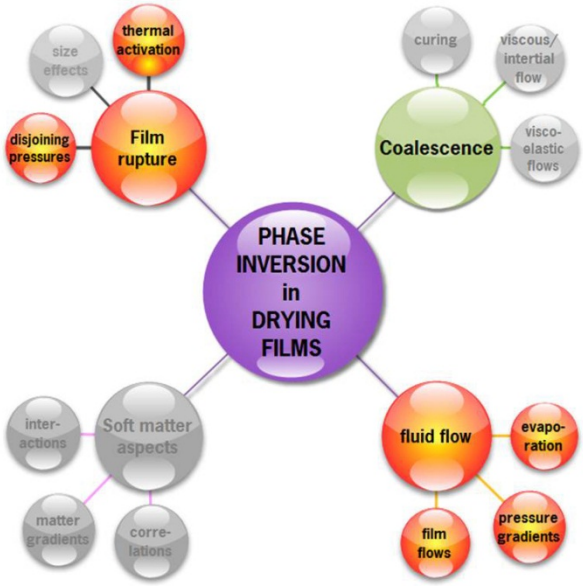

Figure 1.2 Mind map highlighting the complexity of phase inversion in drying films; highlighted are the areas of focus of this thesis.

We started by making some detailed observations of how coalescence occurs in drying films, by combining imaging at the particle scale and on macroscopic length scales; this led to new insight into phase inversion. We also explored the possibilities to manipulate phase inversion and coalescence using responsive surfactants, which change their stabilizing properties upon small changes in temperature. By combining a more physical approach to understand phase inversion and a material chemistry approach to manipulate it, new avenues for getting better grips on this complex problem have been created.

1.2 Emulsions

Emulsions are metastable, biphasic, colloidal systems prepared by dispersing one fluid into an immiscible second fluid [2]. In this entire thesis we consistently use the words “oil”, to indicate a hydrophobic liquid, and water which means aqueous solution often containing

surfactants to stabilize the emulsions. Depending on which phase forms the continuous phase, an emulsion is either an oil-in-water (o/w) emulsion, with water as the continuous phase, or a water-in-oil (w/o) emulsion, when oil is the continuous phase (Figure 1.3).

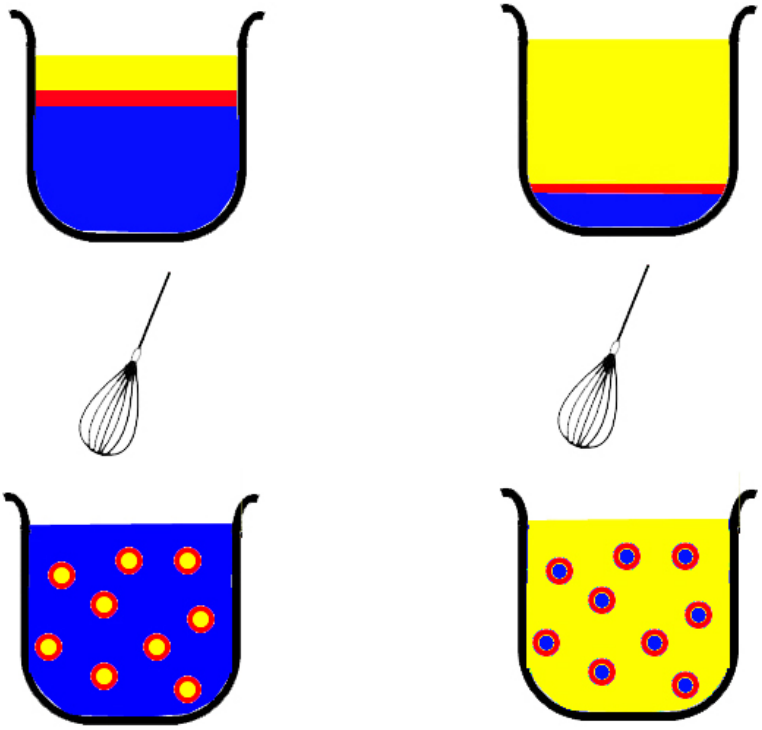

Figure 1.3 Two types of emulsions: oil-in-water and water-in-oil. Blue means water. Yellow means oil. Red means surfactant.

Emulsion droplets possess many of the characteristics of other metastable colloidal systems; they perform Brownian motion[3, 4] and can form amorphous or crystalline packings[5-7]. This makes them a valuable model system to study the properties of colloidal systems. Moreover, o/w emulsions are widely used in an extremely large variety of applications because of their ability to transport or solubilize hydrophobic substances in a continuous water phase. In certain applications, organic solvents can be avoided in solubilizing hydrophobic substances into water by using emulsions as transport “vehicle”. When the water is evaporated the dispersed phase concentrates and ultimately forms a continuous hydrophobic material, e.g.; in painting, paper coating and lubrication. Also, emulsion technology drastically increases the pourability of many hydrophobic substances. One well known example is bitumen used for road surfacing: the hot bitumen, as a melt, is dispersed

as small droplets in water and then remains fluid at room temperature although the droplets solidify. Emulsions are also involved in the food (mayonnaise, salad dressing) and cosmetics (face creams) industries because of their rheological properties which may vary from essentially Newtonian liquids to elastic solids. Moreover, they are efficient drug carriers for various types of targets such as medicines, food and pesticides. Many kinds of surface treatments take advantage of emulsion technology.

1.3 Emulsification

Emulsions can be prepared by application of mechanical energy, for example in the form of shear forces, on two immiscible liquids. This mechanical energy partly is required to provide the extra interfacial free energy of the newly created liquid-liquid interfacial area. In practice, the energy consumption is much larger than this as most of the mechanical energy input is lost through viscous dissipation.

There are several widely used methods to prepare emulsions. Here, we highlight a few of these, and categorize them based on their capacity.

1.3.1 Large scale emulsion preparation

There are many emulsification systems that are widely used in industry such as high pressure systems, membrane emulsifiers, ultrasonic systems, rotor-stator mixers and porous disc mixers, as illustrated in Figure 1.4.

High-pressure emulsification is one the most common methods used in industry. The standard term for these apparatuses is ‘high-pressure homogenizers’. In these set-ups, the material to emulsify is forced, with high pressure, through a dispersion unit, which consists of either a radial diffuser, counter-jet dispergators, or nozzles to disrupt droplets by shear stresses and cavitation[8-13]. The size of the emulsion droplets so obtained is typically below several hundred nanometers in diameter, but with a very wide size distribution. Membrane emulsification is a relatively new process[14, 15]. The dispersed phase is pushed through the pores of a membrane into the continuous phase which is flowing along the membrane and will carry away the produced droplets. Because of much lower operating pressures and stresses as compared to a high-pressure homogenizer, it can be applied to stress-sensitive materials. Moreover it allows to achieve narrow size distributions[16-21]; however, it cannot

produce emulsions at the same volumes as large high-pressure systems. Ultrasonic emulsification is accomplished by applying ultrasonic waves to a biphasic liquid system, to create droplets by cavitation and micro-turbulence. The resulting emulsion droplets can be very small and polydisperse due to intensive energy transmission[22-24]. In rotor-stator mixers, turbulence is created to break the dispersed phase into droplets[25, 26]. The emulsion size depends on the shear forces generated in the turbulent zone within the gap between the spinning rotor and the stationary stator. The size of these droplets decreases with increasing homogenization intensity and duration. The viscosity, total volume size, volume ratio of the continuous phase to the dispersed phase, and the rotor/stator design also play a role in the emulsification process. Small rotor-stator mixers, colloquially known by their trade name Ultra-Turrax, are often used to prepare emulsions in the laboratory.

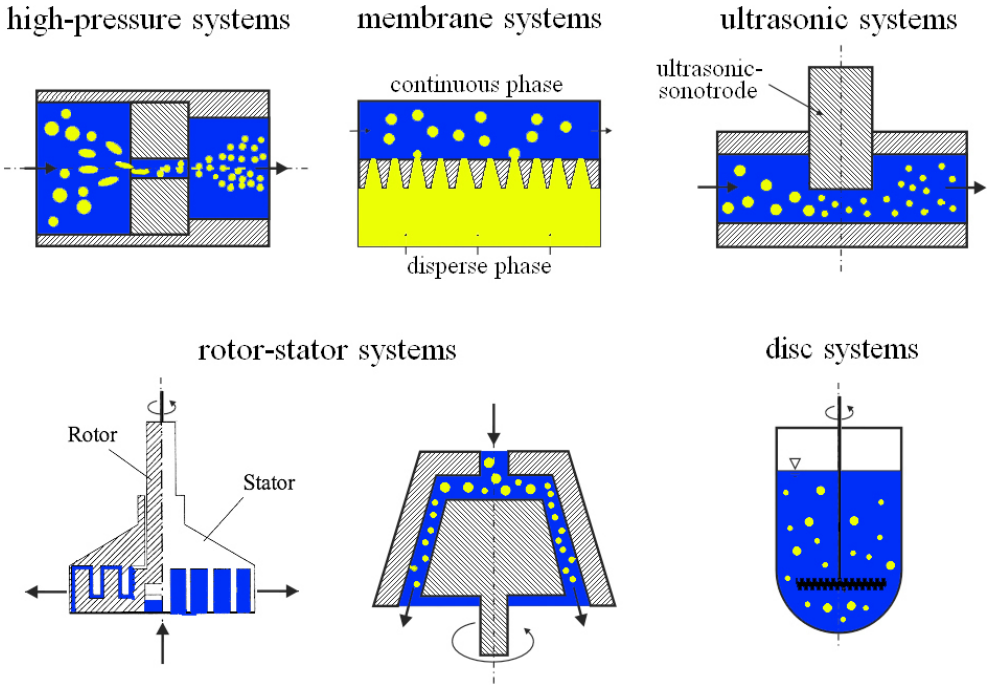

Figure 1.4 Overview of mechanical emulsification systems adapted from Urban et al.[27].

1.3.2 Microfluidic emulsion preparation

In recent years, miniaturization efforts have led to the development of a wide variety of microfluidic methods to prepare well-defined emulsions by using lithographically designed chip reactors. The most common planar microfluidic devices are microfluidic junctions and

flow focusing devices[28]. A T-junction is the simplest microfluidic structure for producing and manipulating droplets; as shown in Figure 1.5, the continuous phase is introduced from the main channel and the dispersed phase flows through a perpendicular channel[29], together forming a T-shape. The combination of shear stresses generated by the continuous phase and evolution of pressure upstream of the emerging droplet causes the tip of the dispersed phase to elongate into the main channel until the neck of the dispersed phase breaks up into a droplet [30, 31]. A flow focusing device, illustrated in Figure 1.4, operates by generating hydrodynamic focusing (extensional) forces close to the exit orifice of the dispersed phase[32, 33]; the dispersed phase (liquid A) flows through the center channel and the continuous phase (liquid B) flows through the two outer channels. Both phases are forced to flow through a small orifice located downstream of the three channels. The continuous phase exerts pressure and shear stress that force the dispersed phase into a narrow thread, which breaks either inside or downstream of the orifice.

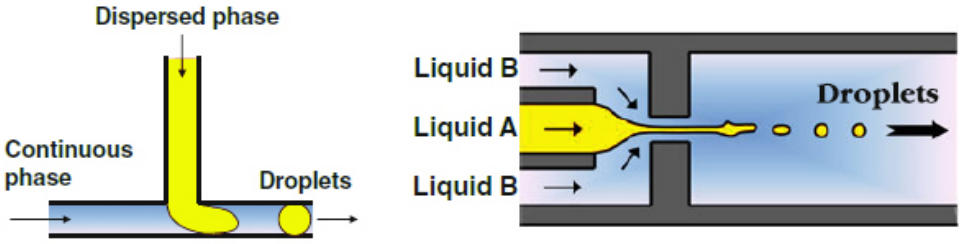

Figure 1.5 Schematic illustration of basic T junction[29] and flow focusing[32] microfluidic emulsifiers.

A wide variety of modifications to these basic designs have been developed to create more complex emulsions, such as double, triple and quadruple emulsions [28]. In Figure 1.6 we highlight a few of these advanced designs, to illustrate the level of sophistication that can be achieved using microfluidic emulsification.

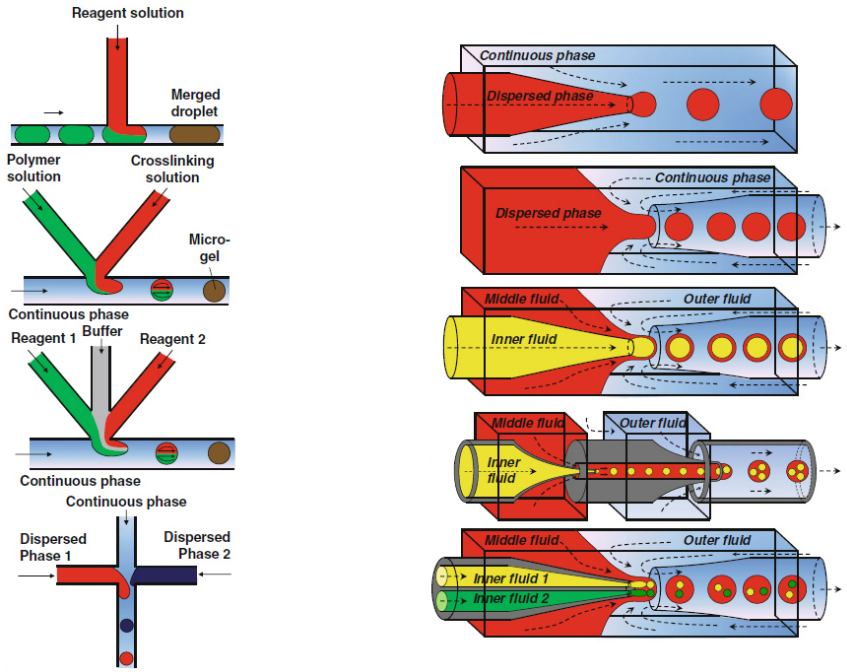

Figure 1.6 Droplet formation from two dispersed phases in a microfluidic junction[34-38] and multiple emulsions in axisymmetric glass capillary devices[39-43].

1.4 Coalescence

Once emulsions are produced, their long term fate in terms of droplets size distribution is controlled by two main mechanisms. The first mechanism, Ostwald ripening, is mediated by the diffusion of the dispersed phase through the continuous phase. This mechanism does not involve any film rupture. Instead there is continuous exchange of matter through the continuous phase. The reason is that in a polydisperse sample, the Laplace pressure that is associated with any curved surface, will be higher in the smaller droplets and lower in the larger drops. As a result, dispersed phase will transport continuously from small to big droplets, making the bigger drops grow and the smaller droplets vanish; ultimately this leads to disproportionation of the droplet population and a reduction in the number of droplets. The kinetics of Ostwald ripening are governed by the solubility of the dispersed phase in the continuous phase; a higher solubility will lead to faster Ostwald ripening. For coating systems, in which the dispersed phase is typically an oligomeric or polymeric fluid, with very low water solubility, this Ostwald ripening is practically absent.

The other mechanism, called coalescence, is of immense importance to coating systems, and most other emulsion formulations. Coalescence is the merging of two drops to form a new, larger droplet. Coalescence thus requires the rupture of the thin liquid film of external phase that separates the initially individual droplets. Upon approaching two droplets at constant pressure, the thin film will drain, at rates set by the film thickness and continuous phase viscosity, until the film reaches an equilibrium thickness when surface forces come into play (see Figure 1.7). The surface forces give rise to a pressure. This pressure, which varies with film thickness, is known as the disjoining pressure Π [44], and can contain a variety of interactions, depending on the nature of the surfaces, such as repulsive electrostatic forces (Π_{elec}), short-range attractive van der Waals interactions (Π_{vdW}) and short-range repulsive steric forces (Π_{steric}). For stable emulsions, the disjoining pressure increases when droplets come closer together, i.e. when the film thins; however, at some critical distance and disjoining pressure, the pressure reaches a maximum, after which it starts to coalescence. As a consequence, the stability of the liquid film is lost, it can rupture and the droplets can coalesce. This critical disjoining pressure (Π_{cr}) is one of the main thermodynamic parameters that determine the stability of emulsions; however, what determines this critical disjoining pressure exactly remains unknown.

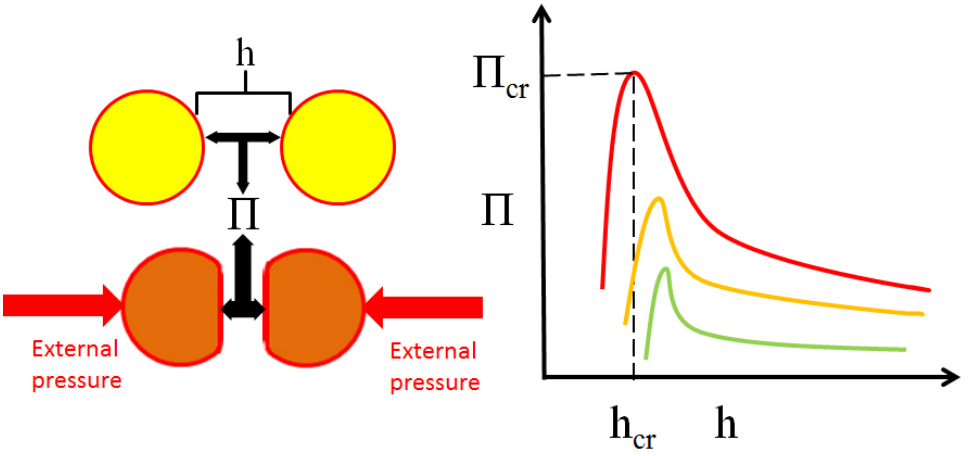

Figure 1.7 The disjoining pressure (Π) between two droplets stabilizes the film between two droplets; the curves show a typical dependence of Π on the film thickness h..

The merging of two droplets can be separated into two separate events; (i) the film rupture, which is caused by thermodynamic instability of the thin liquid film at large enough pressures, and (ii) the fluid dynamics process of the merging (i.e. coalescence) of the two

droplets. The stability of individual thin liquid films has been accurately characterized, for a wide variety of system, using the *liquid surface force apparatus* (LSFA)[45, 46], as well as thin-film balance methods[47-50].

The actual coalescence event for simple liquids, which is a fast process, has also been studied in detail; especially with the availability of high speed cameras, and new fluidic methods to manipulate droplets, this process has been characterized and theoretically described in detail [46, 51-55]. For simple liquids of low viscosity, such as water, coalescence between two isolated droplets occurs within a few microseconds to milliseconds, as shown in the time-sequence in Figure 1.8. For visco-elastic fluids, the situation is much more complex, and coalescence can become much slower, or even occur only partially, as shown in the right panels of Figure 1.8.

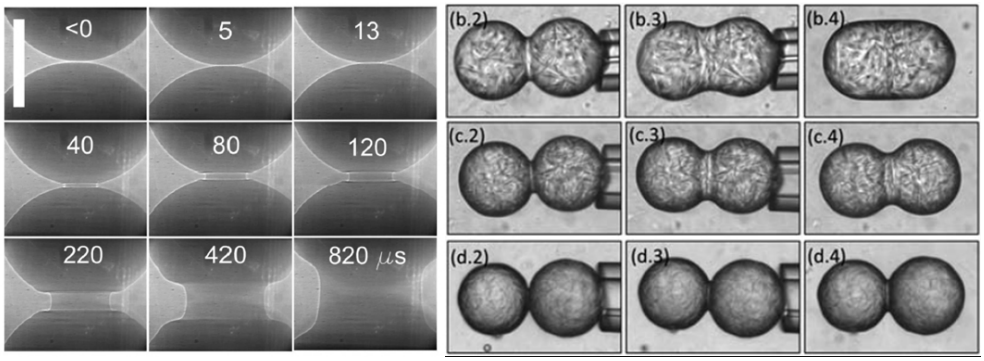

Figure 1.8: left: High speed x-ray imaging time-sequence of the coalescence of two water droplets[56], right: partial coalescence of droplets prepared from a visco-elastic yield stress fluid[57].

1.4. Film formation in drying emulsions

The formation of a paint film from an initially stable resin (emulsion) occurs in various stages [58] as illustrated in Figure 1.9. Initially, as water evaporates, the dispersed droplets concentrate[59] until they come into contact and form a jammed packing. Further evaporation of water creates a capillary pressure that causes the droplets to deform and squeeze together. Similar to dry foams, this ultimately leads to faceted droplets separated by thin water films. The vertices where these films come together are commonly called 'Plateau borders'; these are the main channels for water transport. Finally, when the pressure becomes sufficiently high and exceeds the critical disjoining pressure, individual droplets begin to coalesce and phase inversion takes place[60]. In this final stage, the water films must rupture and disappear so that a homogeneous film can be formed.

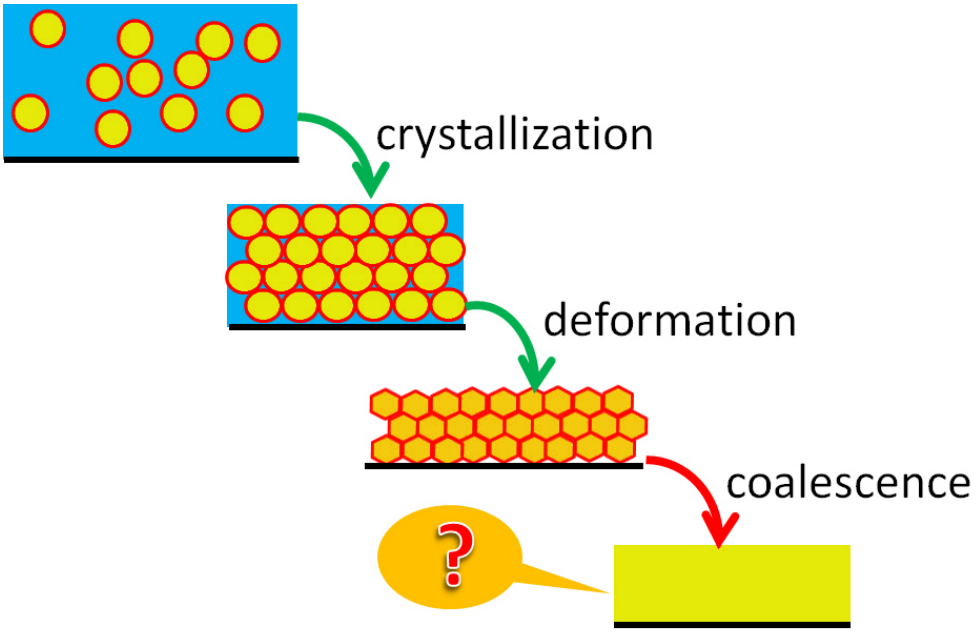

Figure 1.9 A schematic illustration of the stages in the film formation of a drying emulsion.

Film formation in colloidal systems has received a lot of attention in recent decades due to its direct influence on the final properties of the film[61]. A major difficulty in understanding film formation is the practical absence of well-separated stages; in reality, drying, compaction and coalescence all occur simultaneously at different locations within the drying film; as illustrated in Figure 1.10. A dry film at the drying edge is connected to a wet dispersion through a boundary region. Solvent and solutes are transported to this boundary region due to a drying flux towards the dry end of the sample [62]. As drying proceeds, the drying front propagates in the direction opposite to that of the water flux. The dry film grows in size and the wet dispersion decreases in area.

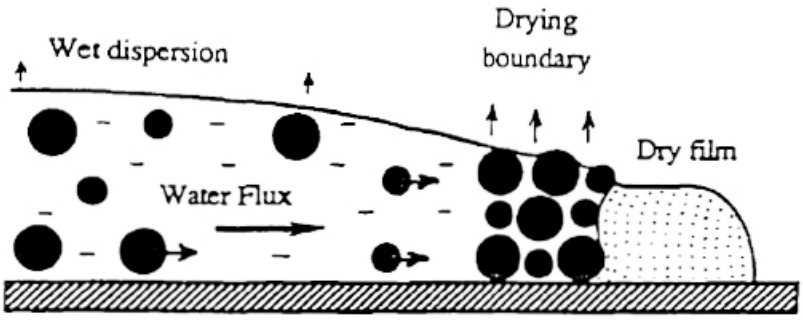

Figure 1.10 Schema representation of drying front in a latex dispersion[58].

Coalescence and film formation in a drying dispersion depend on a wide variety of factors, including the plasticity of the particles, evaporation rates, viscosities of dispersed and continuous phase, surface tension, colloidal interactions, interactions between colloids and solutes (surfactants, polymers), presence of pigments and fillers, film thickness, etc. As a result, capturing this behavior in a single model is extremely difficult; several simplified models, focusing on only few of these aspects, have emerged in the past years. For example, the model proposed by Routh & Russel describes the deformation of soft particles under a uniaxial pressure which is governed by the drying of solvent; depending on the softness of the particles and the evaporation rate, various regimes have been identified, such as regimes of wet sintering, dry sintering, capillary deformation and skin formation[63-70].

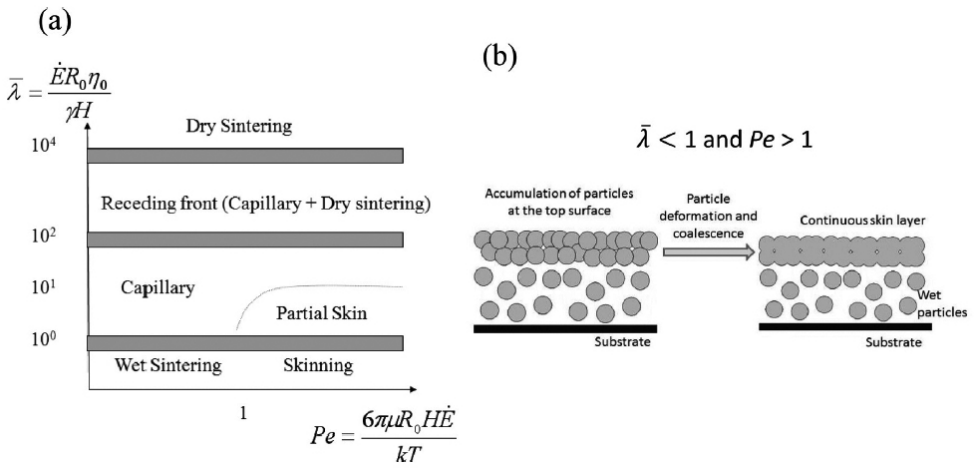

Figure 1.11 a) Deformation phase diagram from the Routh-Russel model for a high Tg latex, as a function of Peclect number *Pe* and λ, which is the ratio of the time needed for water to drain from the thin films versus the typical timescale for water evaporation. b) Illustration of skin formation in a latex where particle softness is sufficient to allow substantial deformation and coalescence to occur in presence of water[70].

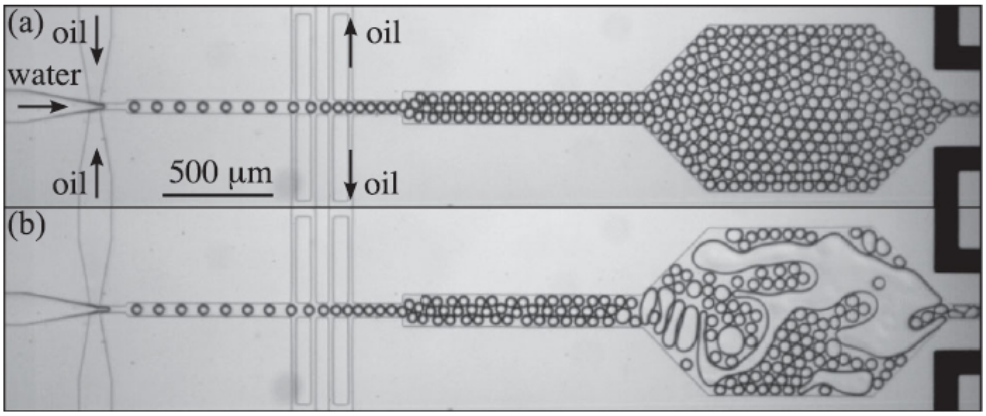

Figure 1.12 Coalescence study on a microfluidic chip.

While these models capture a variety of the observations made in drying practical dispersion formulations, they do not give microscopic insight into the mechanisms that act at the single particle level, which are ultimately responsible for the observed macroscopic behavior.

Surprisingly, a large variety of methods have been employed to study the details of the initial stages of drying films[71-79], while the final and crucial stage, during which phase inversion occurs and a film is formed, remains relatively ill-understood; this is mostly the result of a lack of direct experimental data on the level of individual droplets within the drying emulsion[2]. Some initial steps in this direction have been taken, for example by using a microfluidic reactor to collect droplets to create dense 2 dimensional packings (Figure 1.12), yet many questions remain (despite its immense importance) in understanding water-borne coatings. These questions include: what are the governing parameters on the molecular scale that determine macroscopic coalescence behavior?, how does fluid flow through a drying film influence coalescence kinetics?, are there ways to manipulate coalescence dynamics externally? And can we predict *a-priori* how a certain system will behave?

These are the questions that motivated the work presented in this these, where we aimed to arrive at a new understanding of phase inversion and coalescence in drying films and we explored new routes to manipulate these phenomena using novel responsive polymeric materials. These topics are described in the following chapters.

1.5 Outline of this thesis

In **Chapter 2** we visualize phase inversion in drying emulsions on the single particle level[80, 81] by using an optimized confocal fluorescence imaging method[50, 51]. We used this approach to study coalescence in dense o/w emulsions subjected to a unidirectional drying stress, to mimic a drying film. Here, we observed two different modes of coalescence: coalescence occurs either through a *nucleation-and-growth* mechanism, where coalesced pockets form and grow randomly throughout the sample, or through a *coalescence front* that propagates into the sample from the drying end. We explain these results in terms of the theoretically predicted and experimentally measured *pressure profiles* throughout the drying films, and their relation to the critical disjoining pressure. We find that surfactant concentration plays a significant role through its effect on the critical disjoining pressure at which coalescence occurs. By developing a hydrodynamic model we bridge these length scales and arrive at a microscopic understanding of this complex macroscopic phenomenon[82].

In **chapter 3** we explore the parameter space of our hydrodynamic model, to further investigate the key factors involved in film formation. We show that, those two distinct coalescence behaviors can be obtained within the same model by varying the critical disjoining pressure.

In **chapter 4** we describe the development of a new and well-defined surfactant system to facilitate studies of film formation and phase inversion[83]. The surfactant, which carries a thermoresponsive block, synthesized by ATRP, stabilizes emulsions for at least four months at room temperature. However, by slightly raising the temperature to above the collapse transition of the thermoresponsive block, coalescence between the emulsion droplets occurs; this leads to demixing of the sample within several minutes. We reveal the mechanism for the temperature-triggered coalescence by measurements of the temperature-dependent interfacial tension, and by studying the interfacial morphology of surfactant-covered emulsion droplets.

In **chapter 5** we apply this new surfactant system, developed in chapter 4, in combination with a recently developed microcentrifugation method [84-86] to directly study the coalescence dynamics in densely packed emulsions, under well-defined conditions. We show that, by using a thermoresponsive surfactant[8383, 87], we can manipulate in this way the mode in which coalescence takes place, by changing the critical disjoining pressure.

In **Chapter 6** we summarize our work and discuss it in the perspective of the unanswered questions that remain, including some unfinished work within this project.

Reference

1.BCC Research, 2013.
2. J. Bibette, F. L. Calderon and P. Poulin, Reports on Progress in Physics, 1999, 62, 969-1033.
3. R. A. Buffo and G. A. Reineccius, J. Food Eng., 2002, 51, 267-272.
4. N. A. Mishchuk, A. Sanfeld and A. Steinchen, Advances in Colloid and Interface Science, 2004, 112, 129-157.
5. T. Awad and K. Sato, Colloids and Surfaces B-Biointerfaces, 2002, 25, 45-53.
6. T. El Rhafiki, T. Kousksou, A. Jamil, S. Jegadheeswaran, S. D. Pohekar and Y. Zeraouli, Solar Energy Materials and Solar Cells, 2011, 95, 2588-2597.
7. T. Kousksou, T. El Rhafiki, M. Mandaoui, P. Bruel and Y. Zeraouli, Solar Energy Materials and Solar Cells, 2012, 107, 28-36.
8. F. A. Aguilar, B. Freudig and H. P. Schuchmann, Chemie Ingenieur Technik, 2004, 76, 396-399.
9. G. Kolb, G. Wagner, K. Viardot and J. Ulrich, Chemie Ingenieur Technik, 2001, 73, 84-87.
10. H. P. Schuchmann and T. Danner, Chemie Ingenieur Technik, 2004, 76, 364-375.
11. S. Schultz, G. Wagner and J. Ulrich, Chemie Ingenieur Technik, 2002, 74, 901-909.
12. S. Schultz, G. Wagner and J. Ulrich, Chemie Ingenieur Technik, 2002, 74, 355-359.
13. S. Schultz, G. Wagner, K. Urban and J. Ulrich, Chem. Eng. Technol., 2004, 27, 361-368.
14. C. Charcosset, I. Limayem and H. Fessi, Journal of Chemical Technology and Biotechnology, 2004, 79, 209-218.
15. S. M. Joscelyne and G. Tragardh, Journal of Membrane Science, 2000, 169, 107-117.
16. U. Lambrich and G. T. Vladisavljevic, Chemie Ingenieur Technik, 2004, 76, 376-383.
17. C. Charcosset and H. Fessi, Reviews in Chemical Engineering, 2005, 21, 1-32.
18. U. Lambrich and H. Schubert, Journal of Membrane Science, 2005, 257, 76-84.
19. M. Rayner, G. Tragardh and C. Tragardh, Colloids and Surfaces a-Physicochemical and Engineering Aspects, 2005, 266, 1-17.
20. N. Yamazaki, K. Naganuma, M. Nagai, G. H. Ma and S. Omi, Journal of Dispersion Science and Technology, 2003, 24, 249-257.
21. Q. Z. Zhou, G. H. Ma and Z. G. Su, Journal of Membrane Science, 2009, 326, 694-700.
22. S. Bechtel, N. Gilbert and H. G. Wagner, Chemie Ingenieur Technik, 1999, 71, 810-817.
23. Y. F. Maa and C. C. Hsu, Pharmaceutical Development and Technology, 1999, 4, 233-240.
24. S. Mujumdar, P. S. Kumar and A. B. Pandit, Indian Journal of Chemical Technology, 1997, 4, 277-284.
25. B. Koglin, J. Pawlowski and H. Schnoring, Chemie Ingenieur Technik, 1981, 53, 641-&.
26. Y. F. Maa and C. Hsu, Journal of Controlled Release, 1996, 38, 219-228.
27. K. Urban, G. Wagner, D. Schaffner, D. Roglin and J. Ulrich, Chem. Eng. Technol., 2006, 29, 24-31.
28. G. T. Vladisavljević, I. Kobayashi and M. Nakajima, Microfluid Nanofluid, 2012, 13, 151-178.

29. T. Thorsen, R. W. Roberts, F. H. Arnold and S. R. Quake, Phys. Rev. Lett., 2001, 86, 4163-4166.
30. C.-X. Zhao and A. P. J. Middelberg, Chemical Engineering Science, 2011, 66, 1394-1411.
31. S.-Y. Teh, R. Lin, L.-H. Hung and A. P. Lee, Lab on a Chip, 2008, 8, 198-220.
32. S. L. Anna, N. Bontoux and H. A. Stone, Applied Physics Letters, 2003, 82, 364-366.
33. P. Garstecki, H. A. Stone and G. M. Whitesides, Phys. Rev. Lett., 2005, 94.
34. J. D. Tice, A. D. Lyon and R. F. Ismagilov, Analytica Chimica Acta, 2004, 507, 73-77.
35. B. Zheng, J. D. Tice and R. F. Ismagilov, Analytical Chemistry, 2004, 76, 4977-4982.
36. C.-H. Choi, J.-H. Jung, Y. W. Rhee, D.-P. Kim, S.-E. Shim and C.-S. Lee, Biomedical Microdevices, 2007, 9, 855-862.
37. B. Zheng and R. F. Ismagilov, Angewandte Chemie-International Edition, 2005, 44, 2520-2523.
38. I. Shestopalov, J. D. Tice and R. F. Ismagilov, Lab on a Chip, 2004, 4, 316-321.
39. A. S. Utada, A. Fernandez-Nieves, J. M. Gordillo and D. A. Weitz, Phys. Rev. Lett., 2008, 100.
40. A. S. Utada, L. Y. Chu, A. Fernandez-Nieves, D. R. Link, C. Holtze and D. A. Weitz, Mrs Bulletin, 2007, 32, 702-708.
41. B. J. Sun, H. C. Shum, C. Holtze and D. A. Weitz, Acs Applied Materials & Interfaces, 2010, 2, 3411-3416.
42. A. S. Utada, E. Lorenceau, D. R. Link, P. D. Kaplan, H. A. Stone and D. A. Weitz, Science, 2005, 308, 537-541.
43. L.-Y. Chu, A. S. Utada, R. K. Shah, J.-W. Kim and D. A. Weitz, Angewandte Chemie, 2007, 119, 9128-9132.
44. C. Stubenrauch and R. von Klitzing, J. Phys.-Condes. Matter, 2003, 15, R1197-R1232.
45. R. Aveyard, B. P. Binks, W. G. Cho, L. R. Fisher, P. D. I. Fletcher and F. Klinkhammer, Langmuir, 1996, 12, 6561-6569.
46. B. P. Binks, W. G. Cho and P. D. I. Fletcher, Langmuir, 1997, 13, 7180-7185.
47. T. D. Dimitrova, F. Leal-Calderon, T. D. Gurkov and B. Campbell, Langmuir, 2001, 17, 8069-8077.
48. J. K. Angarska, B. S. Dimitrova, K. D. Danov, P. A. Kralchevsky, K. P. Ananthapadmanabhan and A. Lips, Langmuir, 2004, 20, 1799-1806.
49. P. A. Wierenga, E. S. Basheva and N. D. Denkov, Langmuir, 2009, 25, 6035-6039.
50. T. D. Gurkov, J. K. Angarska, K. D. Tachev and W. Gaschler, Colloids and Surfaces a-Physicochemical and Engineering Aspects, 2011, 382, 174-180.
51. K. D. Danov, N. D. Denkov, D. N. Petsev, I. B. Ivanov and R. Borwankar, Langmuir, 1993, 9, 1731-1740.
52. R. Sudiyo and B. Andersson, Aiche Journal, 2007, 53, 2232-2239.
53. G. F. Christopher, J. Bergstein, N. B. End, M. Poon, C. Nguyen and S. L. Anna, Lab on a Chip, 2009, 9, 1102-1109.
54. A. R. Thiam, N. Bremond and J. Bibette, Phys Rev Lett, 2009, 102, 188304.
55. N. Bremond, A. R. Thiam and J. Bibette, Phys. Rev. Lett., 2008, 100.
56. K. Fezzaa and Y. J. Wang, Phys. Rev. Lett., 2008, 100.
57. A. B. Pawar, M. Caggioni, R. W. Hartel and P. T. Spicer, Faraday Discuss., 2012, 158, 341-350.
58. M. A. Winnik, Curr Opin Colloid In, 1997, 2, 192-199.

59. A. F. Routh and W. B. Russel, AIChE J. FIELD Full Journal Title:AIChE Journal, 1998, 44, 2088-2098.
60. G. A. van Aken, Langmuir, 2002, 18, 2549-2556.
61. J. L. Keddie, Materials Science & Engineering R-Reports, 1997, 21, 101-170.
62. N. D. Denkov, O. D. Velev, P. A. Kralchevsky, I. B. Ivanov, H. Yoshimura and K. Nagayama, Langmuir, 1992, 8, 3183-3190.
63. A. F. Routh and W. B. Russel, Aiche J, 1998, 44, 2088-2098.
64. A. F. Routh and W. B. Russel, Langmuir, 1999, 15, 7762-7773.
65. A. F. Routh and W. B. Russel, Abstracts of Papers of the American Chemical Society, 1999, 218, U621-U621.
66. A. F. Routh and W. B. Russel, Industrial & Engineering Chemistry Research, 2001, 40, 4302-4308.
67. A. F. Routh, W. B. Russel, J. S. Tang and M. S. El-Aasser, Journal of Coatings Technology, 2001, 73, 41-48.
68. F. Routh and W. B. Russel, Aiche Journal, 2002, 48, 917-918.
69. W. B. Russel and A. F. Routh, Abstracts of Papers of the American Chemical Society, 2002, 224, U410-U410.
70. E. Gonzalez, M. Paulis, M. J. Barandiaran and J. L. Keddie, Langmuir, 2013, 29, 2044-2053.
71. F. Bouchama, G. A. van Aken, A. J. E. Autin and G. J. M. Koper, Colloids Surf., A FIELD Full Journal Title:Colloids and Surfaces, A: Physicochemical and Engineering Aspects, 2003, 231, 11-17.
72. H. J. Butt, R. Kuropka and B. Christensen, Colloid & Polymer Science, 1994, 272, 1218-1223.
73. M. C. Goh, D. Juhue, O. M. Leung, Y. Wang and M. A. Winnik, Langmuir, 1993, 9, 1319-1322.
74. S. Hu, J. Rieger, S. V. Roth, R. Gehrke, R. J. Leyrer and Y. Men, Langmuir, 2009, 25, 4230-4234.
75. S. S. Hu, J. Rieger, Y. Q. Lai, S. V. Roth, R. Gehrke and Y. F. Men, Macromolecules, 2008, 41, 5073-5076.
76. J. L. Keddie, P. Meredith, R. A. L. Jones and A. M. Donald, Macromolecules, 1995, 28, 2673-2682.
77. F. Lin and D. J. Meier, Langmuir, 1996, 12, 2774-2780.
78. B. J. Roulstone, M. C. Wilkinson, J. Hearn and A. J. Wilson, Polymer International, 1991, 24, 87-94.
79. Y. Wang, A. Kats, D. Juhue, M. A. Winnik, R. R. Shivers and C. J. Dinsdale, Langmuir, 1992, 8, 1435-1442.
80. J. Brujic, S. F. Edwards, I. Hopkinson and H. A. Makse, Physica a-Statistical Mechanics and Its Applications, 2003, 327, 201-212.
81. J. Brujic, C. M. Song, P. Wang, C. Briscoe, G. Marty and H. A. Makse, Phys. Rev. Lett., 2007, 98, 4.
82. H. Feng, J. Sprakel, D. Ershov, T. Krebs, M. A. C. Stuart and J. van der Gucht, Soft Matter, 2013, 9, 2810-2815.
83. T. E. Kodger and J. Sprakel, Advanced Functional Materials, 2013, 23, 475-482.
84. T. Krebs, D. Ershov, C. G. P. H. Schroen and R. M. Boom, Soft Matter, 2013, 9, 4026-4035.

85. T. Krebs, C. G. P. H. Schroen and R. M. Boom, Chemical Engineering Science, 2012, 71, 118-125.
86. T. Krebs, K. Schroen and R. Boom, Lab on a Chip, 2012, 12, 1060-1070.
87. H. Feng, N. A. L. Verstappen, A. J. C. Kuehne and J. Sprakel, Polymer Chemistry, 2013, 4, 1842-1847.

Part I
Understanding coalescence in dense emulsions

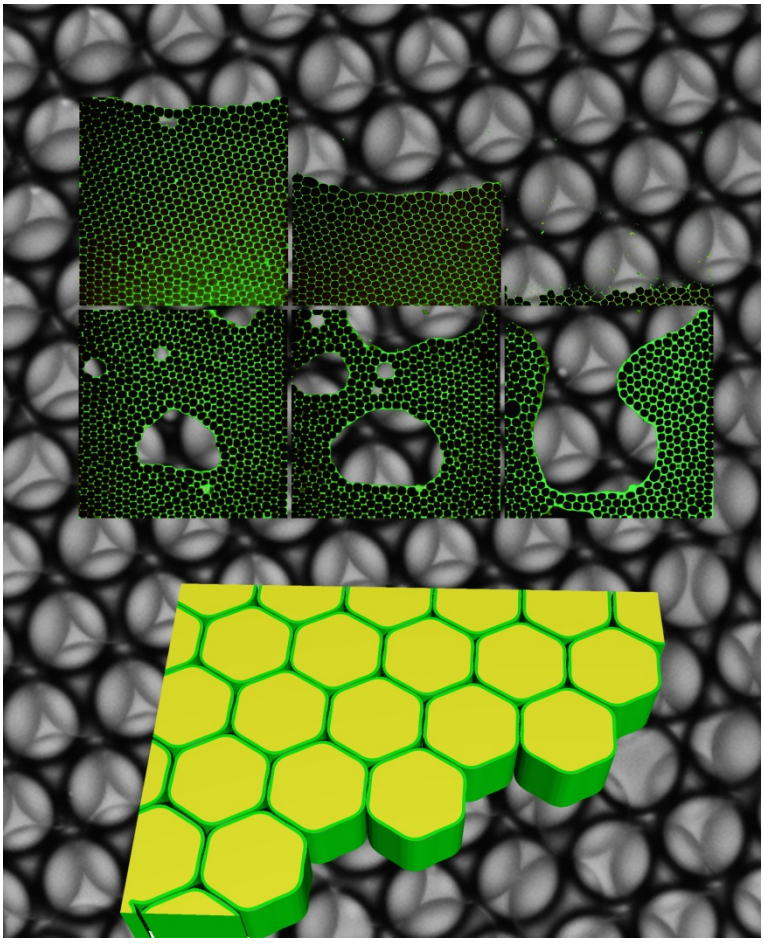

Chapter 2

Two modes of phase inversion in a drying emulsion

We report two different modes of phase inversion in surfactant-stabilized oil-in-water emulsions subjected to a unidirectional drying stress. Coalescence occurs either through a nucleation-and-growth mechanism, where coalesced pockets form and grow randomly throughout the sample, or through a coalescence front that propagates into the sample from the drying end. This drying-induced coalescence results from the development of a pressure gradient from the drying front into the bulk of the sample, established by limited water transport through the Plateau borders. Depending on the steepness of this pressure profile, coalescence occurs throughout the sample or only at the drying front. Moreover, we find that surfactant concentration plays a significant role through its effect on the critical disjoining pressure at which coalescence occurs. Very stable emulsions, characterized by a high critical pressure, tend to develop steep pressure profiles, which favours front-dominated coalescence, while unstable emulsions, with low critical pressures develop shallow pressure gradients, favouring nucleation-and-growth dominated coalescence. These result offer new insight into the microscopic mechanisms governing the complex and poorly understood macroscopic phenomena during phase inversion of drying emulsions.

This chapter was published as:
H. Feng, J. Sprakel, D. Ershov, T. Krebs, M. A. C. Stuart and J. van der Gucht, Two modes of coalescence in a drying emulison, *Soft Matter*, **2013**, 9, 2810-2815

2.1 Introduction

When a thin layer of an oil-in-water emulsion is dried on a substrate, evaporation of water eventually leads to the formation of a film of the dispersed phase. Despite its widespread practical importance in the fields of paints, coatings and adhesives, a detailed understanding of the complex process of phase inversion in concentrated emulsions is not available to date.

It is known that film formation occurs in a sequence of stages[1]: (1) as water evaporates, the dispersed droplets concentrate[2] until they come into contact and form a jammed packing. (2) Further evaporation of water creates a capillary pressure that causes the droplets to deform and squeeze together. Similar to dry foams, this ultimately leads to faceted droplets separated by thin water films. (3) Finally, when the pressure becomes sufficiently high, the individual droplets begin to coalesce and phase inversion takes place[3]. In this final stage, the water films must rupture and disappear so that a homogeneous film can be formed.

While a large variety of methods have been employed to study the details of the initial stages of drying films[4-12], the final and crucial stage, during which phase inversion occurs and a film is formed, remains incompletely understood; this is mostly the result of a lack of direct experimental data on the level of individual droplets within the drying emulsion[13].

In this article we therefore visualize phase inversion in drying emulsions on the single particle level [14, 15] and on macroscopic length scales. By developing a hydrodynamic model we bridge these length scales and arrive at a microscopic understanding of this complex macroscopic phenomenon.

2.2 Materials and methods

2.2.1 Materials

Polydimethysiloxane (PDMS) viscosity 100 mPa.s, sodium dodecyl sulfate (99% purity), and Nile Red (99% purity) were purchased from Sigma.

2.2.2 Emulsion preparation

Monodisperse emulsions are produced in a T-junction microfluidic device [2, 16, 17]. The continuous phase is a 10 mmol/L SDS solution, while the dispersed phase is silicone oil.

The cross-flow at the T-junction shears the oil to pinch off droplets of well-defined size into the continuous phase, as illustrated in supporting information, Figure A2.1. The droplet size can be adjusted by varying the flow speeds of the two phases [2]. Here we produce droplets of 50 μ m in diameter, which can be observed readily by both confocal and bright-field microscopy.

2.2.3 Confocal Microscopy

The silicone oil is fluorescently labeled by the solvochromic oil-soluble dye Nile Red. The emission of this dye at wavelengths above 560 nm is enhanced for molecules located at the oil/water interface with respect to those surrounded by oil only; this enables us to selectively highlight the interfaces of the droplets (see supporting information, Figure A2.2) [15].

2.2.4 Drying experiments

The drying experiments are carried out in a shallow glass sample chamber formed by two parallel glass slides separated by a spacer of 120 μm. One side is not sealed, but exposed to the air; this leads to unidirectional drying, similar to that experienced in drying films. The conditions are fixed at 26˚C and 60% relative humidity by placing the samples in a home-built climate control box. The drying experiments are conducted in emulsions with initial concentrations of SDS in the water phase of 10, 30, and 100 mmol/L. For each of these concentrations we run 8 samples in parallel to obtain sufficient statistics. The set-up is illustrated in Figure 2.1. All emulsions were prepared at approximately the same initial volume fraction of 60%.

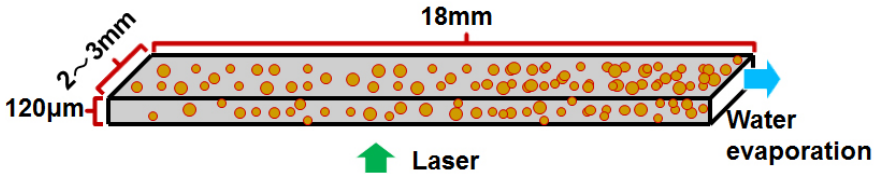

Figure 2.1 Scheme of drying experiment chamber

2.2.5 Centrifugation experiments

The critical disjoining pressure, at which the film that separates two emulsion droplets ruptures and coalescence takes place, is measured using centrifugation. The emulsion

samples are centrifuged with a fixed centrifugal force equivalent to 20000g. The temperature is fixed at 30℃ to prevent crystallization of the surfactant SDS [18]. After an initial gradual ramping-up of the gravitational acceleration, we let the samples reach mechanical equilibrate at 20000g for 8 hours. From the relative volumes of the coalesced oil phase on top and the remaining compressed emulsion, and knowing the density difference between oil and water, we can extract the critical disjoining pressure [19, 20].

2.3 Results and discussion

2.3.1 Macro and microscopic observations

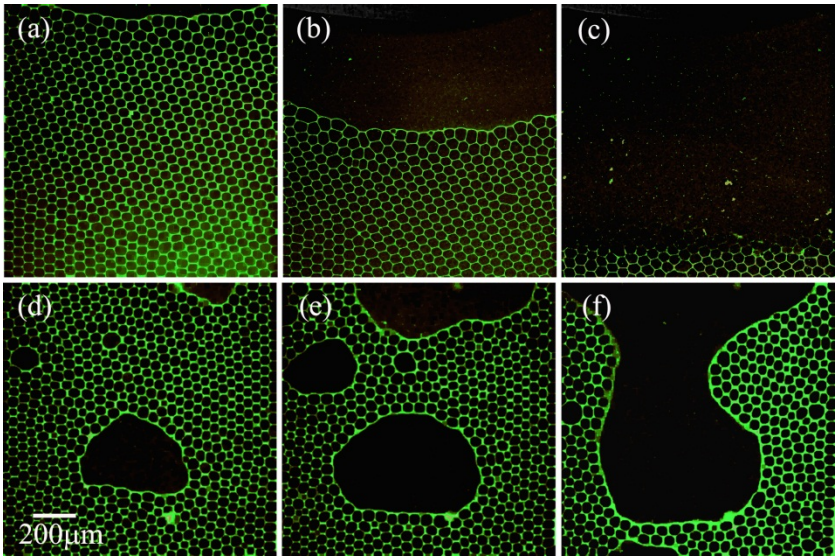

Figure 2.2 Confocal microscopy images of drying emulsions at various stages. (a-c) 'Front' coalescence at an initial SDS concentration of 100 mmol/L. (d-f) 'Bulk' coalescence at an initial SDS concentration of10 mmol/L.

The compressed emulsions appear as a honeycomb-like hexagonal packing, due to the monodispersity of the emulsion droplets created by microfluidics; see Figure 2.2. Note that almost all water films are flat, indicative of a very dense packing of the droplets, well above the close packing limit. During the drying of the emulsions, we see two distinct types of behaviour, depending on the initial surfactant concentration. At high surfactant concentrations coalescence occurs exclusively at the drying end of the sample and propagates into the sample as a well-defined front (Figures 2.2 a-c and 2.3a). At low surfactant concentrations however, coalescence starts at random positions throughout the

sample from which large liquid pockets grow; this is reminiscent of a nucleation-and-growth process (Figure 2.2 d-f and 2.3a). In the remainder of this paper we will refer to these two distinct modes of coalescence as 'front' and 'bulk' coalescence, respectively. Another interesting observation that can be made from these images is that in all samples coalescence occurs almost exclusively between oil droplets of different size (or between droplets and the macroscopic bulk oil phase), with the exception of the initial nucleation events.

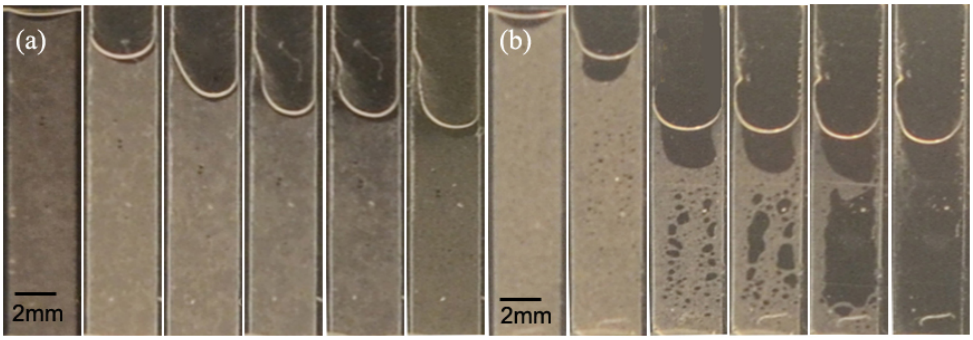

Figure 2.3 Images of drying emulsions at various stages. (a) 'Front' coalescence occurs at an initial SDS concentration of 100 mmol/L. (b) 'Bulk' coalescence occurs at an initial SDS concentration of 10mmol/L.

To quantify the coalescence process, we calculate the fraction, α, of emulsion that has coalesced as a function of time. We extract this information from the macroscopic images, as shown in Figure 2.3; dark areas, in which there is no more diffuse scattering, represent coalesced areas and the light areas represent the not-yet coalesced emulsion. For each initial surfactant concentration, we average 8 parallel samples to obtain reliable statistics. The trends are very clear: coalescence proceeds more slowly as the SDS concentration increases, as shown in Figure 2.4. We can also see that the fluctuations, expressed by the variance, shown as error bars in Figure 2.4, decrease with increasing surfactant concentration. For low surfactant concentrations, of 10 and 30 mmol/L, there is an initial stage where coalescence proceeds slowly. This persists until there is a sudden increase in coalescence rate, after approximately 1000 minutes; this fast coalescence mode then persists until the entire sample has coalesced and the fraction α approaches 100%. For higher surfactant concentrations, i.e. 100 mmol/L SDS, coalescence is very slow and halts altogether after approximately 300 minutes.

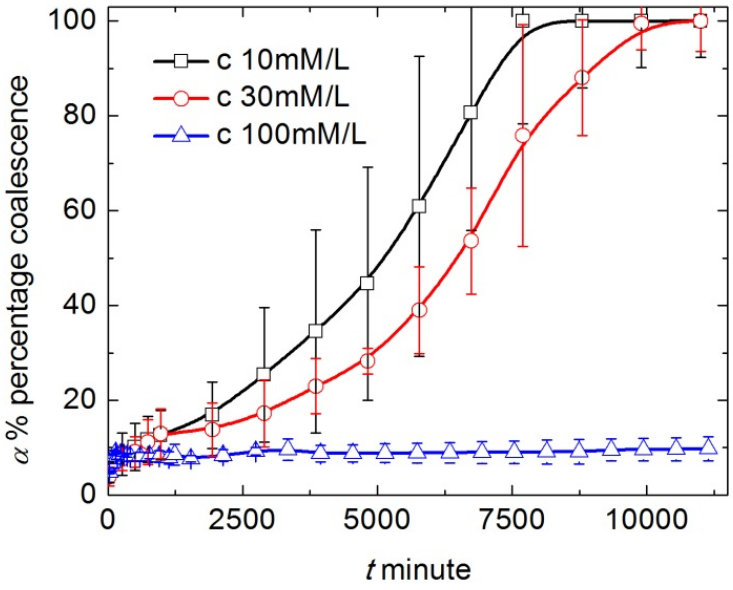

Figure 2.4 Percentage of coalesced emulsion as a function of time from drying experiments for different initial surfactant concentrations.

We see clear differences in the coalescence kinetics between low and high surfactant concentrations, suggesting that the initial stability of the emulsion plays an important role. This immediately triggers the question, what microscopic mechanisms are at play causing these differences in macroscopic behaviour.

A first insight can be obtained, by separating the contributions of front and bulk coalescence in the kinetic plots; for a description of this data analysis we refer to the supporting information (Figure A2.3). In all samples, irrespective of the surfactant concentration, coalescence starts at the front. At low SDS concentration, the accelerating bulk coalescence then takes over; for example for 10 mmol/L SDS concentration this occurs after 2000 minutes (Figure 2.5a). After even longer times, coalescence is so wide-spread that it becomes impossible to distinguish bulk and front coalescence from our images; this occurs after approximately 4000 minutes for 10mmol/L SDS (Figure 2.5a). The effect of surfactant concentration also emerges clearly from Figure 2.5: the higher the SDS concentration, the slower the process, although the overall pattern remains the same. At high SDS concentration, bulk coalescence is even entirely suppressed up to 8000 minutes (~6 days), which is the maximum duration length in our experiment.

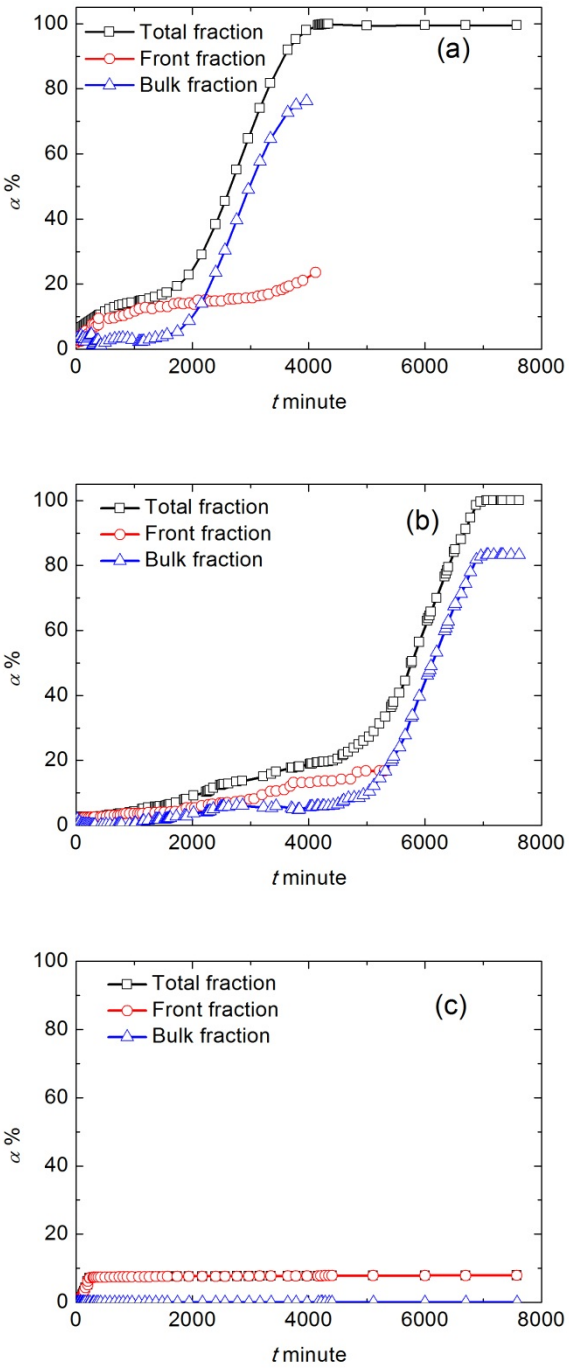

Figure 2.5 Front and bulk contributions to the coalescence as a function of time for initial SDS concentrations of 10 (a), 30 (b), and 100 (c) mmol/L.

2.3.2 Pressure prolife

To achieve an understanding of what occurs in these emulsions to cause these two distinct modes of coalescence, we first realize that the stability of an emulsion is due to the disjoining pressure acting between the surfaces of the dispersed phase. When the actual disjoining pressure reaches a critical value, the film can rupture and coalescence can take place. It is therefore important to determine the pressures and their critical values as they occur in a drying system. To measure the actual capillary pressure profiles, from the drying front into the bulk of the sample, and as a function of time, we determine the curvature of the Plateau borders throughout the sample. Since we visualize the interfaces, curvatures can be measured in the microscopy images as shown in Figure 2.6. The pressure can then be evaluated from the Laplace law, $P=-\gamma/r$, in which γ is the surface tension and r the radius of curvature of the Plateau border. The interfacial tension was measured separately, and was found to decrease from 50 to 11mN/m when the SDS concentration increased from 0 to 10mmol/L, which is close to the CMC of SDS. Then it remains constant at SDS concentrations above the CMC (see Supporting information, Figure A2.4).

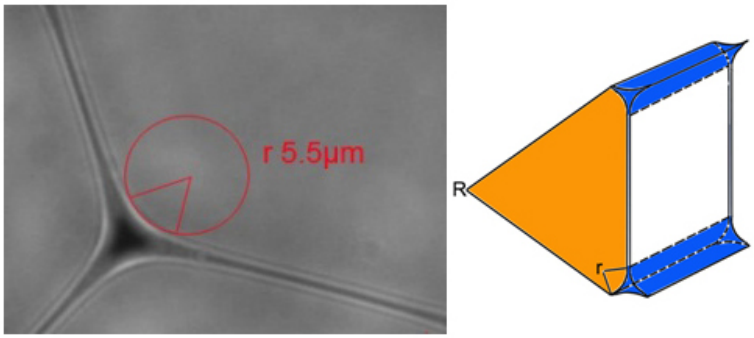

Figure 2.6 Schematic depiction of a Plateau border. Bright field microscopy image of a jammed emulsion, showing the Plateau borders between three droplets and its radius of curvature.

The results, presented in Figure 2.7, show that the pressure is initially low, but increases in time. Moreover, the pressures at the dry end increase faster, so that substantial pressure gradients develop (Figure 2.7). This can be easily understood; drying requires the flow of water from the bulk to the drying front. Such water flow can only occur if a pressure gradient exists and the more the emulsion becomes concentrated, the narrower the Plateau borders and the steeper the pressure drop required to drive fluid to the evaporation site.

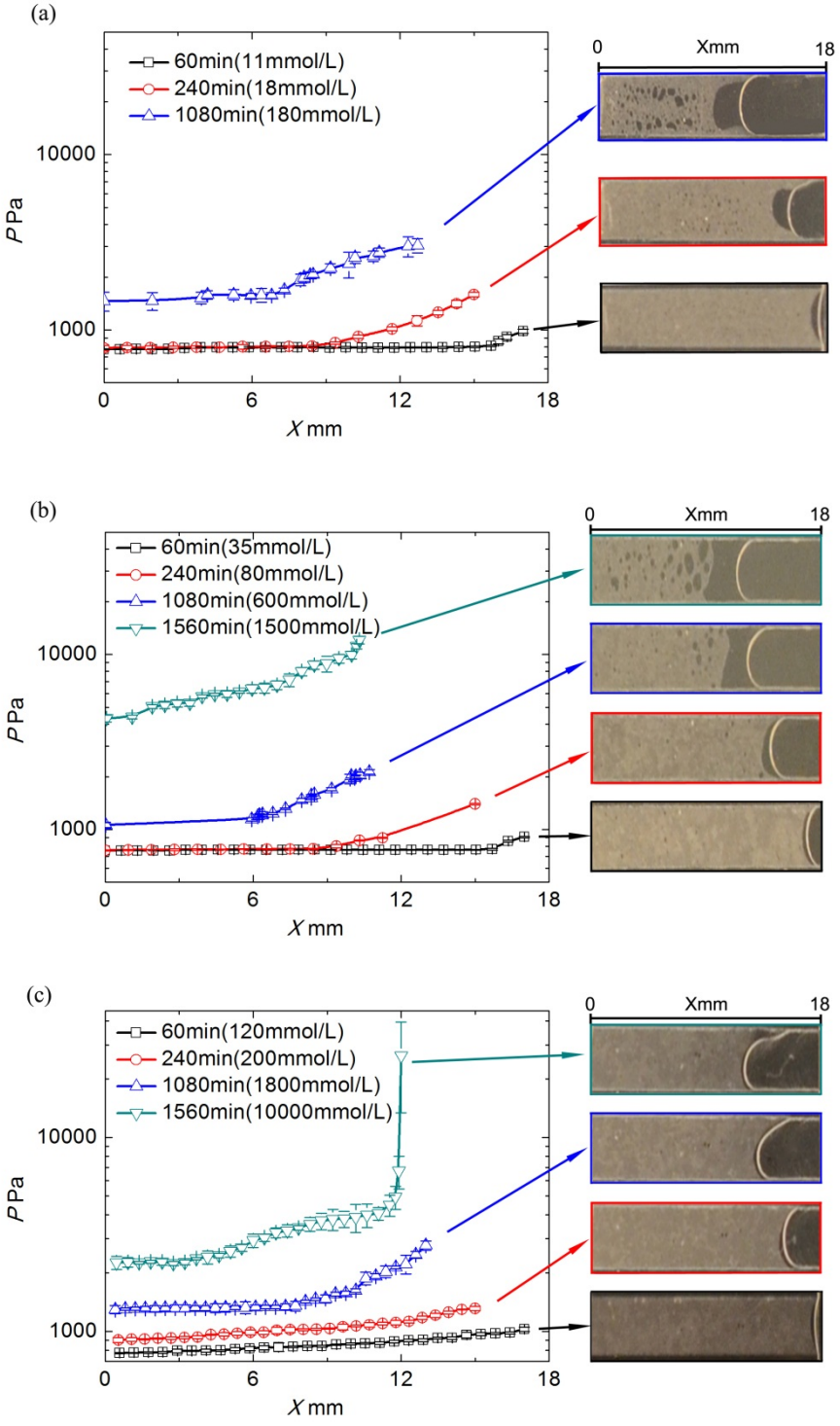
(a)
60min(11mmol/L)
240min(18mmol/L)
1080min(180mmol/L)
10000
1000
P Pa
0
6
12
18
X mm
0
Xmm
18
(b)
60min(35mmol/L)
240min(80mmol/L)
1080min(600mmol/L)
1560min(1500mmol/L)
10000
1000
P Pa
0
6
12
18
X mm
0
Xmm
18
(c)
60min(120mmol/L)
240min(200mmol/L)
1080min(1800mmol/L)
1560min(10000mmol/L)
10000
1000
P Pa
0
6
12
18
X mm
0
Xmm
18

Figure 2.7 Pressure profiles as function of position and time for initial SDS concentrations of 10 (a), 30 (b), and 100 (c) mmol/L. X=0 corresponds to the bottom of the sample, while the largest X-value in each curve represents the drying front of the sample. The images to the right show the corresponding state of the emulsions; their mean SDS concentrations, taking into account the evaporated water, are indicated in the legend.

It should be anticipated that when the pressure at a particular location reaches the critical value that exceeds the maximum disjoining pressure (P*), coalescence will occur [21, 22]. To assess the probability of coalescence at a given location and pressure it is necessary to determine this critical disjoining pressure for our system. We obtain P* for the emulsion as a function of SDS concentration by centrifugation experiments. The results are shown in Figure 2.8. The critical disjoining pressure increases dramatically at low SDS concentration before reaching its maximum value around 1000mmol/L. The critical disjoining pressures that we find are about a factor of 5 lower than values found by Bibette et al[23], probably because the droplet size in our experiments is at least an order of magnitude larger. Furthermore, we find that the critical pressure keeps on increasing far above the CMC, while the surface tension stays constant beyond the CMC; this suggests that it is not only the adsorbed amount of surfactant that determines the stability of the liquid films. Probably the exchange kinetics of surfactants plays key a role in determining the critical disjoining pressure.

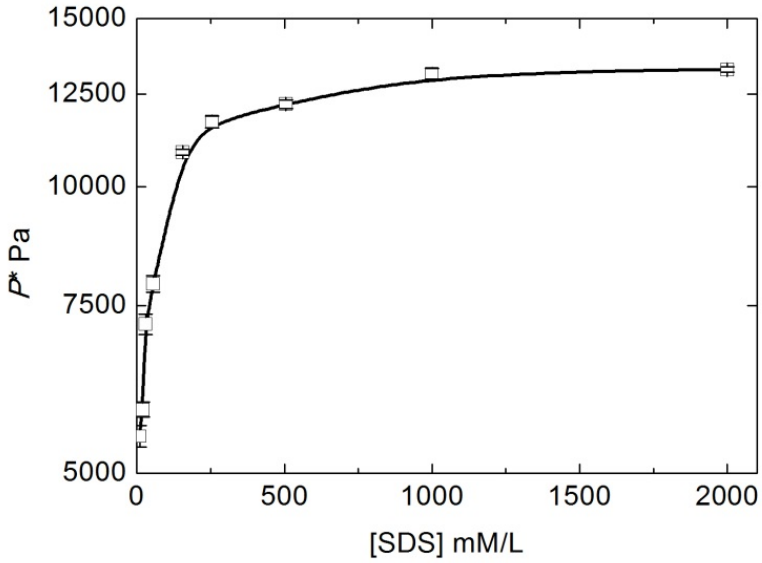

Figure 2.8 Critical disjoining pressures as a function of SDS concentration

2.3.3 Hydrodynamic mode

To understand our observations and the development of the steep pressure gradients, we use a hydrodynamic model for the flow of water in the drying emulsion in the stages prior to coalescence. Water flow is assumed to occur predominantly through the Plateau borders, and to be controlled by viscous drag and the pressure gradient. The interfaces of the Plateau borders are assumed to be immobile, generating a no-slip boundary condition, while the size of the Plateau borders (r) adjusts according to the local pressure, in order to satisfy the Laplace law[24]. As shown in the supporting information, these assumptions, together with mass conservation of both water and oil[25], can be expressed in the following differential equation:

$$\frac{\partial \varepsilon}{\partial \tau} = \frac{\partial}{\partial \xi}\left((\varepsilon^{1/2} - \varepsilon^{3/2}) \frac{\partial \varepsilon}{\partial \xi} \right) \quad (1)$$

where ε is the volume fraction of water at a certain distance from the bottom of the sample, which is related to the size of the Plateau borders:

$$\varepsilon = \alpha \left(\frac{r}{R} \right)^2 \quad (2)$$

Here R is the size of the emulsion droplets and α is a geometric constant of order unity. The local Laplace pressure is directly related to this by Laplace's law, $P = \gamma \alpha^{1/2} / R \varepsilon^{1/2}$. In equation 1, τ is a dimensionless time, $\tau = kt\gamma/\alpha\eta R$, with k a numerical pre-factor of order 10^{-3}, and $\xi = x/R$ is the dimensionless distance from the bottom of the sample. The pressure gradient may have an extra contribution from osmotic gradients, of which mobile surfactant is an obvious one. Water moving towards the dry front transports surfactant, which then accumulates at the dry end, causing a concentration gradient and a concomitant osmotic pressure gradient. For our Ansatz, we first neglect this osmotic pressure gradient, which is a reasonable assumption if diffusion is fast enough to level out concentration gradients. Surfactant transports towards the drying end may also lead to Marangoni effect causing transport in direction perpendicular to x, we also ignore them here. A more detailed investigation, taking surfactant accumulation and diffusion into account, will be presented elsewhere.

To solve equation 1 for the water volume fraction profile, and the pressure profile that follows from that, we need boundary conditions. At the bottom, where the sample is closed,

there is no net flux, so that the gradient must vanish: $d\varepsilon/d\xi=0$ at $\xi=0$. The boundary condition at the dry end of the sample is determined by the rate of evaporation (see supporting information for details):

$$\varepsilon^{\frac{1}{2}}\frac{\partial \varepsilon}{\partial \xi}=\frac{\partial \xi_2}{\partial \tau} \text{ at } \xi=\xi_1 \tag{3}$$

where ξ_1 denotes the position of the emulsion/air interface. The change of the latter represents the overall volume change of the sample, so that $d\xi_2/d\tau$ is directly proportional to the evaporation rate of water. We solve equation 1 with the appropriate boundary conditions numerically, by using a boundary immobilization method to map the moving boundary problem onto a fixed domain.

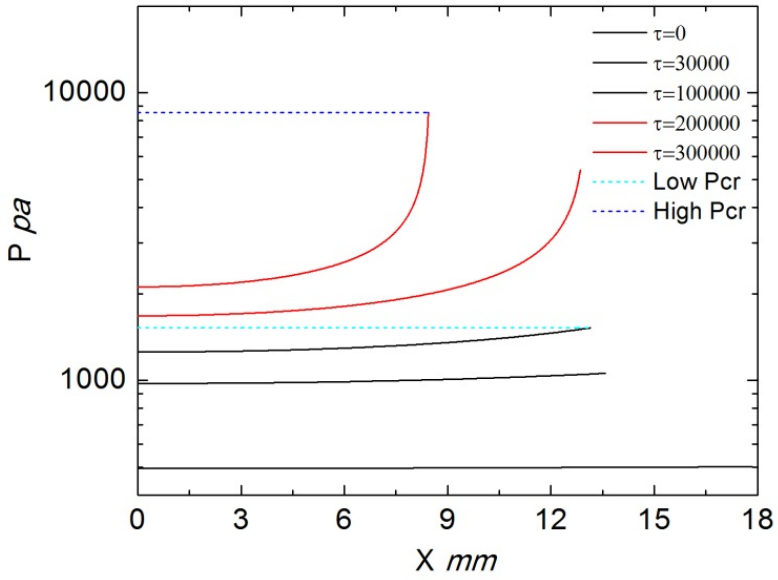

Figure 2.9 Pressure profiles in the drying emulsion from Hydrodynamic model simulation. (while R is 25 μ m, α is 0.094)

Figure 2.9 shows the calculated pressure profiles for various times. Clearly, drying increases the pressure throughout the system. Initially, the pressure profile is flat, but as drying goes on, the profile becomes steeper. If the critical disjoining pressure is low, as is the case for low surfactant concentrations (lower dashed line in Figure 2.9), the pressure cannot reach very high values, because coalescence occurs once the pressure exceeds the

critical threshold. As a result, the Plateau borders remain relatively wide and water transport towards the dry end can proceed much faster. Pressure gradients are therefore leveled out, leading to a rather flat pressure profile. This means that the critical pressure can be reached everywhere in the sample, so that bulk coalescence can take over quickly. By contrast, if the critical pressure is high, very steep pressure profiles can be reached. This is caused by the fact that narrow pores can develop, which induce strong pressure drops, because they clog the system from the drying end to the bottom of the sample. In this case, the pressure in the bulk never reaches the critical pressure and coalescence can occur only at the front.

2.4 Conclusions

We have observed two distinct modes of coalescence in a drying emulsion; one that proceeds as a nucleation and growth process throughout the sample and another where a coalescence front propagates into the sample from the dry end. Which mode dominates is determined by a balance between the established pressure profile and the local critical disjoining pressure in the emulsion. For very stable emulsions, narrow plateau borders can develop, leading to steep pressure gradients; the actual pressure only exceeds the critical pressure in a narrow zone around the drying front and front coalescence results. The opposite occurs for unstable emulsions; only shallow pressure profiles develop before coalescence commences throughout the bulk of the sample. Our results offer insight into the microscopic mechanisms that underlie the complex phenomena of coalescence in concentrated systems. While a lot of water can get trapped in the very stable emulsions in which only front coalescence takes place, phase inversion reaches completion much more efficiently for unstable emulsions that display bulk coalescence. Complete removal of the continuous phase is an essential requirement for the formation of homogeneous films of various types of emulsion paints. This poses a contradictory constraint on those systems; while stability is important for maintaining an emulsion during storage, this same stability inhibits good film formation.

References

1. M. A. Winnik, Curr Opin Colloid In, 1997, 2, 192-199.
2. A. F. Routh and W. B. Russel, AIChE J. FIELD Full Journal Title:AIChE Journal, 1998, 44, 2088-2098.
3. G. A. van Aken, Langmuir, 2002, 18, 2549-2556.
4. F. Bouchama, G. A. van Aken, A. J. E. Autin and G. J. M. Koper, Colloids Surf., A FIELD Full Journal Title:Colloids and Surfaces, A: Physicochemical and Engineering Aspects, 2003, 231, 11-17.
5. H. J. Butt, R. Kuropka and B. Christensen, Colloid & Polymer Science, 1994, 272, 1218-1223.
6. M. C. Goh, D. Juhue, O. M. Leung, Y. Wang and M. A. Winnik, Langmuir, 1993, 9, 1319-1322.
7. S. Hu, J. Rieger, S. V. Roth, R. Gehrke, R. J. Leyrer and Y. Men, Langmuir, 2009, 25, 4230-4234.
8. S. S. Hu, J. Rieger, Y. Q. Lai, S. V. Roth, R. Gehrke and Y. F. Men, Macromolecules, 2008, 41, 5073-5076.
9. J. L. Keddie, P. Meredith, R. A. L. Jones and A. M. Donald, Macromolecules, 1995, 28, 2673-2682.
10. F. Lin and D. J. Meier, Langmuir, 1996, 12, 2774-2780.
11. B. J. Roulstone, M. C. Wilkinson, J. Hearn and A. J. Wilson, Polymer International, 1991, 24, 87-94.
12. Y. Wang, A. Kats, D. Juhue, M. A. Winnik, R. R. Shivers and C. J. Dinsdale, Langmuir, 1992, 8, 1435-1442.
13. J. Bibette, F. L. Calderon and P. Poulin, Reports on Progress in Physics, 1999, 62, 969-1033.
14. J. Brujic, S. F. Edwards, I. Hopkinson and H. A. Makse, Physica a-Statistical Mechanics and Its Applications, 2003, 327, 201-212.
15. J. Brujic, C. M. Song, P. Wang, C. Briscoe, G. Marty and H. A. Makse, Phys. Rev. Lett., 2007, 98, 4.
16. A. A. Maan, K. Schroen and R. Boom, J. Food Eng., 107, 334-346.
17. T. Krebs, K. Schroen and R. Boom, Lab on a Chip, 2012, 12, 1060-1070.
18. P. Kékicheff, C. Grabielle-Madelmont and M. Ollivon, Journal of Colloid and Interface Science, 1989, 131, 112-132.
19. G. A. van Aken and F. D. Zoet, Langmuir FIELD Full Journal Title:Langmuir, 2000, 16, 7131-7138.
20. G. Narsimhan, Colloids and Surfaces, 1992, 62, 41-55.
21. J. Bibette, T. G. Mason, G. Hu and D. A. Weitz, Phys. Rev. Lett., 1992, 69, 981-984.
22. S. Tcholakova, N. D. Denkov, I. B. Ivanov and B. Campbell, Advances in Colloid and Interface Science, 2006, 123–126, 259-293.
23. J. Bibette, D. C. Morse, T. A. Witten and D. A. Weitz, Phys. Rev. Lett., 1992, 69, 2439-2442.
24. S. A. Koehler, S. Hilgenfeldt and H. A. Stone, Langmuir, 2000, 16, 6327-6341.
25. A. Bhakta and E. Ruckenstein, Advances in Colloid and Interface Science, 1997, 70, 1-124.

Appendix

Emulsion preparation

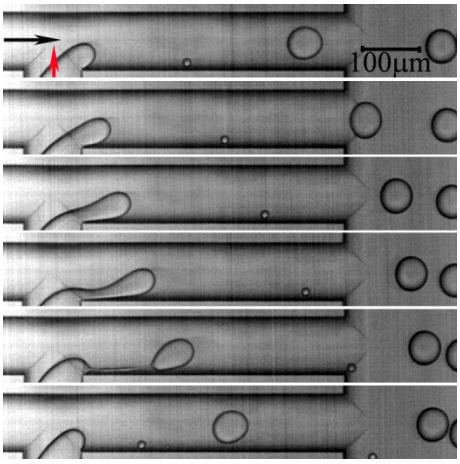

Figure A2.1. Production of monodisperse emulsions in a T-junction microfluidic device. Black long arrow shows the flow direction of the continuous phase (10mmol/L SDS). Red short arrow shows the flow direction of the dispersed phase (Nile Red-labelled silicone oil). During droplet pinch-off, small satellite droplets are formed due to the high viscosity ratio. These small satellite droplets were removed by making use of their very small creaming rate: in a sufficiently high container the cream layer that develops consists almost exclusively of the large droplets.

Visualization of emulsions with confocal microscopy

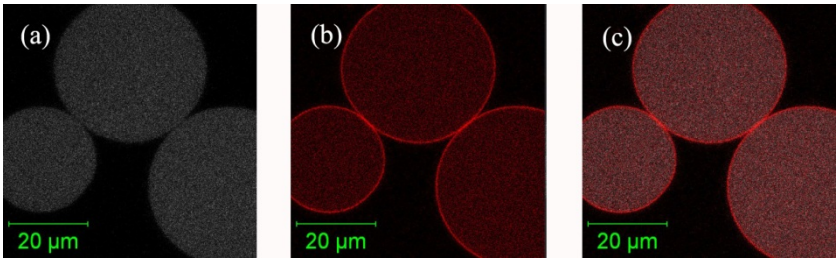

Figure A2.2. Confocal microscopy images of a silicone oil in water emulsion with 10mmol/L SDS surfactant, produced by vortexing. (a) Emission between 505 and 530nm colored with gray. (b) Emission for wavelengths larger than 560nm colored with red. (c)

Overlap of images (a) and (b) (give a reference here to the original Nile Red interface visualization paper).

Analysis of images to obtain bulk and front coalescence

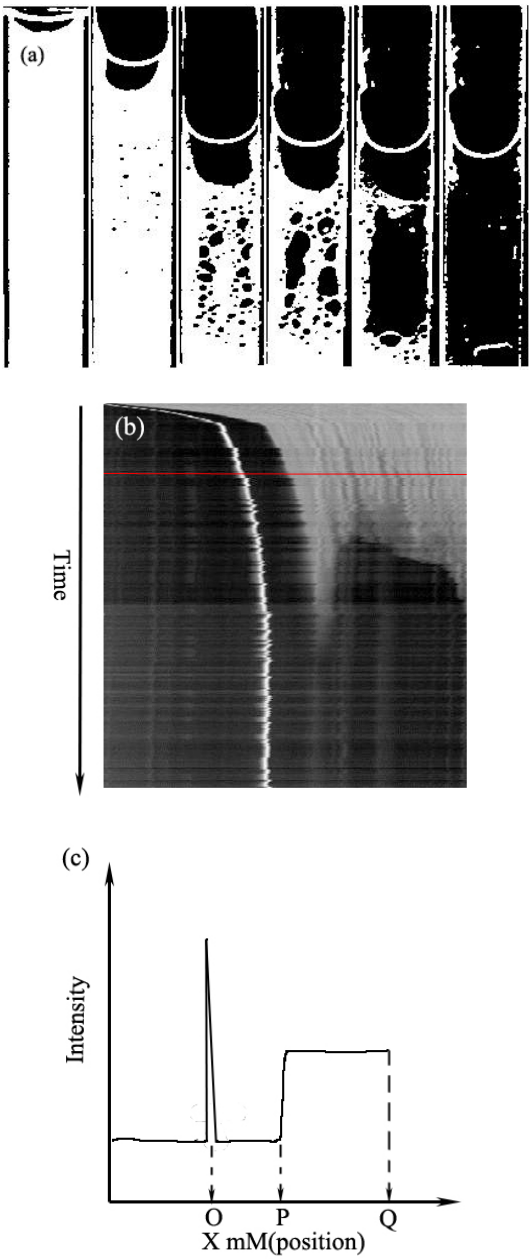

Figure A2.3. Analysis of the images of the drying samples. (a) The grayscale images,

presented in Figure 2.3 in the main text, are first converted to binary images using a gray level threshold. In these images, the black pixels below the interface with the air (which is white) represent coalesced emulsion, while the white pixels denote non-coalesced emulsion. (b) From the binary images, we create kymographs (using an ImageJ plugin). In the kymographs, the vertical axis indicates time, while the horizontal axis denotes vertical position (from top to bottom). The pixel intensity indicates the average intensity along a horizontal slice in the binary image. The bright white trace represents the position of the drying front, and the dark regions to the right of it represent coalesced regions. (c) An intensity profile along the sample at one particular time. The point marked with O corresponds to the drying front; the point marked P corresponds to the coalescence front (where continuous oil and emulsion meet). The front contribution to the coalescence is calculated from the distance between O and P, while the bulk contribution is obtained from the average pixel intensity in the region between P and Q.

Measurement of interfacial tension between silicone oil and SDS solution

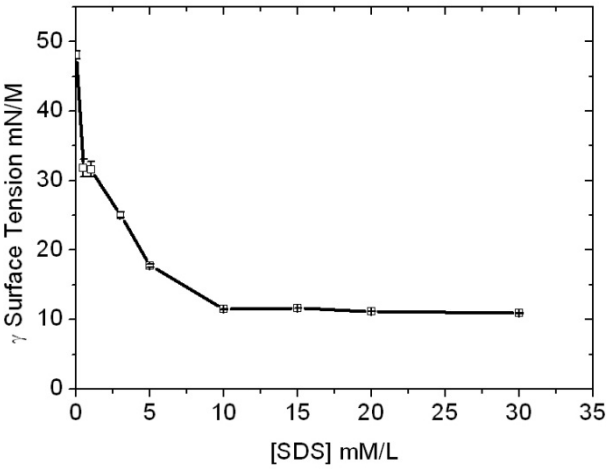

Figure A2.4. Interfacial tension between PDMS oil and aqueous SDS solution as a function of SDS concentration. Measurements were done using a pendant drop tensiometer (Sinterface, PAT1) at 298 K.

Chapter 3

Hydrodynamic model for drying emulsions

We present a hydrodynamic model for the water flow in a jammed emulsion, subjected to a unidirectional drying stress. Water flows through the Plateau borders towards the drying end, driven by gradients in the capillary pressure. Our model predicts the pressure gradients that arise, and allows us to explain the different modes of coalescence observed experimentally in chapter 2. From these results, we estimate the boundaries (critical pressure and evaporation rate) between bulk and front coalescence.

3.1 Introduction

Film formation in drying emulsions has been studied intensively in recent decades, both experimentally and theoretically. The process occurs in three stages [1]: (1) evaporation of water, leading to a dense packing of oil droplets; (2) deformation of the droplets; and (3) coalescence of the droplets. In our understanding of these stages, there are still many questions remaining. In particular, the last stage, that of droplet coalescence, is still poorly understood.

In **chapter 2**, we have found experimentally that there are two modes of phase inversion in surfactant-stabilized oil-in-water emulsions subjected to a unidirectional drying stress[2]. Coalescence occurs either through a nucleation-and-growth mechanism, where coalesced pockets form and grow randomly throughout the sample, or through a coalescence front that propagates into the sample from the drying end. We argued that which of these two modes occurs is determined by the steepness of the pressure profile in the emulsion. In this chapter, we present a hydrodynamic model that allows us to predict how the pressure profiles in the emulsion develop. We will then relate these calculated pressure profiles to our observations of chapter 2.

3.2 Description of the model

Our model aims to describe the last stages of film formation, in which the emulsion has already formed a jammed packing of deformed, faceted droplets (Figure 3.1). The structure of such a jammed emulsion is very similar to that of a dry foam and the equations that describe water flow in it are also similar to the equations used for foam drainage[3-9]. Water remains confined in the thin films (of thickness h) that separate two droplets, in the network of channels at which three films meet (called the Plateau borders), and in the nodes that connect four such channels. The Plateau borders, depicted schematically in Figure 3.2, have a length L and a triangular-like cross-section $A=cr^2$, with r the radius of curvature of the Plateau channel and $c \approx 0.161$[6]. To simplify the analysis, we assume that most of the water is contained within the Plateau borders, so that the volume of the films and the nodes can be neglected. This is valid for strongly jammed emulsions with very thin films ($L \gg r \gg h$). In this case, the local volume fraction of water ε in the emulsion can be written as:

$$\varepsilon = \alpha \left(\frac{r}{L}\right)^2 \quad (1)$$

where α is a geometrical factor that depends on the geometry of the Plateau channels and on the number of channels per droplet. For a regular polyhedral packing of droplets, $\alpha \approx 0.17$.[6]

Water evaporates at the top of the emulsion (at $z = z_2$, see Figure 3.1), which leads to an upward flow of water through the Plateau borders, towards the drying end. The flow through a single Plateau channel can be described by Poiseuille's law, which relates the average flow velocity in the channel v_c to the pressure gradient across the channel:

$$v_c = -k \frac{\nabla P r^2}{\eta} \quad (2)$$

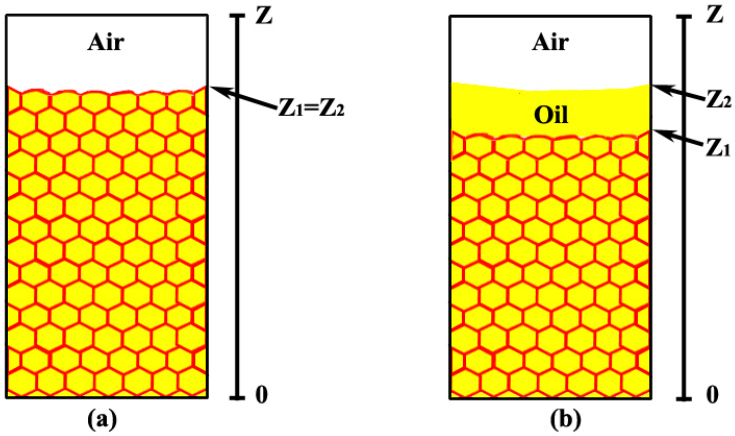

Figure 3.1 Schematic picture of a jammed emulsion subjected to a unidirectional drying stress, (a) before and (b) after coalescence has started to occur at the drying front. The emulsion/continuous oil interface is located at $z=z_1$ and the oil/air interface at $z=z_2$.

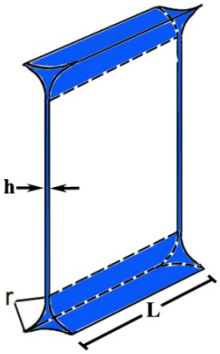

Figure 3.2 The geometry of a Plateau border in a jammed emulsion. Each Plateau border has a length *L* and a radius of curvature *r*.

Here, η is the viscosity and k is a numerical prefactor, which depends on the geometry of the channel and on the interfacial viscosity of the oil/water interface (which determines the slip velocity at the interface). It can be calculated by solving the Stokes equation. Since in our 1d model we are interested only in the average z-component of the velocity, we have to average over all the different channel orientations in the emulsion. This gives a value of k on the order of 10^{-3}.[6] The pressure gradient ∇P in equation 2 includes gradients in the capillary pressure (given by Laplace's law, $P = -\gamma/r$) and – if there is a soluble surfactant present in the water phase – also in osmotic pressure (P_{os}):

$$\frac{\partial P}{\partial z} = \frac{\gamma}{r^2}\frac{\partial r}{\partial z} - \frac{\partial P_{os}}{\partial z} = \frac{\gamma \alpha^{1/2}}{2L\varepsilon^{3/2}}\frac{\partial \varepsilon}{\partial z} - \frac{\partial P_{os}}{\partial z} \qquad (3)$$

where we have used equation (1) to obtain the second form. Gravitational forces also contribute to the pressure gradient, but for thin emulsion layers (or for the horizontal experimental set-up of chapter 2) this contribution can be neglected.

To obtain an equation for the distribution of water in the emulsion layer, we use the continuity equation, which describes mass conservation:

$$\frac{\partial \varepsilon}{\partial t} = -\frac{\partial(\varepsilon v)}{\partial z} \qquad (4)$$

Here, v is the net velocity of water in the z-direction. Because the total volume must be filled with either water or oil, a net flow of water towards the dry end through the channels must lead to a counter-flow of emulsion droplets in the opposite direction. By writing a mass balance also for the oil fraction, one obtains that the overall net water velocity is smaller than the velocity in the channels[3]:

$$v = v_c(1-\varepsilon) \qquad (5)$$

Substitution of equations 2, 3, and 5 in equation 4 leads to the following partial differential equation:

$$\frac{\partial \varepsilon}{\partial \tau} = \frac{\partial}{\partial \xi}\left((\varepsilon^{1/2} - \varepsilon^{3/2})\frac{\partial \varepsilon}{\partial \xi}\right) - (\varepsilon^2 - \varepsilon^3)\frac{\partial \Pi}{\partial \xi} \qquad (6)$$

where we have introduced a dimensionless length scale $\xi = z/L$, a dimensionless time $\tau = t/t_0$ with $t_0 = \frac{2\sqrt{\alpha}\eta L}{k\gamma}$, and a dimensionless osmotic pressure $\Pi = P_{\mathrm{os}} \cdot \frac{2L}{\sqrt{\alpha}\gamma}$.

The osmotic pressure depends on the local concentration of dissolved surfactant c and on the interactions between surfactant molecules. Here, we will assume that the osmotic pressure gradient is negligible compared to the gradient in capillary pressure, so that the last term in equation 6 can be neglected. In Appendix 2, we show how inhomogeneous surfactant distributions can be included in the model.

Equation 6 is a non-linear parabolic partial differential equation. Its solution $\varepsilon(\xi,\tau)$ gives the water profile as a function of position and time. To find solutions, appropriate initial and boundary conditions are needed. We assume that initially, at time zero, the sample is completely homogeneous:

$$\varepsilon(\xi,0)=\varepsilon_0 \qquad (7)$$

We assume here that the initial volume fraction is close to the random close packing limit, $\varepsilon_0 \approx 0.36$. It should be noted that the assumption of highly jammed emulsion is not valid at this volume fraction, but this is not crucial for the trends that we predict here.

At the bottom of the layer, at $\xi = 0$, the emulsion is in contact with an impenetrable substrate. This means that the flux must vanish here, so that the first boundary condition is:

$$\frac{\partial\varepsilon}{\partial\xi}=0 \quad \text{at } \xi=0 \qquad (8)$$

To obtain the boundary condition at the drying end of the sample, we consider the total volume of water in the sample, $\mathrm{V} = \mathrm{A}\int_0^{z_1}\varepsilon dz$, where A is the cross-sectional area of the layer. Any change in the amount of water, dV/dt, is due to evaporation at the dry end, so that:

$$A\int_0^{z_1}\frac{\partial\varepsilon}{\partial t}\mathrm{d}z+\varepsilon(z_1)A\frac{dz_1}{dt}=A\frac{dz_2}{dt} \qquad (9)$$

Here, the first term corresponds to changes in the water content throughout the film, the second term denotes the change in emulsion volume due to movement of the emulsion/oil interface (at z_1), and the last term denotes the total volume change of the emulsion, which must be accompanied by a change in the oil/air interface, z_2 (because the volume of oil is constant). Using equations 6 and 8, equation 9 can be written as

$$\left[(\varepsilon^{1/2}-\varepsilon^{3/2})\frac{\partial\varepsilon}{\partial\xi}\right]_{\xi=\xi_1}+\varepsilon(\xi_1)\frac{d\xi_1}{d\tau}=\frac{d\xi_2}{d\tau}=-\dot{E} \qquad (10)$$

with $\xi_1 = z_1/L$ and $\xi_2 = z_2/L$. Here, $\dot{E}$ is the dimensionless evaporation rate. Equation 10 is a mixed boundary condition at $\xi = \xi_1$. We can distinguish two different regimes. At the beginning, before coalescence occurs, no continuous oil layer is formed yet. This means that ξ_1 and ξ_2 coincide, and $\frac{d\xi_1}{d\tau}=-\dot{E}$. However, as time progresses the pressure at the drying end increases and after some time it becomes so high that the water films rupture and the emulsion droplets coalesce. This happens when the pressure locally exceeds the critical disjoining pressure for film rupture (see chapter 2). The latter depends on the concentration and the type of surfactant used to stabilize the emulsion. In our model, we

assume that coalescence occurs instantaneously as soon as the local pressure reaches a critical value, or, equivalently, as soon as the local volume fraction decreases below a critical value ε_{cr}. As soon as coalescence begins to occur (at the drying end, where the pressure is highest), an oil layer develops on top of the sample and ξ_1 and ξ_2 no longer coincide. In this regime, we assume that the volume fraction at the dry end equals the critical value:

$$\varepsilon(\xi_1, \tau) = \varepsilon_{cr} \tag{11}$$

Equation 10 then describes how the emulsion/oil interface moves. Equation 6, together with initial condition 7 and boundary conditions 8 and 10 (or 11), can be solved numerically as described in Appendix 1.

3.3 Results

The dimensionless form of our model leaves a limited number of parameters that determine the evolution of the volume fraction profiles. These are the initial volume fraction ε_0 and sample thickness *H*, the dimensionless evaporation rate $\dot{E}$, and the critical volume fraction where coalescence begins to occur, ε_{cr}. Of these, ε_{cr} has the largest effect on the evolution of the profiles. We therefore vary this parameter, and fix the others: $\varepsilon_0 = 0.36$, $H = 100$, and $\dot{E} = 8 * 10^{-5}$. The effect of varying the evaporation rate will be discussed below. Figure 3.3 and 4 show volume fraction profiles calculated for two different critical volume fractions. In Figure 3.3, the critical volume fraction is relatively high (corresponding to a relatively low critical disjoining pressure): $\varepsilon_{cr} = 0.1$. It can be seen that the water content throughout the emulsion decreases gradually, with only a relatively small gradient. When ε drops to ε_{cr}, it can no longer decrease further, because water films rupture below this value. Coalescence then leads to the formation of an oil layer on top of the emulsion. The emulsion/oil interface moves rapidly towards $\xi = 0$.

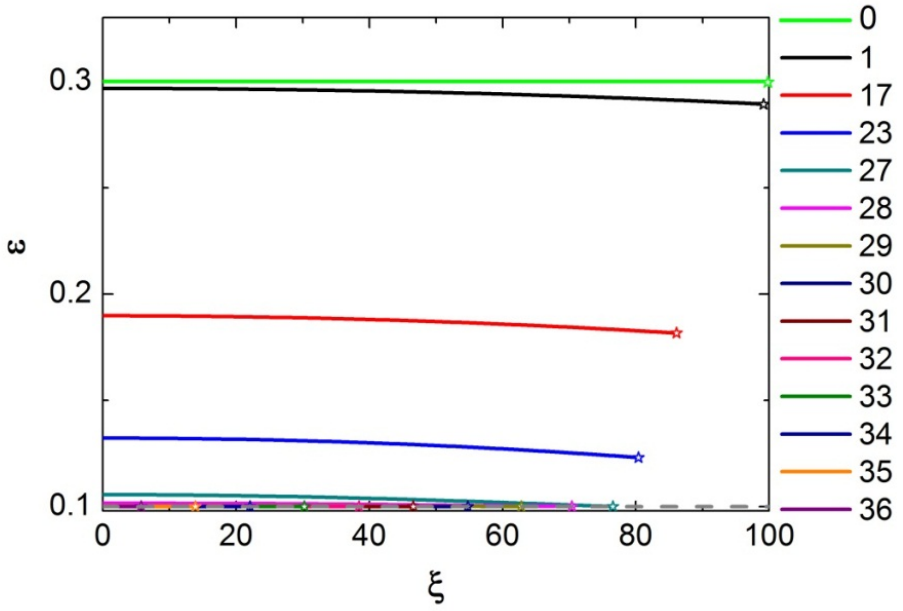

Figure 3.3 Calculated water volume fraction profiles for various dimensionless store time ($10000\,\tau$) and for a critical volume fraction $\varepsilon_{cr} = 0.1$. The star indicates ξ_1. The grey dashed line indicates ε_{cr}.

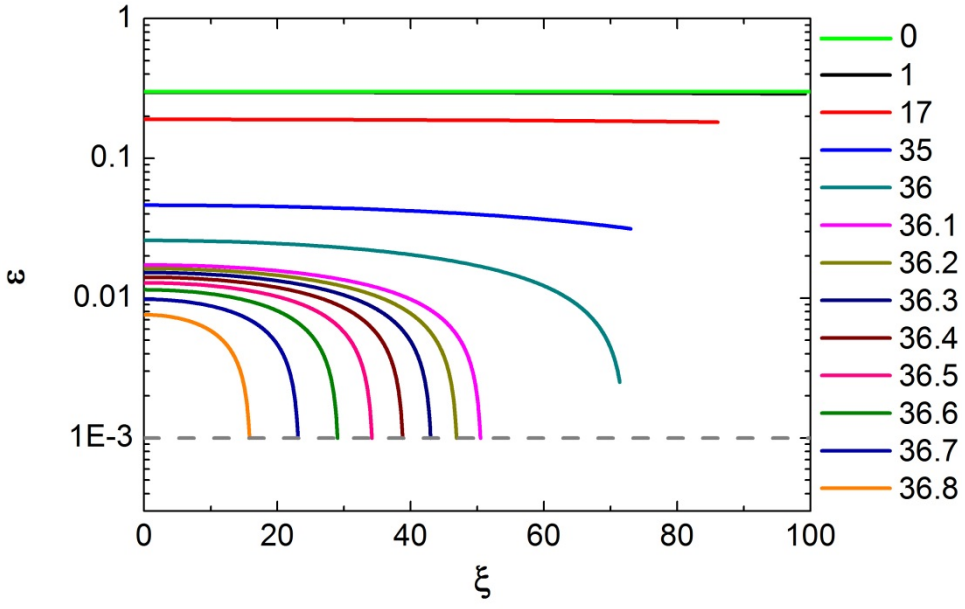

Figure 3.4 Calculated water volume fraction profiles for various dimensionless store time ($10000\,\tau$) and for a critical volume fraction $\varepsilon_{cr} = 0.001$. The grey dashed line indicates ε_{cr}.

In Figure 3.4, profiles are shown for a much lower critical volume fraction (corresponding to a higher critical disjoining pressure), $\varepsilon_{cr} = 0.001$. The differences with Figure 3.3 are obvious. First, the volume fraction has to decrease to 0.001 before coalescence starts to occur. This means that coalescence starts later. Secondly, the profiles become much steeper. The reason for this is that the Plateau borders become much thinner in this case, impeding the water flows from the bulk of the emulsion towards the drying end. This impediment prevents the water concentration profiles to level off: a steep pressure profile must build up.

3.3.1 Comparison to experiments

In Figures 3.3 and3. 4, we have presented results using dimensionless quantities. To compare these results to experiment, we need to convert these to measurable quantities. Here, we will consider conditions that mimic the experimental system of **chapter 2**. Table 3.1 shows the parameters that we use.

Table 3.1 Parameters in the model

Parameter	Meaning	Value
α	Geometrical factor for Plateau border	0.17
k	Prefactor in Poiseulle's law	0.001
L	Plateau border length	25 μm
η	Viscosity	0.01 Pa s
γ	Interfacial tension	0.01 N/m
$H \cdot L$	Initial sample thickness	2.5 mm
ε_0	Initial volume fraction	0.36
$\dot{E}$	Dimensionless evaporation rate	8×10^{-5}
t_0	Characteristic time scale, $2\sqrt{\alpha}\eta L/k\gamma$	0.02 s
v_2	Velocity of oil/air front	1.2×10^{-7} m/s

Using these parameters, we can convert the volume fraction profiles to pressure profiles, using $P = (\gamma/L)\sqrt{\alpha/\varepsilon}$. This is done in Figure 3.5 a and b, for the curves of Figure 3.3 and 4, respectively. The critical disjoining pressures for these two figures are 953Pa (for $\varepsilon_{cr} = 0.1$) and 5734Pa (for $\varepsilon_{cr} = 0.001$). It is clear that the pressure profiles remain relatively shallow when the critical disjoining pressure is low, while very steep pressure gradients arise near the front when the critical disjoining pressure is high.

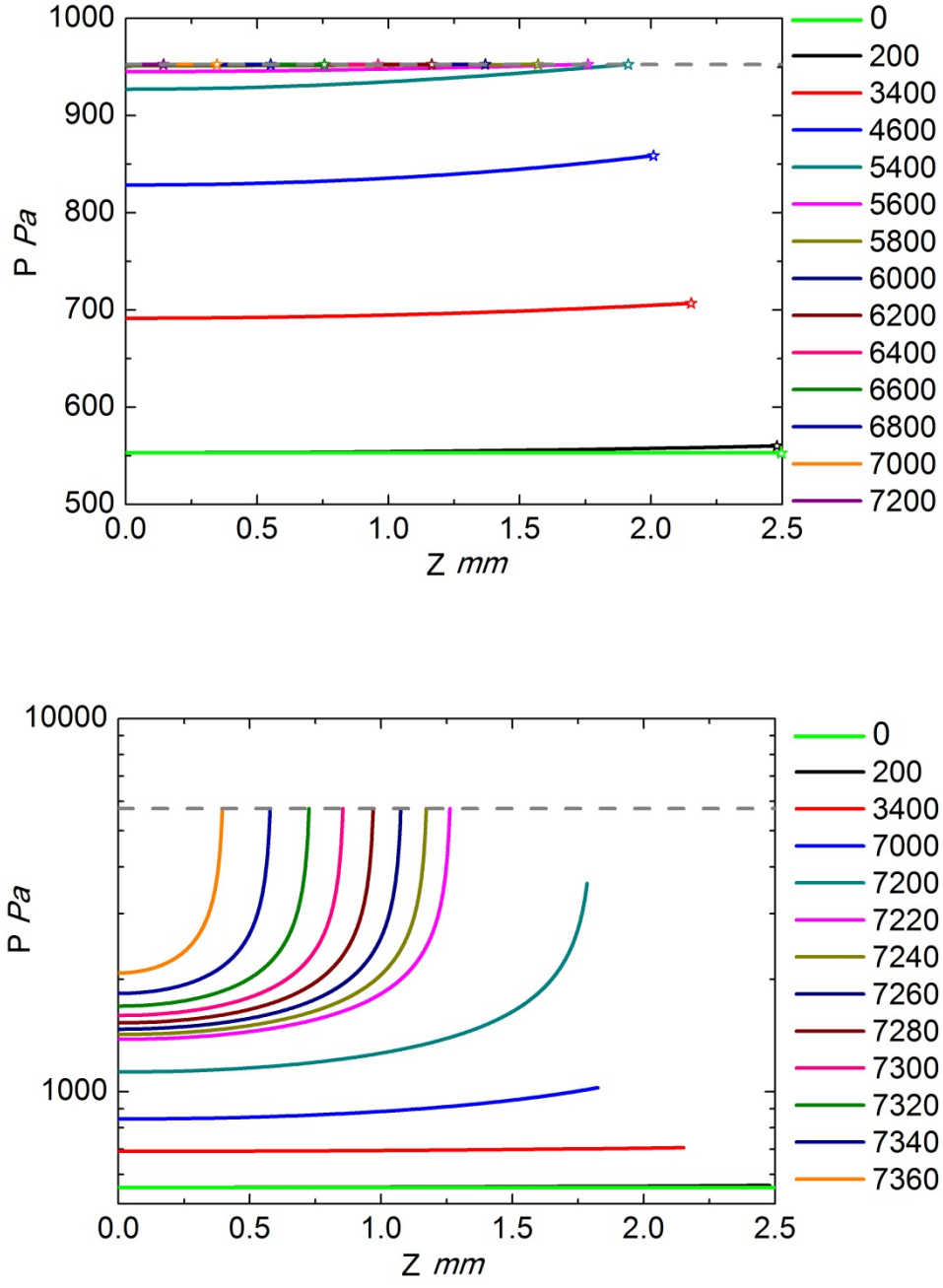

Figure 3.5 Calculated pressure profiles for various time and for critical disjoining pressures of 553Pa (a) and 5734Pa (b). Different curves correspond to different times, expressed in seconds (for the parameters of Table 1).

In chapter 2, we have seen that, depending on the critical disjoining pressure (which depends on the surfactant concentration), two modes of coalescence occur. When the critical disjoining pressure is low (for low surfactant concentration), coalescence starts at the front, but soon occurs throughout the whole emulsion layer. Figure 3.5a explains why: the pressure reaches the critical value at the front first, so that coalescence starts there. However, after that the pressure profile quickly levels off and P approaches the critical value throughout the whole layer. This causes water films to break everywhere in the sample. We called this bulk coalescence in chapter 2.

By contrast, when the critical pressure is high (for high surfactant concentration), the pressure gradient becomes much steeper and hardly levels off. This means that only at the front the actual pressure is close to the critical pressure so that only there droplets can coalesce.

3.3.2 Thickness of the coalescence zone

As discussed above the mode of coalescence is determined by the gradient in the pressure (or volume fraction) profile. When the pressure profile is shallow, coalescence can occur in a larger region than when the profile is steep. We can estimate the thickness of the region where coalescence can occur by introducing an extrapolation length

$$\lambda = -\frac{\varepsilon}{\partial\varepsilon/\partial\xi}\bigg|_{\xi=\xi_1} = \frac{1}{L}\frac{P}{\partial P/\partial z}\bigg|_{z=z_1} \qquad (12)$$

which expresses the typical length scale (expressed in units of L) over which the pressure increases to its highest value. A small value of λ indicates that the pressure is close to the critical value only near the front, while a large value of λ means that this is so in a much wider region. Figure 3.6 shows the extrapolation length as a function of time for different values of ε_{cr}. Figure 3.6b shows λ as a function of the relative position of the front, ξ_1/H, for the same values of ε_{cr}. First, λ decreases gradually, indicating that the pressure profiles become steeper. After coalescence begins to occur at the front, λ increases again, because the profiles become flatter. For large values of ε_{cr} (low P_{cr}), λ increases quickly to very large values, so that coalescence can occur in a very wide region (bulk coalescence). For small ε_{cr} (high P_{cr}), however, coalescence proceeds completely before any increase in λ occurs. Here, coalescence can occur only near the front.

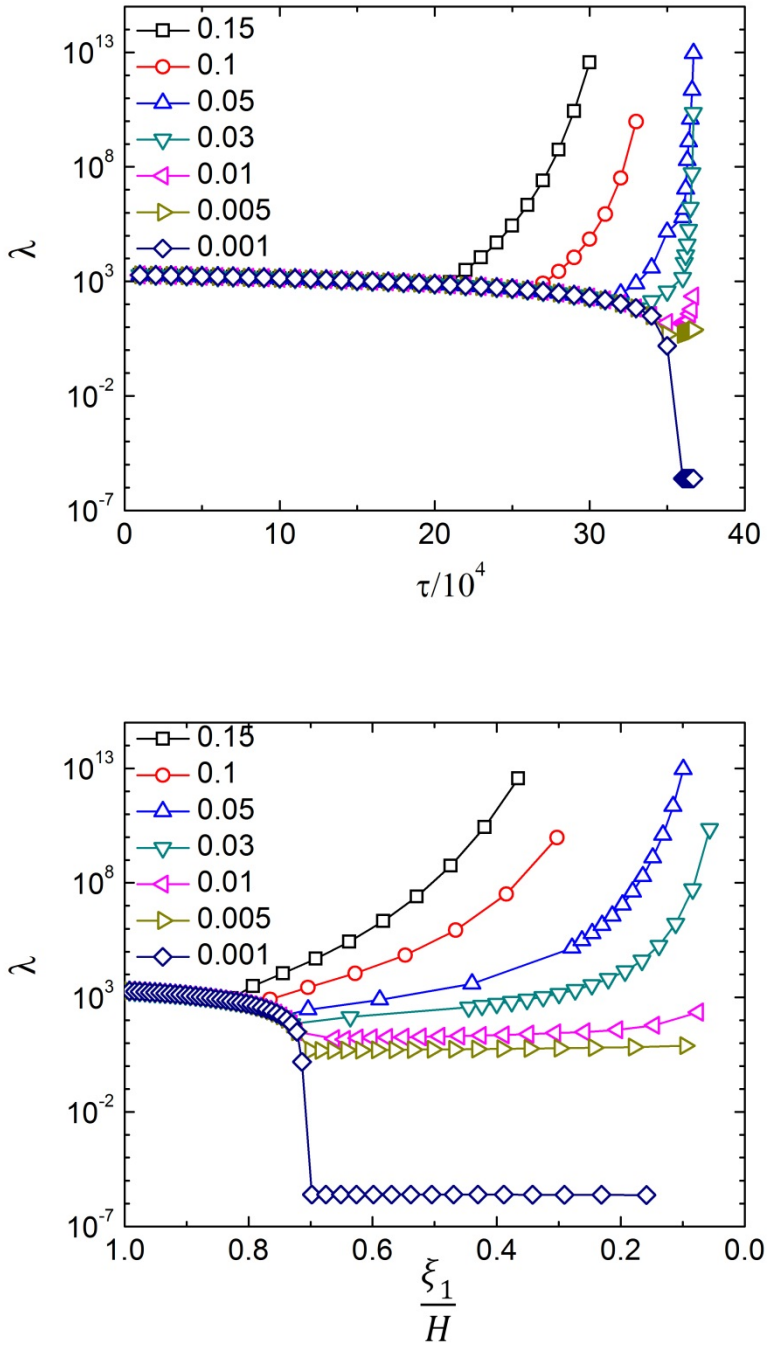

Figure 3.6 Evolution of the extrapolation length λ, indicating the length scale (expressed in units of L) over which the pressure profile decays, as a function of time (a) and as a function of ξ_1/H (b), for several values of the critical volume fraction.

To estimate the boundary between the two modes of coalescence, we consider the value of λ right at the moment that coalescence begins (this is where the kink in the curves occurs in figures 6a and b). We can estimate this value, which we denote $\boldsymbol{\lambda^*}$, from equations 10 and 11; using $\boldsymbol{\varepsilon(\xi_1) = \varepsilon_{cr}}$ and $\frac{\boldsymbol{d\xi_1}}{\boldsymbol{dt}} = \frac{\boldsymbol{d\xi_2}}{\boldsymbol{dt}} = -\boldsymbol{\dot{E}}$, we find:

$$\lambda^* = \frac{\varepsilon_{cr}^{3/2}}{\dot{E}} \tag{13}$$

Hence, the extrapolation length at the moment where coalescence begins increases as the critical volume fraction for coalescence increases and the evaporation rate decreases. When evaporation is slower, pressure gradients have more time to equalize, leading to shallower profiles and a larger extrapolation length. It follows that bulk coalescence is more likely to occur when the evaporation rate is low. We expect that the boundary between bulk and front coalescence occurs for a critical value of λ^*, which we assume to be on the order of unity. For λ^* below this critical value, front coalescence prevails, while above it bulk coalescence is more likely. This leads to a 'state diagram' of coalescence in drying emulsions as shown in Figure 3.7.

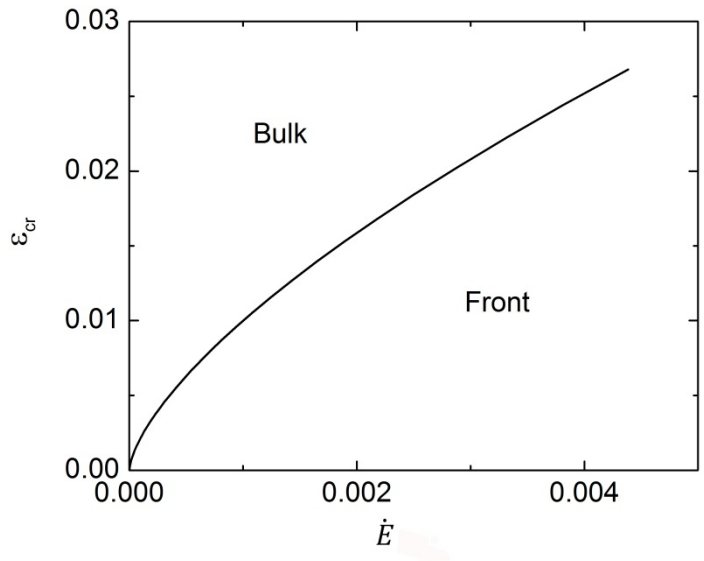

Figure 3.7 'State diagram', showing under which conditions ($\boldsymbol{\varepsilon_{cr}}$ and $\dot{E}$) bulk and front coalescence are expected to occur. The line shows the boundary, given by equation 13 with $\lambda_b^* = 1$.

3.4 Concluding remarks

We have presented a hydrodynamic model for the water flow in a drying emulsion. Our model predicts the pressure profiles that build up and can explain, at least qualitatively, our experiments of chapter 2 where we observed two different modes of coalescence. The model is still quite primitive, however, and in some ways oversimplified.

For example, in our calculations we have assumed a constant evaporation rate. In reality, the evaporation slows down strongly once coalescence has begun to occur at the front and a continuous oil layer forms on top of the emulsion. Our calculations therefore strongly overestimate the rate of the drying process. Also the steepness of the pressure profile is probably overestimated. A more realistic model should include an evaporation rate that depends on the thickness of the oil layer on top of the emulsion. This layer can be considered as a diffusive barrier for water transport; the evaporative flux then depends on the solubility of water in the oil, on the vapour pressure and on the layer thickness.

A second simplification, as already mentioned, is that we have neglected osmotic contributions to the pressure gradient due to variations in surfactant concentration. The water flows in the emulsion constitute an effective flux of dissolved surfactant towards the drying end. If this flux is large compared to the diffusive flux, surfactant will accumulate near the front and raise the osmotic pressure there. This gradient in osmotic pressure adds to the capillary pressure gradient. In the later stages of drying, the surfactant concentration can rise to very high values. This leads to a decrease of the chemical potential of water. Once the chemical potential of water in the Plateau borders at the front drops to the level of that in the vapour phase, evaporation stops altogether. In appendix 2, we show how surfactant transport can be included in our model.

Appendix 1 Numerical solution method

Equation 6, together with initial condition 7 and boundary conditions 8 and 10 (or 11), must be solved numerically. The problem is a moving boundary problem, because the boundary at $\xi = \xi_1$ is not stationary, but moves downward as the drying proceeds. We therefore employ a boundary-immobilization method, by introducing a reduced spatial variable $s = \xi/\xi_1(\tau)$. For the partial derivatives, we must employ the chain rule:

$$\frac{\partial}{\partial \xi} \rightarrow \frac{1}{\xi_1}\frac{\partial}{\partial s} \text{ and } \frac{\partial}{\partial \tau} \rightarrow \frac{\partial}{\partial \tau} - \frac{s}{\xi_1}\frac{\partial \xi_1}{\partial \tau}\frac{\partial}{\partial s} \tag{A1}$$

Substitution leads to:

$$\xi_1^2 \frac{\partial \varepsilon}{\partial \tau} - s\xi_1 \frac{\partial \xi_1}{\partial \tau}\frac{\partial \varepsilon}{\partial s} = \frac{\partial}{\partial s}\left(\left(\varepsilon^{\frac{1}{2}} - \varepsilon^{\frac{3}{2}}\right)\frac{\partial \varepsilon}{\partial s}\right) \tag{A2}$$

where the osmotic pressure term has been left out. The boundary immobilization method has introduced a pseudo-convective term (second term on the left). We use a finite-element method to solve this partial differential equation[10]. First, the weak form of the PDE is constructed by multiplying by an arbitrary weighting function $w(s)$ and integrating over the whole domain, $s \in [0,1]$. This gives:

$$\int_0^1 w\left\{\frac{\partial \varepsilon}{\partial \tau} - s\xi_1 \frac{\partial \xi_1}{\partial \tau}\frac{\partial \varepsilon}{\partial s} - \frac{\partial}{\partial s}\left(\left(\varepsilon^{\frac{1}{2}} - \varepsilon^{\frac{3}{2}}\right)\frac{\partial \varepsilon}{\partial s}\right)\right\} ds = 0 \tag{A3}$$

We perform partial integration on the second term to reduce the order of integration,

$$\int_0^1 w\left\{\frac{\partial \varepsilon}{\partial \tau} - s\xi_1 \frac{\partial \xi_1}{\partial \tau}\frac{\partial \varepsilon}{\partial s}\right\} ds + \int_0^1 \frac{\partial w}{\partial s}\left(\varepsilon^{\frac{1}{2}} - \varepsilon^{\frac{3}{2}}\right)\frac{\partial \varepsilon}{\partial s} ds - \left[w\left(\varepsilon^{\frac{1}{2}} - \varepsilon^{\frac{3}{2}}\right)\frac{\partial \varepsilon}{\partial s}\right]_{s=0}^{s=1} = 0 \tag{A4}$$

In the last term, we substitute boundary conditions 8 and 10 (after the appropriate substitution $s(\xi)$). This gives

$$\int_0^1 w\left\{\frac{\partial \varepsilon}{\partial \tau} - s\xi_1 \frac{\partial \xi_1}{\partial \tau}\frac{\partial \varepsilon}{\partial s}\right\} ds + \int_0^1 \frac{\partial w}{\partial s}\left(\varepsilon^{\frac{1}{2}} - \varepsilon^{\frac{3}{2}}\right)\frac{\partial \varepsilon}{\partial s} ds - w(1)\left[\xi_1 \frac{d\xi_2}{d\tau} - \varepsilon(1)\xi_1 \frac{d\xi_1}{d\tau}\right] = 0 \tag{A5}$$

To solve this equation, we discretize ε on a finite element grid consisting of *N* nodes. The solutions are approximated by interpolation between the values at the nodes, $\varepsilon(s,\tau) = \mathbf{n} \cdot \mathbf{e}(\tau)$, where $\mathbf{e}(\tau)$ is a vector that stores the volume fractions at the nodes and $\mathbf{n}$ is the interpolation vector consisting of standard shape functions. We use simple linear 2-node elements, both for the volume fractions and the weight functions *w(s)* (Galerkin method). Substitution of the approximated solutions and weighting functions and carrying out the integrals in the weak form of the PDE (A5) element-by-element yields a sparse set of *N* non-linear equations for the ε values at the nodes. These equations are solved using Newton's iteration method. If the pseudo-convective terms in the PDE become large

compared to the diffusive terms, spurious oscillations arise in the solution, which make the solution method unstable. This is remedied by using a Petrov-Galerkin scheme[10]

Appendix 2 Concentration gradients

Equation 6 also contains a contribution of the osmotic pressure to the pressure gradient. Osmotic pressure gradients arise if the water phase contains a soluble surfactant (or any other soluble ingredient). The flow towards the dry end drags the surfactant along, leading to an accumulation at the dry end. This accumulation is counteracted by diffusion. The conservation equation for the surfactant is

$$\frac{\partial(\varepsilon c)}{\partial t} = -\frac{\partial}{\partial z}\left[\varepsilon D\frac{\partial c}{\partial z} - \varepsilon v c\right] \tag{A6}$$

where c is the surfactant concentration, D the diffusion coefficient of the surfactant, and v is the net water velocity. Here, we have neglected the contribution of adsorbed surfactant. Using equation 6, this can also be written as

$$\frac{\partial(\varepsilon c)}{\partial t} = \frac{\partial}{\partial \xi}\left[\varepsilon \widetilde{D}\frac{\partial C}{\partial \xi} + C\left(\varepsilon^{\frac{1}{2}} - \varepsilon^{\frac{3}{2}}\right)\frac{\partial \varepsilon}{\partial \xi} - C(\varepsilon^2 - \varepsilon^3)\frac{\partial \Pi}{\partial C}\frac{\partial C}{\partial \xi}\right] \tag{A7}$$

where we have introduced a reduced concentration $C = cL^3$ and a dimensionless diffusion coefficient $\widetilde{D} = D(t_0/L^2)$. The relation between the reduced osmotic pressure Π and the reduced concentration C depends on the type of surfactant. It can be obtained from experimental data.

Again, we need an initial condition and boundary conditions:

$$C(\xi, 0) = C_0, \tag{A8}$$

$$\frac{\partial C}{\partial \xi} = 0 \text{ at } \xi = 0, \tag{A9}$$

$$\left[\varepsilon \widetilde{D}\frac{\partial C}{\partial \xi} + C\frac{d\xi_2}{d\tau}\right] = 0 \quad \text{at } \xi = \xi_1 \tag{A10}$$

where the last condition comes from the conservation of the total amount of surfactant. The simultaneous solution of these equations and the equations that describe the water flow (equation 6) yields both pressure and surfactant concentrations profiles.

Reference

1. M. A. Winnik, Current Opinion in Colloid & Interface Science, 1997, 2, 192-199.
2. H. Feng, J. Sprakel, D. Ershov, T. Krebs, M. A. C. Stuart and J. van der Gucht, Soft Matter, 2013, 9, 2810-2815.
3. A. Bhakta and E. Ruckenstein, Advances in Colloid and Interface Science, 1997, 70, 1-124.
4. A. Saint-Jalmes, Soft Matter, 2006, 2, 836-849.
5. S. J. Cox, D. Weaire, S. Hutzler, J. Murphy, R. Phelan and G. Verbist, Proceedings of the Royal Society of London Series a-Mathematical Physical and Engineering Sciences, 2000, 456, 2441-2464.
6. S. A. Koehler, S. Hilgenfeldt and H. A. Stone, Langmuir, 2000, 16, 6327-6341.
7. D. Weaire, S. Hutzler, S. Cox, N. Kern, M. D. Alonso and W. Drenckhan, J. Phys.-Condes. Matter, 2003, 15, S65-S73.
8. H. A. Stone, S. A. Koehler, S. Hilgenfeldt and M. Durand, J. Phys.-Condes. Matter, 2003, 15, S283-S290.
9. S. Hilgenfeldt, S. A. Koehler and H. A. Stone, Physical Review Letters, 2001, 86, 4704-4707.
10. K.-J. Bathe, Finite element procedures, Prentice hall Englewood Cliffs, 1996.

Part I
Manipulating coalescence in dense emulsions

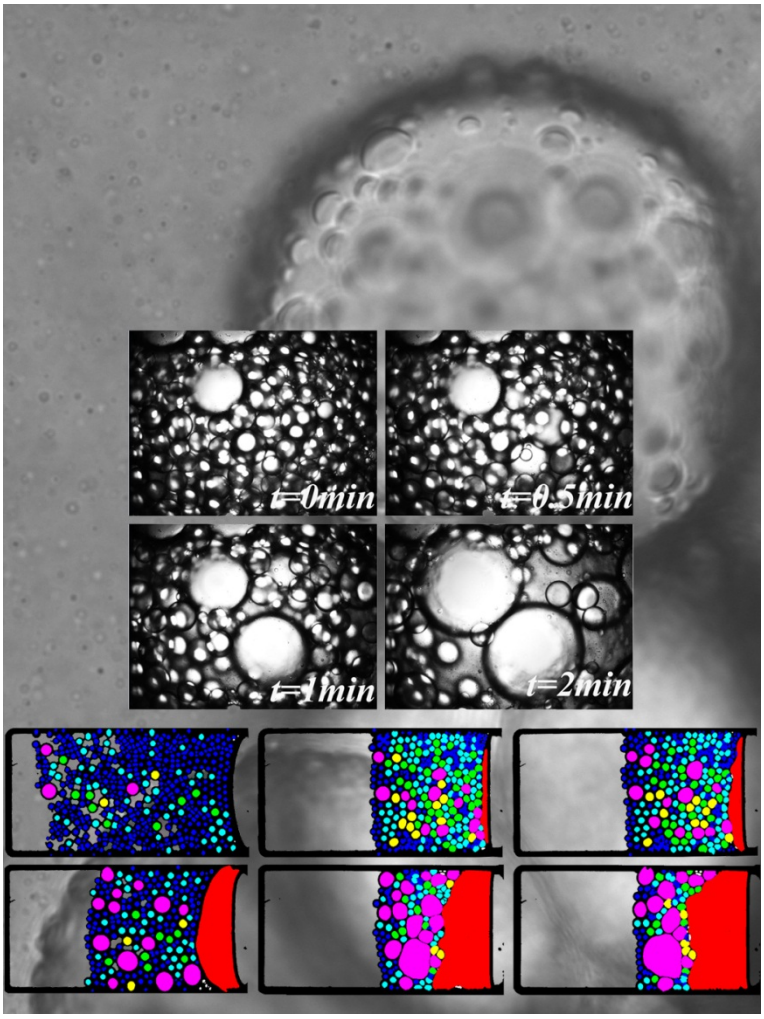

Chapter 4

Well-defined temperature-sensitive surfactants for controlled emulsion coalescence

In a variety of applications, emulsion formulations are required, which exhibit excellent shelf stability yet can be broken or perform phase inversion at a desired time. Here we approach these contradictory constraints through the synthesis of well-defined thermoresponsive surfactants based on di(ethylene glycol)methacrylate and poly(ethylene glycol)methacrylate using Atomic Transfer Radical Polymerization. The surfactants show a Lower Critical Solution Temperature (LCST) of approximately 37°C, independent of molecular weight, which is ascertained by both Differential Scanning Calorimetry as well as Dynamic Light Scattering. Below the LCST, the surfactants stabilize the emulsions for at least four months. Above this temperature the hydrophilic block collapses and coalescence between the emulsion droplets occurs; this leads to demixing of the sample within several minutes. We reveal the mechanism for the temperature-triggered coalescence by measurements of the temperature-dependent interfacial tension and by studying the interfacial morphology of surfactant-covered emulsion droplets.

This chapter was published as:
H. Feng, N. A. L. Verstappen, A. J. C. Kuehne and J. Sprakel, Well-defined temperature-sensitive surfactants for controlled emulsion coalescence *Polymer Chemistry*, **2013**, 4, 1842-1847.

4.1 Introduction

The stabilization of liquid-liquid interfaces through the adsorption of surfactants plays an important role in many industrial processes in which emulsions are produced or used. The main aim in the development of new surfactants is to provide prolonged shelf-life by preventing the coalescence of emulsion droplets. The coalescence of two individual liquid droplets requires the close approach of the two liquid interfaces and the subsequent rupture of the liquid film that separates them[1-7]. Surfactants, which are adsorbed onto these interfaces, reduce the interfacial tension and prevent close approach of the droplets through steric or electrostatic repulsion[8-12]. Strong repulsive interactions between the droplet surfaces lead to high stability against coalescence. While stability of an emulsion against coalescence is often the main aim in the formulation of emulsion systems, many applications of emulsions do not only require high stability against coalescence, but also on demand breaking or phase inversion of the emulsion. For example, in the application of alkyd emulsions as waterborne paints, prolonged shelf-stability is required, yet upon application of the paint to a surface, a coating must be formed; this requires coalescence of all droplets to form a continuous film of the dispersed material. Furthermore, in emulsion synthesis and separation processes, in which two-phase systems are used to react or extract certain components from complex mixtures, on demand breaking of the emulsion and separation of the oil and water phases is required to recover the individual product.

At first, these requirements seem contradictive: The emulsion needs to be stable on the shelf, yet be de-stabilized on demand by a given stimulus. With the development of novel classes of responsive building blocks, it becomes possible to meet these apparently conflicting requirements and to provide an emulsion with both high stability and on-demand breaking or phase inversion.

Previously, light-triggered surfactants have been developed by introducing light-responsive azobenzene side-groups, which undergo cis-trans isomerization upon exposure to light[13, 14]. The conformational change leads to a small variation in polarity of the polymer, thus changing its adsorption properties at the oil-water interface. In this way, reversible switching between oil-in-water and water-in-oil emulsions has been demonstrated. The first generation of these light-responsive surfactants shows only small changes in interfacial tension upon a change in wavelength[15]. However, a second generation of non-ionic surfactants have recently been developed, where the azobenzene group is located in

between the hydrophobic tail and hydrophilic ethylene oxide group. Here the surface tension changes significantly after switching[16].

While these materials represent promising switchable systems, light-responsive surfactants have the drawback of being colored to allow light absorption. For many industrial applications, such as in coatings and paints, coloration is unacceptable. Moreover, in separation processes of sensitive compounds, such as proteins or other biomolecules, high light exposure doses might induce undesired photochemical changes in the molecules. New material systems, in which emulsion breaking is induced under mild conditions are thus required.

Recently, we have reported the synthesis of a simple thermoresponsive surfactants using chain transfer free radical polymerization of poly(n-isopropyl acrylamide).[17] Through physical adsorption of these surfactants at the interface, temperature-triggered self-assembly of colloidal particles and an on-demand phase inversion of emulsions has been achieved. While such surfactants display many advantages over the light-responsive systems, such as their colourless appearance, low cost and mild triggering conditions, the preparation with free radical polymerization yields an ill-defined and polydisperse product.

In this paper we describe the synthesis and characterization of a well-defined thermoresponsive surfactant using Atom Transfer Radical Polymerization (ATRP). From an alkyl-functional ATRP initiator we grow a hydrophilic block consisting of a combination of poly(ethylene glycol)methacrylate (PEGMA) and di(ethylene glycol)methacrylate (DEGMA). This polymer exhibits a lower critical solution temperature (LCST) that is independent of molecular weight[18]. We prepare a systematic range of surfactants, in which only the ratio of hydrophilic to hydrophobic blocks vary while all other properties remain unchanged. We characterize these surfactants, using light scattering and differential calorimetry, and we demonstrate that they can be used to prepare emulsions that are stable for at least four months at room temperature. Yet these same emulsions can be completely phase separated within minutes upon changing the temperature above the LCST. Moreover, we study the mechanism with which a simple temperature trigger can lead to droplet coalescence.

4.2 Materials & Methods

All reagents were purchased from Sigma-Aldrich and used as received.

4.2.1 Alkyl-functional ATRP initiator

We first prepare an ATRP initiator functionalized with a hexadecyl tail. The reaction proceeds as follows; in a roundbottomflask, hexadecanol (82 mmol) and triethylamine (90.2 mmol), are dissolved in dry dichloromethane (DCM) (200 mL). α-bromoisobutyryl bromide (98.4 mmol) is dissolved in 30 mL DCM and added dropwise to the reaction mixture. The reaction is stirred for 18 hours at room temperature. The white precipitate (ammonium bromide) is removed by filtration. The filtered solution is washed 3 times with a 1 mM NaOH-solution. The organic phase containing the product is dried by adding anhydrous Mg_2SO_4 and subsequently decolourizing carbon is added to remove coloured impurities. After filtration the solvent is removed by rotary evaporation. The product is obtained as a brown oil that crystallizes after a few days at room temperature. The conversion is >99% as determined by ^{1}H NMR and the yield after purification is 48.4%.

4.2.2 Surfactant synthesis

The hydrophilic part of the synthesized surfactants consists of PEGMA and DEGMA. By adjusting the molar ratio of these two monomers, the LCST can be tuned between 90 °C, for homo-PEGMA, and 28°C for homo- DEGMA blocks[19]. Here we chose a molar ratio of 8% PEGMA and 92% DEGMA, which results theoretically in an LCST of 37 °C [19].

The reaction mixture consist of the monomers PEGMA, DEGMA, and N,N,N',N'',N''-Pentamethyldiethylenetriamine (PMDETA) as ligand. All compounds are dissolved in toluene, with a constant mass ratio of monomer to solvent of 1:7. Quantities of reagents are given in Table 4.1. After degassing the solution with nitrogen for 10 minutes, CuCl is added as a catalyst. After purging with nitrogen for another 10 minutes, the alkyl-functional ATRP initiator is added, thus starting the reaction. The reaction is left to proceed for 3 hours at 60 °C.

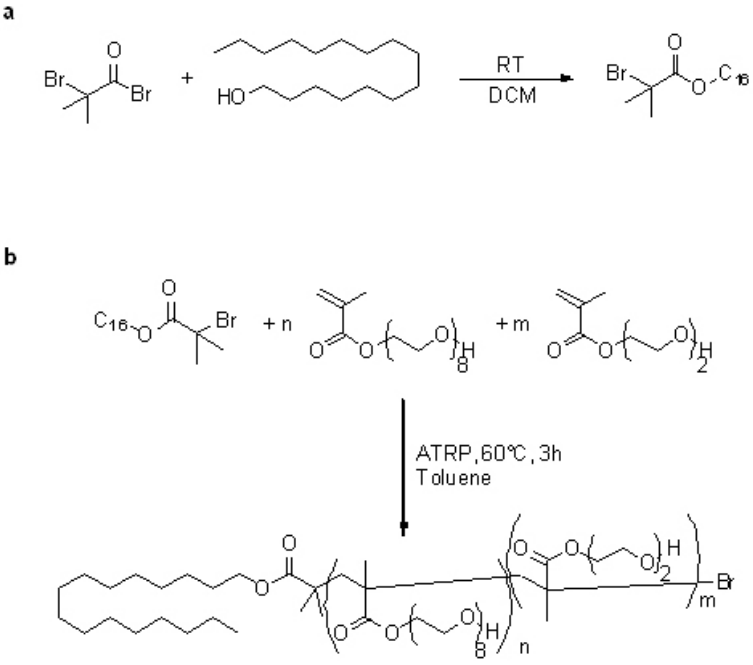

Figure 4.1 Reaction schemes: (a) synthesis of the initiator at room temperature in dichloromethane and (b) the polymerization of the surfactants by ATRP in toluene, where the ratio of the monomers is; n/m = 0.087.

The reaction is quenched by exposing the reaction mixture to air. It is then diluted by adding approximately 3x the reaction volume of toluene and passed over an aluminium oxide column to remove the catalyst-ligand complex. After evaporation of the solvent, the product is dissolved in deionized water and purified by dialysis against deionized water until the product is colourless. Then the surfactant is obtained by freeze drying. All products appeared as a light yellow, highly viscous oil.

For all surfactants, the same synthetic protocol is applied. Only the ratio between monomers and initiator is varied to synthesize polymers with a target degree of polymerization of N=38, N=76, N=114. The specific composition of all the reaction mixtures can be found in Table 1.

^{1}H-NMR (400 MHz, $CDCl_3$) (ppm): 4.3 - 3.9 (br, PEG CH_2), 3.7 – 3.5 (br, PEG CH_2), 3.5 – 3.4 (br PEG OH), 3.4 – 3.3 (br PEG CH_2), 2.0 – 1.6 (m br backbone CH_2), 1.3 – 1.1 (br, C_{16} CH_2), 1.1 – 0.9 (br, backbone & C_{16} CH_2), 0.9 – 0.7 (br, backbone CH_3). ^{13}C-NMR (100 MHz, $CDCl_3$) (ppm): 72.0 (PEG CH_2), 70.5 (PEG CH_2), 69.0 – 68.0 (PEG CH_2), 64.0 (PEG CH_2), 59.0 (backbone CH_2), (other signals too small).

Table 4.1 Composition of reaction mixtures and analysis of the degree of polymerisation (DP), molecular weight (Mw), polydispersity (PDI) and lower critical solution temperature (LCST), from gel permeation chromatography (GPC), ^{1}H-NMR end group analysis, dynamic light scattering (DLS), differential scanning calorimetry (DSC).

	Initiator (mmol)	PEGMA (mmol)	DEGMA (mmol)	PMDETA (mmol)	CuCl (mmol)	Target DP	Obtained DP	Mw (kg/mol)	PDI	LCST DLS (°C)	LCST DSC (°C)
N=38	0.675	2.054	23.503	1.021	1.030	38	32	7.5	1.33	34	32.0
N=76	0.337	2.020	23.503	0.511	0.514	76	58	13.1	1.68	34	33.7
N=114	0.253	2.362	26.442	0.383	0.385	114	63	14.3	1.51	34	33.5

4.2.3 Characterization

To determine the LCST of the surfactants we perform both differential calorimetry and light scattering measurements. Differential scanning calorimetry (MicroCal VP-DSC, GE Healthcare, Northampton USA) is performed on surfactant solutions in de-ionized water at 0.05 g/L at heating rates of 1 °C/min. The size of the micelles formed by these surfactants, dissolved in de-ionized water at 5 g/L is measured as a function of temperature using Dynamic Light Scattering on a home-built light scattering set-up with a fixed detection angle of 90°. Interfacial tensions are measured by pendant drop tensiometry with a thermostated sample chamber between 20-50℃.

Emulsions, consisting of a 5 g/L surfactant solution and decane are prepared using a mechanical homogenizer (IKA Ultra Turrax Tube Drive). An emulsion of low polydispersity, consisting of a 5g/L surfactant solution and poly-dimethylsiloxane (PDMS) silicone oil is prepared using a T-junction microfluidic device. Stability is judged both by visual inspection and by observation using brightfield microscopy with a 20x air objective. Temperature-triggered coalescence and the morphology of the oil-water interface are studied through heating the emulsions, contained within hermetically-sealed glass sample chambers, on a microscope-mounted Instec thermal stage (TSA02i) within a temperature range of 25-60 °C.

4.3 Result and discussion

To synthesize well-defined surfactants, which exhibit thermoswitchable stabilization of emulsions, we choose a mixture of PEGMA and DEGMA with a reported LCST of 37°C[19]. This copolymer has the advantageous properties that its LCST is independent of chain length and shows little to no hysteresis upon cooling[18].

We prepare a systematic series of surfactants with increasing chain-length of the

hydrophilic block; the synthesis and characterisation are summarised in Table 1. The polydispersity, as obtained from gel permeation chromatography (GPC), reveals polydispersity indices (PDI) between 1.3 and 1.7, which is a significant improvement over the previously reported thermoresponsive surfactants[17]. Note that the total conversion is relatively low, ranging from 85 to 58%, as determined by comparing the target degree of polymerization (DP) with the DP obtained from both GPC and ^{1}H-NMR end-group analysis. This is probably because the activity of the initiator is reduced due to limited accessibility as a result of the tethered alkyl chain. The synthetic protocol appears to work well for low molecular weights, while the synthesis of the higher molecular weight surfactants do not yield the target PDs. Despite the purity of all reagents, it appears that the chain length is limited to N~50-60 for the method applied.

Since the conversion of the monomers during the synthesis is as low as 30%, it is important to verify that the molar ratio of PEGMA to DEGMA aimed for, is indeed present in the final product. Since the LCST of these copolymers is very sensitive to the exact ratio of these two monomers[18], we can use measurements of the LCST to establish the copolymer compositions. Differential Scanning Calorimetry shows a distinct peak in heat capacity, indicative for a clear LCST phase transition. For all three surfactants the transition appears at the same temperature of 34 °C, with small margins of errors (see Figure 4.2a & Table 4.1). As the LCST has been reported to be independent of molecular weight, we can therefore establish that the PEGMA/DEGMA ratio is constant amongst the three surfactants under investigation[19].

Dynamic light scattering shows that the surfactants form micelles with a radius between 25-75 nm at room temperature. With increasing temperature, we observe a clear growth in apparent hydrodynamic radius to 200-500 nm, depending on the molecular weight of the surfactant (Figure 4.2b). We identify the LCST from the light scattering experiment by determining the temperature of the steepest gain in micelle radius. Also here we find an LCST of approximately 34°C, independent of chain length (Table 1).

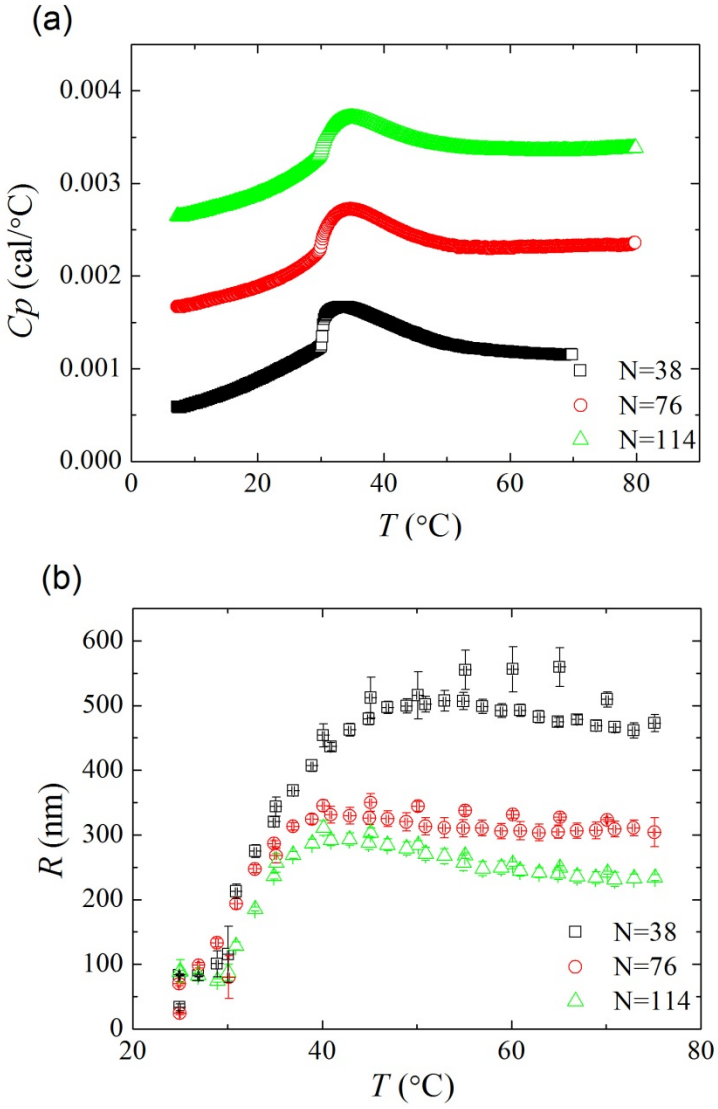

Figure 4.2 Characterization of the thermoresponsive surfactants using Differential Scanning Calorimetry (a) and Dynamic Light Scattering (b)

At the LCST, it is expected that the hydrophilic block collapses and demixes from water; consequently, we would expect that the initially stable micelles would aggregate and ultimately display macroscopic demixing from the aqueous solvent. Surprisingly, instead of macroscopic demixing, we observe that the micelles grow to a well-defined and stable size upon heating the surfactant solution above the LCST. We speculate that this might be the result of a morphological transition of the self-assembled objects. While the surfactant,

below the LCST, with its small alkyl tail and relatively large swollen hydrophilic headgroup, exhibits a conical packing parameter,[20] upon heating above the LCST, the hydrophilic head collapses and the shape of the surfactant transitions into a more cylindrical packing parameter. Such changes in the shape of the surfactant are known to induce changes in the morphology of the micelles they form. This means that the well-defined increase in size we observe here could be the result of a spherical-to-wormlike micelle transition. While further research is required to substantiate this claim, it would be a fascinating feature of these systems where micelle morphology can be tuned through a simple temperature switch.

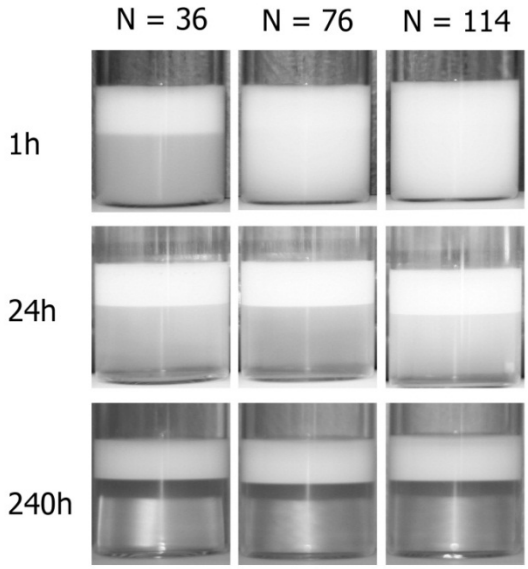

Figure 4.3 Time series of the decane-in-water emulsions, stabilized with the surfactants N=38, N=76, N=114; all images taken at room temperature.

All surfactants prepared above are able to emulsify decane in water (top row in Figure 4.3). After four months at room temperature, the emulsions of N=38, N=76 and N=114 are still stable; this highlights the excellent performance of these thermoresponsive surfactants at a temperature below the LCST.

To showcase that emulsions can be broken on demand by a thermal stimulus, we prepare an emulsion with high droplet volume fractions, of approximately 60 vol%. We then heat the emulsion to well above the LCST, while observing it on a brightfield microscope.

Initially, the emulsion consists of many small droplets, which do not coalescence at room temperature over several months. Upon heating, coalescence of smaller droplets into larger ones occurs all across the sample almost immediately. After approximately 2 minutes, only few small droplets remain and the demixing is practically complete (Figure 4.4). While we only show data for N=76 in Figure 4.4, identical results were obtained for N=38 and N=114. Movies of this process can be found in the online S1.

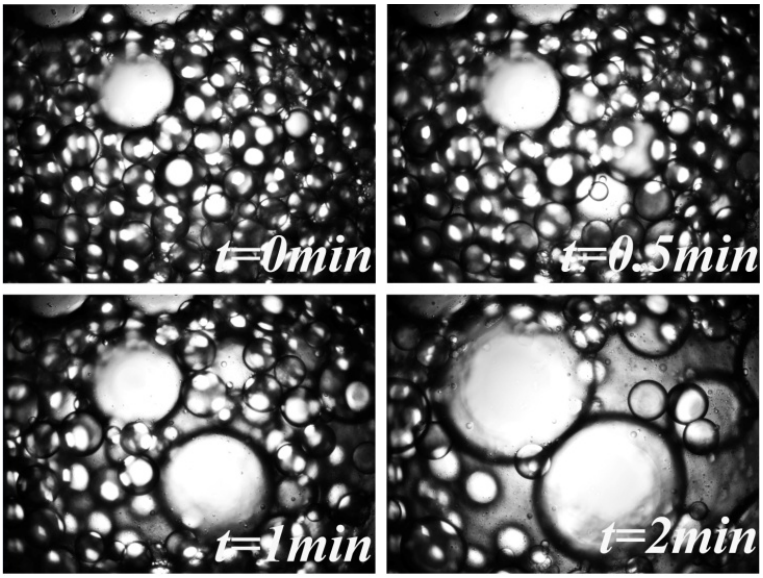

Figure 4.4 The coalescence of an emulsion with N=76 as surfactant, heated above the LCST. Pictures are made with a bright field microscope.

To understand the mechanism underlying the thermally triggered coalescences, in a previously stable emulsion, we measure the interfacial tension between an aqueous surfactant solution, at a concentration of 5 g/L, and PDMS silicone oil as a function of temperature. We clearly see a large increase of more than a factor of two in the interfacial tension when the system is brought above the LCST of the thermoresponsive surfactant (Figure 4.5a). This increase in surface tension, or reduction in the surface pressure, indicates that the total adsorbed amount of surfactant decreases. This is a first indication of the link between collapse of the thermoresponsive block and the subsequently observed emulsion breaking. By measuring the concentration dependence of the interfacial tension between oil and an aqueous surfactant solution we can determine the critical micelle concentration (CMC) of our surfactants; at room temperature, below the collapse transition, the CMC is found to be approximately 0.1 g/L(Figure 4.5b).

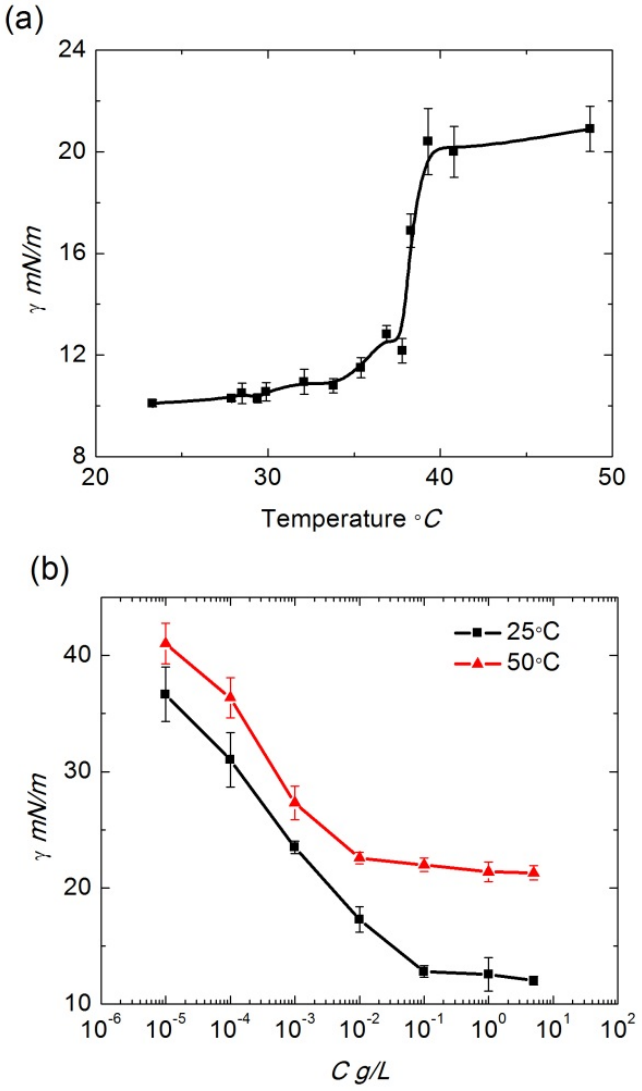

Figure 4.5 The interfacial tension as a function of temperature at 5g/L(a) and interfacial tension as function of concentration at two main regime temperatures(b).

The formation of micelles is governed by a balance between the energetically favourable grouping of hydrophobic blocks in a micellar core and the entropically unfavourable compression of the hydrophilic head groups in the micellar corona. Consequently, changes in the solvation of the head group will influence the CMC; above the LCST the solvent quality for the hydrophilic blocks decreases, which can be expected to result in a decrease of the CMC. We indeed observe that the critical micelle concentration has been reduced by

approximately one order of magnitude to 0.01 g/L above the LCST(Figure 4.5b).

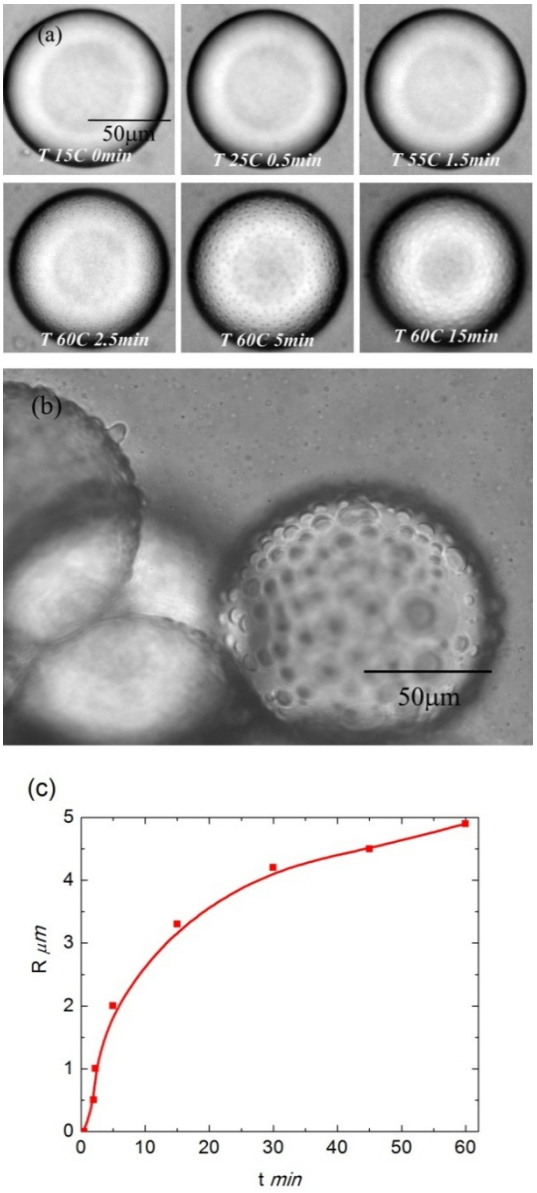

Figure 4.6 Interfacial demixing and formation of surfactant coacervate microdroplets at oil-water interfaces, microscopy images over time show the process (a) and the microdroplets can be clearly identified in a zoomed in image (b). Average radius of the microdroplets as a function of time is shown in (c).

Observation of the surface morphology of individual emulsion droplets during the collapse transitions yield additional information for the mechanism of emulsion breaking in this system. We heat a sample with a few isolated droplets from 15℃ to 60℃ at a heating rate

of 20℃/min; around the LCST distinct droplets of a third immiscble phase form at the oil-water interface. We think this is a coacervate of the collapsed surfactant (Figure 4.6a&b). These interfacially-pinned microdroplets grow in time when the sample is maintained at 60° C (Fig.6c) and appear to age logarithmically to macroscopic dimensions. This suggests a true phase separation that is pinned to the interface of the oil-water droplets. Note that this process is fully reversible; when we subsequently cool the samples the interfacial droplets disappear completely. Movies of this process can be found in the SI (movies S2 and S3). We can envision that bridging of emulsions droplets by these interfacially pinned coacervate droplets provides a mechanism for the coalescence and macroscopic emulsion breaking we observe.

4.4 Conclusions

In this paper we present the successful synthesis of well-defined thermoresponsive surfactants, which stabilize emulsions for over four months below their LCST. The emulsions can be broken on demand within minutes when heated above the LCST. This is mediated by desorption of the surfactants from parts of the surface, as evidenced by surface tension measurements, and the subsequent interfacially-pinned phase separation of the surfactant. Our results suggest that these well-defined thermoresponsive surfactants form an interesting platform to study droplet coalescence and triggered phase inversion in emulsion systems. Moreover, the ability to break a very stable emulsion on demand has industrial relevance for several applications, such as in film formation of waterborne emulsion paints and the recovery of products during emulsion-based extraction and reaction processes.

References

1. D. Li, Journal of Colloid and Interface Science, 1996, 181, 34-44.
2. M. A. Winnik, Current Opinion in Colloid & Interface Science, 1997, 2, 192-199.
3. A. F. Routh and W. B. Russel, Aiche Journal, 1998, 44, 2088-2098.
4. G. L. Brown, J Polym Sci, 1956, 22, 423-434.
5. F. Dobler and Y. Holl, Trends Polym Sci, 1996, 4, 145-151.
6. D. P. Sheetz, J Appl Polym Sci, 1965, 9, 3759-&.
7. W. A. Henson, D. A. Taber and E. B. Bradford, Ind Eng Chem, 1953, 45, 735-739.
8. S. Acevedo, X. Gutierrez and H. Rivas, Journal of Colloid and Interface Science, 2001, 242, 230-238.
9. I. Gülseren and M. Corredig, Food Hydrocolloid, 2012, 29, 193-198.
10. R. Pons, P. Taylor and T. F. Tadros, Colloid Polym Sci, 1997, 275, 769-776.
11. S. Tcholakova, N. D. Denkov, I. B. Ivanov and B. Campbell, Advances in Colloid and Interface Science, 2006, 123–126, 259-293.
12. O. D. Velev, T. D. Gurkov, S. K. Chakarova, B. I. Dimitrova, I. B. Ivanov and R. P. Borwankar, Colloid Surface A, 1994, 83, 43-55.
13. S. Khoukh, P. Perrin, F. B. de Berc and C. Tribet, Chemphyschem, 2005, 6, 2009-2012.
14. J. Ruchmann, S. Fouilloux and C. Tribet, Soft Matter, 2008, 4, 2098-2108.
15. L. Yang, N. Takisawa, T. Hayashita and K. Shirahama, J Phys Chem-Us, 1995, 99, 8799-8803.
16. T. G. Shang, K. A. Smith and T. A. Hatton, Langmuir, 2003, 19, 10764-10773.
17. T. E. Kodger and J. Sprakel, Adv. Funct. Mater., 2012.
18. J. F. Lutz, O. Akdemir and A. Hoth, J Am Chem Soc, 2006, 128, 13046-13047.
19. J. F. Lutz and A. Hoth, Macromolecules, 2006, 39, 893-896.
20. J. Israelachvili, Academic Press, 2010.

Chapter 5

Switching between two modes of coalescence in dense thermoresponsive emulsions

In this paper we describe a new approach to measure critical disjoining pressures and study coalescence dynamics in responsive emulsions using a recently developed micro-imaging-centrifugation method. We first measure the thermodynamic properties of thermoresponsive emulsions by analyzing equilibrium volumes of continous oil and water phases and densely packed emulsion under constant gravitational stress. We then show that the same microfluidic-based centrifugation method, combined with high-speed synchronised imaging, can be used to quantitatively study the dynamics of emulsion coalescence. Surprisingly, we reveal two distinct modes of coalescence in a dense emulsion, which can be triggered with a simple temperature jump and can be explained on the basis of the critical disjoining pressure.

Submitted for publication in a slightly modified form as:
H. Feng, J. Sprakel, D. Ershov, T. Krebs, K. Schroen, M. A. C. Stuart and J. van der Gucht; Switching between two modes of coalescence in dense thermoresponsive emulsions

5.1 Introduction

The formation of a homogeneous film from a previously dispersed phase, for example during the drying of emulsions or dispersions, is an essential stage in the surface application of dispersed coating systems. Especially for waterborne paints, which by definition are dispersions of liquid or solid particles in a continuous water phase, the way in which the final film forms is crucial in determining its properties. With the political and societal incentives to phase out the emission of hazardous organic compounds from both consumer and industrial coatings and adhesives, this has become an even more pressing issue. A thorough understanding of how film formation takes place at all length scales, and how it can be manipulated, is required to improve the quality of waterborne paints to the standards of their solvent-based counterparts. Nonetheless, despite the direct implications, this understanding is largely lacking, which is exacerbated by the absence of model materials and measurement techniques. Especially, probing film formation at the length scale of individual particles has proven to be cumbersome.

It is generally accepted that film formation takes place in several subsequent steps. (1) Evaporation of the continuous water phase leads to concentration of the dispersed droplets until they come into physical contact and form a jammed packing[1]. (2) Further evaporation of the continuous phase creates a capillary pressure that causes the droplets to deform and squeeze together; just like dry foams, this ultimately leads to faceted droplets separated by thin, nanometric, water films. (3) Eventually, the capillary pressure exceeds the critical pressure required to break individual water films and droplets begin to coalesce leading to phase inversion[2]. While the initial stages of film formation have been studied extensively[1, 3-6], the final and essential stage of collective coalescence remains poorly understood. While the fluid dynamics of the coalescence of two isolated droplets has been studied in detail[7, 8], the activated processes and corresponding randomness of the events that leads up to coalescence, which are especially important in dense packings of droplets, remain virtually unexplored due to the complexity of events. Recently, we reported that film formation in a drying emulsion film can occur in two distinct modes; coalescence can occur either localized to the drying front or in a random manner throughout the bulk of the film[9]. The type of coalescence that is observed was shown to depend sensitively on a balance between the critical pressure required for film rupture and the hydrostatic pressure profile that develops during evaporation. In these experiments, drying was used to develop a pressure

gradient to induce phase inversion; however, this also necessarily introduced the complication of a non-constant surfactant concentration, hence a variable critical pressure, throughout the experiment. To further advance our understanding of film formation, new methods are required in which these phenomena can be systematically studied and manipulated under well-defined conditions.

In this paper, we apply a new method of microcentrifugation[10-12] to directly study the coalescence in densely packed emulsions, under well-defined conditions. We show direct measurements of temperature-dependent critical disjoining pressures and coalescence rates. Surprisingly, we find that, our thermoresponsive emulsion allows tuning of the mode in which coalescence occurs; we show that a simple temperature trigger allows switching from coalescence occurring exclusively at the oil-emulsion front to coalescence occurring randomly throughout the entire packed layer of emulsion. These findings shed new light on the mechanisms of coalescence in dense emulsions at the length scale of the individual droplets.

5.2 Experimental Section

All reagents were purchased from Sigma-Aldrich and used as received.

5.2.1 Thermoresponsive surfactants

The synthesis of the thermally responsive surfactant and its characterization, were discussed in a previous paper[8]. In short, a polymer of di(ethylene glycol)methacrylate and poly(ethylene glycol)methacrylate is grafted to an alkyl tail through Atom Transfer Radical Polymerization[13]. The thermally responsive surfactant has a lower critical solution temperature (LCST) around 34°C in aqueous solution, as measured by light scattering and calorimetry[8].

5.2.2 Emulsions

Monodisperse emulsions of silicone oil in water, are prepared in a flow-focusing microfluidic device as Figure 5.1 shows. The dispersed phase presenting by red arrow, here silicone oil with a viscosity of 100mPa s is hydrodynamically focused at the nozzle by the

continuous phase presenting by blue arrows, here a 5 g/L solution of the thermoresponsive surfactant. This induces droplets to form at the nozzle. The size of the droplets can be tuned by varying the flow rates of both continuous and dispersed phases[14, 15]. The final diameter is chosen here to be 200μm due to the design of the chambers used in the microcentrifugation experiments; in this way we achieve a single layer of droplets in the coalescence chambers. Note that, upon loading the emulsions in the sample chambers, some coalescence occurs due to wall effects; this does not influence the further analysis of our experiments.

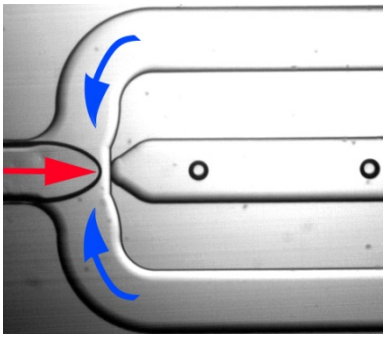

Figure 5.1 The schema of flow focusing junction.

5.2.3 Microcentrifugation

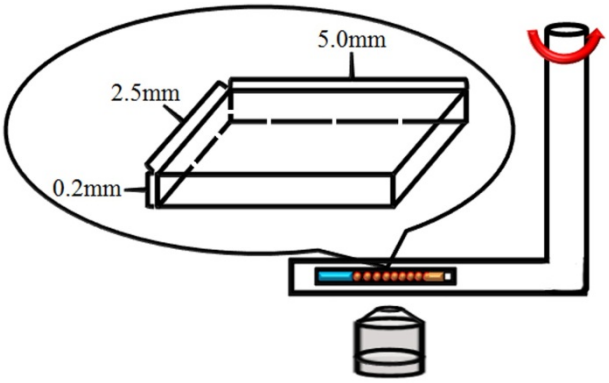

Figure 5.2 Schematic illustration of the microcentrifuge mounted on an inverted microscope.

Coalescence is induced by applying a constant gravitational force in a recently developed microcentrifugation method. In this method, a constant centrifugal force is applied to a microfluidic chamber (Micronit Microfluidics BV, the Netherlands) that holds a monolayer of emulsion droplets. Here we expand this method by incorporating temperature control

which allows us to trigger the collapse of the thermoresponsive surfactant. The set-up is schematically illustrated in Figure 5.2. A detailed description of the method is presented elsewhere[16]. We heat the sample through a stream of warm air and monitor the temperature of the measurement cell through an infrared thermometer. Images of the sample are captured using a high-speed camera, synchronized with the rotating sample chamber, mounted on a brightfield microscope. In our experiments we apply a constant centrifugal acceleration of 450g and vary the temperature between 25 and 45°C, which represent temperature both above and below the LCST of the surfactant. Experiments were conducted 5 times to ensure reproducibility of our results.

5.2.4 Image Analysis

To extract quantitative information from the images we develop an image processing routine in Matlab. First, we spatially filter all images to reduce high-frequency noise that is due to small dust particles. We then discard images in which the synchronization between the moving sample and the camera was not ideal, resulting in only partial capture of the sample cell. This is done by detecting the edges of the sample chamber, and requiring that each image used for further processing has two black edges that demarcate the glass sample walls (see SI). We then use an edge detection algorithm to locate areas of continuous intensity in our thresholded images to identify the position and size of all droplets and the continuous water and oil phases.

5.3 Results & Discussion

Emulsions of silicone oil–in-water, stabilized by our thermoresponsive surfactant[13], are prepared by microfluidics and then collected in small sample chambers designed for the microcentrifugation experiments. The droplets are prepared with diameters of approximately 200 microns, which thus form a single layer in the sample chambers with smallest dimension, orthogonal to the imaging plane, of also 200 micrometers. Initially, droplets are present throughout the sample, but upon applying a constant gravitational stress of 450g, in which g is gravitational constant, the droplets, which have a lower density then the continuous phase, move towards the emulsion-air interface moving to the right side of the images. Within a few seconds, they become jammed and deform due to the gravitational stress, as shown in the image sequence in Figure 5.2; subsequently, the

droplets begin to coalesce. This leads to an increase in the volume of the continuous oil phase and a reduction in the volume of the packed emulsion.

To extract quantitative information from the large number of images collected during an experiment, we apply an image processing routine (see Materials & Methods). An example of images after passing through this algorithm are shown in the bottom row of Figure 5.3; each droplet, as well as the oil and water bulk are recognized and colored individually.

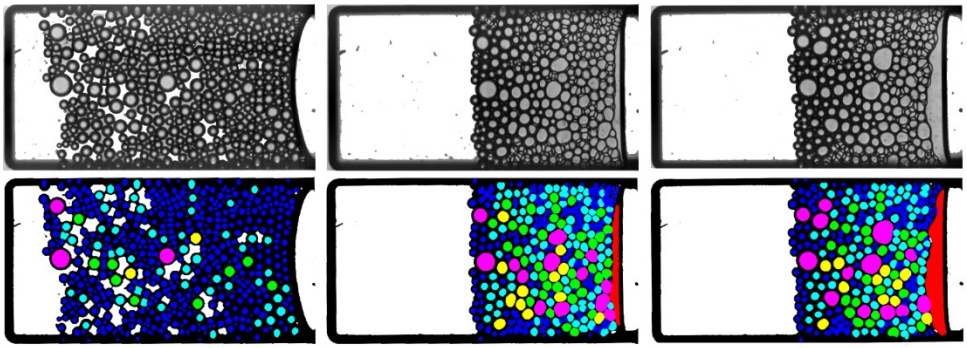

Figure 5.3: Microcentrifugation experiment on an oil-in-water emulsion, stabilized by a thermoresponsive surfactant based on poly(di-ethylene glycol methacrylate) at 450g and 25 °C. (top) Images obtained from the experiment after cropping to the region-of-interest, (bottom) images after parsing through the image analysis routine, in which individual droplets and bulk water and oil phases are recognized.

5.3.1 Critical disjoining pressure

Upon bringing two emulsion drops together, the water film that separates the droplets becomes thinner. This leads to a restoring pressure that acts to separate the droplets, which is known as the disjoining pressure. For the coalescence of two droplets, the film between them needs to rupture before the two oil drops can merge. This can only occur if the pressure applied to the droplets exceeds a critical disjoining pressure Π^*. In our microcentrifugation experiments we can directly measure Π^*. In steady-state, when the emulsion is left to equilibrate sufficiently long at fixed gravitational acceleration, a well-defined gradient in pressure builds-up in the concentrated emulsion. The pressure within this packed layer is highest at the oil-front and lowest at the water-end of the emulsion and is determined by the gravitational pressure that emulsion droplets apply on each other. Coalescence will occur at the front, until the total volume of the emulsion, that pushes on the front, is reduced to the point where the pressure exerted on the droplets at the front drops below the critical disjoining pressure.

Thus, by analyzing the volume of both the bulk oil phase and the total volume of the packed emulsion, at steady-state, and knowing the density difference $\Delta\rho$, between oil and water, the disjoining pressure can be quantitatively determined. Assuming that the densely packed emulsion layer has the same density as the oil, thus ignoring the volume occupied by the thin water films, the critical disjoining pressure measured at 450g can be expressed as $\Pi^* = 450\Delta\rho h$, where h is the height of packed emulsion which can be obtained from the images. At room temperature, below the LCST of the thermoresponsive block of our surfactant, we find a critical disjoining pressure, for droplets of approximately 200 micrometers, of around 300 Pa (Figure 5.4). As the critical disjoining pressure is a function of the droplet size, making a direct comparison with values reported for other surfactants in literature difficult, this disjoining pressure is approximately two orders of magnitude lower than that for the common, and highly effective, surfactant sodium dodecyl sulfate[9, 17]. Nevertheless, this is sufficient to stabilize these emulsions against coalescence for several months under ambient conditions[18].

When we increase the temperature, to above the LCST of the surfactant, we see a gradual but significant decrease of the critical disjoining pressure; at 45 °C, it has decreased by a factor of 6 to only $\Pi^* \approx 50$ Pa (Figure 5.4). Note that the decrease in disjoining pressure is not abrupt at the LCST: Π^* gradually decreases when increasing the temperature above the LCST; a similar effect was seen for the adhesive forces between two surfaces coated with thermoresponsive surfactants[19].

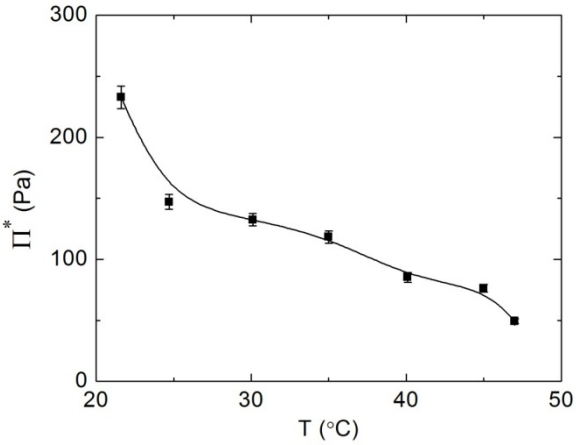

Figure 5.4 Critical disjoining pressure Π^* for 200 micron oil-in-water droplets, stabilized by a thermoresponsive surfactant as a function of temperature, error bars indicate the average of 5 parallel experiments

The significant decrease in critical disjoining pressure with increasing temperature above the LCST also sheds new light on our previous observation that an emulsion, stabilized by these surfactants, could be triggered from stable to unstable with increasing the temperature[18]; when an emulsion is prepared at osmotic pressures between the critical disjoining pressure at room temperature and that above the LCST, it will be stable at room temperature. Once the temperature is raised, the osmotic pressure will remain the same yet exceed the decreased critical disjoining pressure, leading to rapid destabilization.

5.3.2 Coalescence dynamics

The ratio of the actual osmotic pressure in the emulsion and the critical disjoining pressure determines whether coalescence can occur; however, this consideration is based on thermodynamic arguments and thus only gives insight into equilibrium properties of the system. Once the critical disjoining pressure is (locally) exceeded, coalescence can occur. The kinetics of this process are governed by a complex interplay of the time scale for film rupture, typically assumed to be an activated process, film drainage, governed by hydrodynamic factors such as the film thickness and viscosity of the continuous phase, and in some cases, when the dispersed phase itself is highly viscous, the viscous flows associated with droplet merging.

In our experimental approach, the kinetics of coalescence can be ideally studied; we record images at a frame rate of 5000 fps to capture still frames of the fast spinning sample cell. As the coalescence we observe occurs over relatively long time scales, we choose to analyse only 5 images/s; more images are available and can be used for systems in which these processes occur much faster. Our image analysis gives access to the area of the bulk oil phase at the front of the sample, indicated in red, at the right hand side of the images in Figure 5.3. As we know the height of the lithographically produced sample chamber precisely, we can track the change in volume of the bulk oil phase V_{oil}, as shown in Figure 5.5. Also here we can clearly see the effect of our switchable surfactant. While coalescence occurs relatively slowly, with a rate $^{dV_{oil}}/_{dt} = 0.0008 mm^3/s$ at 25°C, below the LCST of the surfactant, increasing the temperature to around the LCST, 35°C, or above the LCST, at 45°C, greatly enhances the coalescence rate. These results are summarized in the inset in Figure 5.5, which show the coalescence rates as a function of temperature.

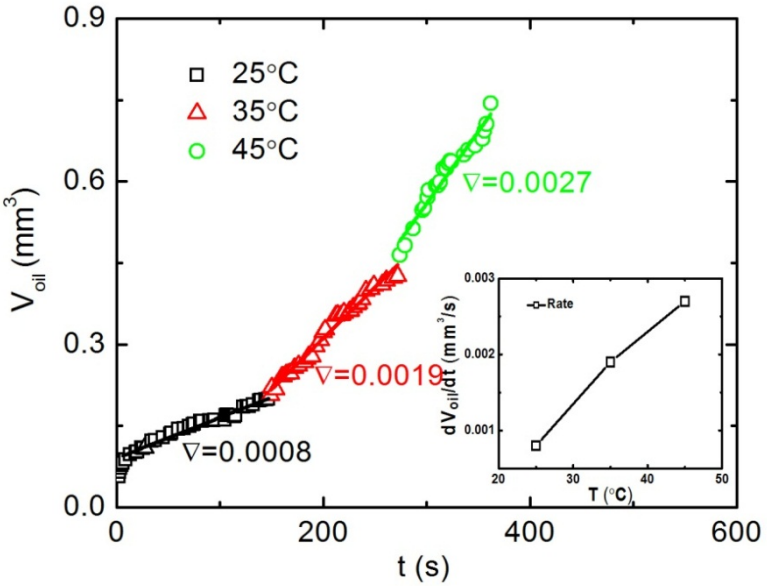

Figure 5.5 Coalescence kinetics measured by tracking the volume of the bulk oil phase V_{oil} as a function of time, drawn lines are linear regressions through the data to extract the coalescence rates, $^{dV_{oil}}/_{dt}$, which are given in the inset.

As mentioned above, multiple factors influence the coalescence kinetics; one important contribution is the time required for the breaking of the thin film between two droplets. We can assume that film breaking is an activated process, as it occurs through an intermediate stage in which the total surface of the drops connected through a small liquid bridge[20] is larger than that of the two individual drops; this intermediate state thus possesses a higher free energy, which provides an activation barrier against coalescence. The rate of transitions over this barrier, required for droplet coalescence, will depend on the absolute height of this energy barrier, but also on the difference $\Delta\Pi = \Pi - \Pi^*$ between actual pressure Π and critical disjoining pressure Π^*. If the difference is negative, the film is stable and coalescence will not occur; if the difference is positive, but small, transitions over the energy barrier will occur but infrequently, leading to low coalescence rates, and when the difference becomes larger, individual coalescence events become more frequent, thus increasing the macroscopic coalescence rate.

As an increase in temperature decreases the critical disjoining pressure for our thermoresponsive surfactants, but the gravitational acceleration remains constant, increases

in temperature in effect increase ΔΠ, and thus increase the coalescence rate. Interestingly, this enhanced rate of coalescence and emulsion breaking is thus a direct macroscopic manifestation of the microscopic collapse of the surfactants when the sample is heated above their LCST.

5.3.3 Modes of coalescence

While the analysis above, where we only consider the increase in volume of the bulk oil phase, gives direct access to the coalescence rates, it does not describe how the coalescence process occurs spatially. Recently, we showed that the coalescence in concentrated emulsions can occur in two distinct modes[9]. When the critical disjoining pressure is relatively low, coalescence occurs throughout the bulk of the sample in which several nuclei of coalesced drops form, which subsequently rapidly grow until the entire sample has been destabilized. By contrast, when the critical disjoining pressure of the system is high, the pressure is only high enough to induce coalescence at the front end of the sample; in this scenario, coalescence only occurs at the front where the emulsion meets the bulk oil phase. These observations suggest that the thermoresponsive emulsions we use here, in which we can gradually tune the disjoining pressure through small changes in temperature, could be suitable to induce a change from front to bulk coalescence on demand.

At temperatures below the LCST of the surfactant, we indeed observe that coalescence only occurs at the front end of the sample, as shown in Figure 5.3. This is further corroborated by the fact that the droplet size in the packed emulsion remains constant; as drops only coalesce with the bulk oil phase, no coarsening is observed (Table 5.1). Full droplet size distributions are available in the supporting information.

Interestingly, when we increase the temperature, thus decrease the disjoining pressure, the coalescence process proceeds completely differently. Across the packed emulsion, droplets begin to coalesce, leading to rapid disproportionation of the emulsions, as can be clearly seen in Figure 5.6. Correspondingly, the mean droplet radius increases as shown in Table I. This highlights that the mode of coalescence, either occurring throughout the bulk of the sample, or being restricted to the front, is indeed determined by the disjoining pressure. Moreover, the introduction of thermoresponsivity to the emulsions allows us to trigger these two distinctly different modes on demand.

Table 5.1 Mean droplets radius, extracted from the image analysis, as a function of time and temperature

26°C	Time (s)	2	10	40	100	150
	<R> (μm)	181	180	182	182	183
46°C	Time (s)	2	10	40	100	150
	<R> (μm)	183	188	209	217	224

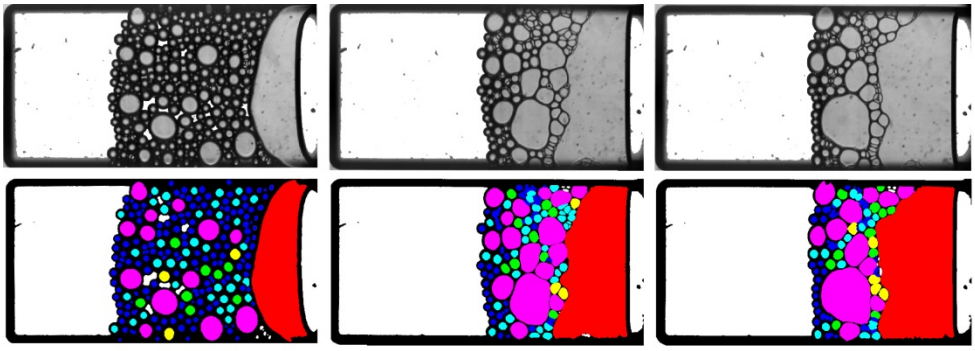

Figure 5.6: Microcentrifugation experiment on an oil-in-water emulsion, stabilized by a thermoresponsive surfactant based on poly(di-ethylene glycol methacrylate) at 450g and 45 °C, showing bulk coalescence. (top) Images obtained from the experiment after cropping to the region-of-interest, (bottom) images after parsing through the image analysis routine, in which individual droplets and bulk water and oil phases are recognized.

5.4 Conclusion

Despite a wealth of research on the coalescence kinetics of two individual droplets dispersed in a continuous phase, the phase inversion and film formation in dense emulsions remains ill understood; this is partially due to the complex nature of the problem in which equilibrium thermodynamics (critical disjoining pressures), activated processes (film rupture) and fluid dynamics (film drainage, fluid transport through the packed emulsion) interplay. Moreover, suitable methods to study coalescence in dense emulsions remain scarce; especially when control over the applied forces, thermodynamic properties and onset of coalescence are required.

Here we reported on a new approach to study coalescence in dense thermoresponsive emulsions using a microfluidic-based microcentrifugation method. We have shown that both thermodynamic and kinetic properties can be measured through automated image analysis, and that the temperature-responsivity of the surfactants can be used to trigger different modes of coalescence on demand. These developments form a stepping stone for further investigations into the governing mechanisms that dominate phase inversion and film formation.

Reference

1. A. F. Routh and W. B. Russel, AIChE J. FIELD Full Journal Title:AIChE Journal, 1998, 44, 2088-2098.
2. G. A. van Aken, Langmuir, 2002, 18, 2549-2556.
3. G. A. van Aken and F. D. Zoet, Langmuir, 2000, 16, 7131-7138.
4. S. S. Hu, J. Rieger, Y. Q. Lai, S. V. Roth, R. Gehrke and Y. F. Men, Macromolecules, 2008, 41, 5073-5076.
5. A. M. Koenig, T. G. Weerakkody, J. L. Keddie and D. Johannsmann, Langmuir, 2008, 24, 7580-7589.
6. S. S. Hu, J. Rieger, S. V. Roth, R. Gehrke, R. J. Leyrer and Y. F. Men, Langmuir, 2009, 25, 4230-4234.
7. J. D. Paulsen, J. C. Burton and S. R. Nagel, Physical Review Letters, 2011, 106, 114501.
8. J. D. Paulsen, J. C. Burton, S. R. Nagel, S. Appathurai, M. T. Harris and O. A. Basaran, Proc. Natl. Acad. Sci. U. S. A., 2012, 109, 6857-6861.
9. H. Feng, J. Sprakel, D. Ershov, T. Krebs, M. A. C. Stuart and J. van der Gucht, Soft Matter, 2013, 9, 2810-2815.
10. T. Krebs, D. Ershov, C. G. P. H. Schroen and R. M. Boom, Soft Matter, 2013, 9, 4026-4035.
11. T. Krebs, C. G. P. H. Schroen and R. M. Boom, Chem. Eng. Sci., 2012, 71, 118-125.
12. T. Krebs, K. Schroen and R. Boom, Lab on a Chip, 2012, 12, 1060-1070.
13. H. H. Feng, N. A. L. Verstappen, A. J. C. Kuehne and J. Sprakel, Polymer Chemistry, 2013, 4, 1842-1847.
14. W. L. Ong, J. S. Hua, B. L. Zhang, T. Y. Teo, J. L. Zhuo, N. T. Nguyen, N. Ranganathan and L. Yobas, Sens. Actuator A-Phys., 2007, 138, 203-212.
15. T. T. Fu, Y. N. Wu, Y. G. Ma and H. Z. Li, Chem. Eng. Sci., 2012, 84, 207-217.
16. T. Krebs, C. Schroen and R. M. Boom, Chemical Engineering Science, 2012, 71, 118-125.
17. J. Bibette, D. C. Morse, T. A. Witten and D. A. Weitz, Physical Review Letters, 1992, 69, 2439-2442.
18. H. Feng, N. A. L. Verstappen, A. J. C. Kuehne and J. Sprakel, Polymer Chemistry, 2013, 4, 1842-1847.
19. T. E. Kodger and J. Sprakel, Advanced Functional Materials, 2013, 23, 475-482.
20. J. Lyklema, 2005, vol. V.

Appendix

Image analysis

We spatially filter all images to reduce high frequency noise, which mainly originates from small dust particles on the outside of the sample cell. We then define an area at near the end of the sample cell, indicated by the green area in Figure S1a, to use for image selection. We then select images based on the unique pattern of intensity values when crossing the two, black, walls of the cell. This is done to remove images in which only a part of the sample cell is imaged, due to minor mis-synchronisations between camera and centrifuge. The selected images are cropped to display only the sample cell; a reconstructed movie of the coalescence dynamics from these selected images can be found in the online supplementary information (movies S3 & S5, sped up 10x). We then apply the Matlab command “PixelList” to recognise all continuous areas of intensity in the images. This gives access to the area of each of these continuous spaces, as illustrated in Figure A5.1; reconstructions of the recorded movies after this image processing step can also be found in the supplementary information, as movies S4&S6 (sped up 10x). The continous oil phase, used to track the amount of coalescence that has occured, shown as the big red area in Figure A5.1b, can then be automatically followed in time. In the same way, the sizes of individual droplets can be automatically followed.

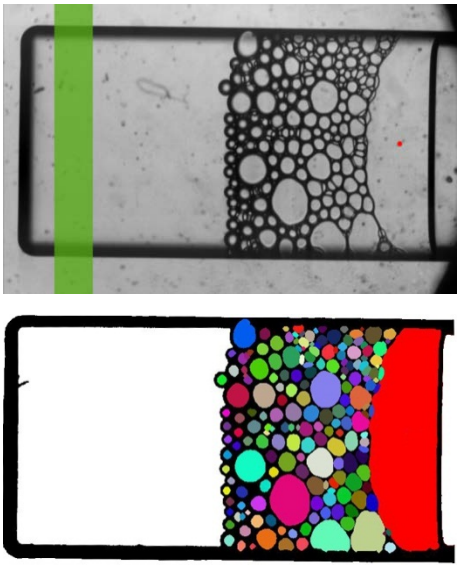

Figure A5.1 Images analyze scheme.(a) is about algorithm (b) is result.

From this data we can easily extract the evolution of the droplet size distributions in time; as shown in Figure A5.2. For front coalescence, the distributions do not change significantly (Figure A5.2a) , as droplets only coalesce with the large oil reservoir, which doesnt lead to disproportionation of the remaining droplets. By contrast, for bulk coalescence, the distributions of droplet sizes shifts to larger average sizes (Figure.A5.2b); as coalescence occurs everywhere also disproprotionation occurs.

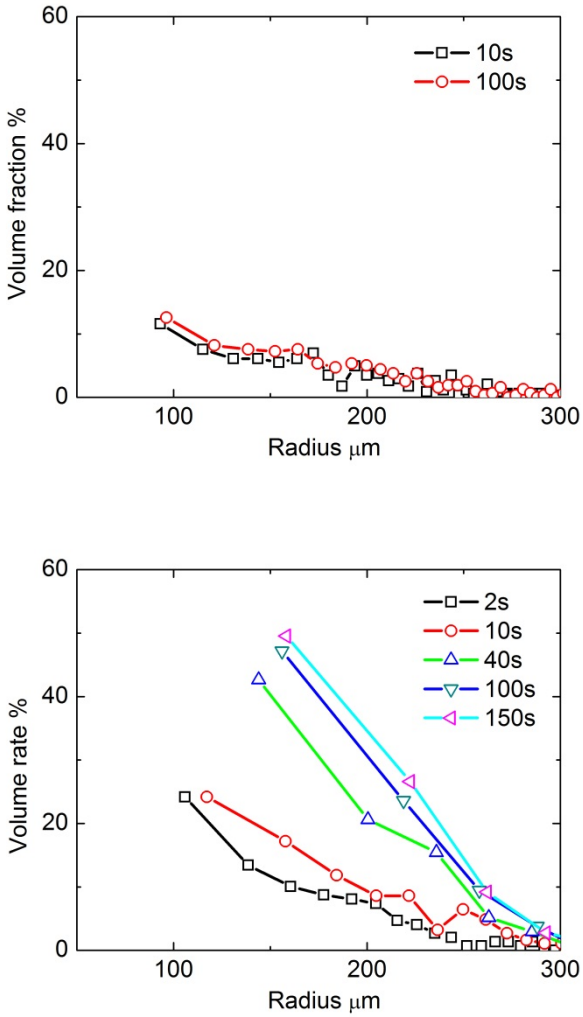

Figure A5.2 The droplets distribution VS time at different coalescence modes. (a) is in front coalescence (b) is in bulk coalescence

Chapter 6

Summary and general discussion

In this final Chapter, we present a summary of this dissertation highlighting the main results. As scientific progress can only be partly measured by the answers we find, we also discuss new and open questions resulting from our studies and give an outlook on future topics of study.

Coatings and paints play a significant role in daily life; they prolong the lifetime of materials by offering protection against, for example, corrosion, weathering or fouling, and literally add color to our lives. Due to their widespread use, their environmental consequences have become focus of increasingly strict regulations and public awareness. There has been a strong effort to replace traditional solvent-based coatings with waterborne coatings to reduce or eliminate the volatile organic compounds (VOC) that traditionally formed the main component of paints. A pronounced shift from solvent-based to water-based systems has already taken place for decorative (consumer) coatings. However, for more demanding applications in industry, the replacement of solvent-based paints with greener waterborne formulations still has a long way to go, due to their lower performance in terms of both mechanical, durability and aesthetic aspects. The development of waterborne coatings with the same or better performance than solvent-borne systems is thus an important step towards the further vanishing of VOC-rich coatings. Ultimately, the final aim is to replace all solvent-borne coatings with VOC-free paint formulations.

Waterborne paints form a very promising candidate, yet several key aspects of their properties during storage, handling and during their lifetime as a coating, remain poorly understood. Waterborne coatings are complex multiphase systems, containing a wide variety of dissolved and dispersed components in the common aqueous continuous phase. During the drying of the paint, after application, this complex mixture must undergo a phase inversion to achieve a homogeneous film of the resin from its initial dispersed state. While this state governs the structure, and thus final properties of the coating film, its complexity precludes a deep understanding to date. This is due to the complexity of the drying and phase inversion process, which is governed by a seemingly immense number of chemical and physical parameters.

We therefore adopted a simplification approach, minimizing the number of parameters to obtain a first-pass insight into the phase inversion process. We started by directly visualizing how coalescence occurs in a drying 2D emulsion film, both on the single-particle scale, with confocal microscopy, and by macroscopic imaging. Based on these observations, we built a hydrodynamic model that explains some of the key governing parameters in the film formation process. Furthermore, we explored the possibilities to manipulate phase inversion and coalescence, by developing new thermoresponsive surfactants. These new strategies allow us to obtain new insights into this complex problem.

Understanding coalescence in dense emulsions

The first part of this thesis focusses on understanding how coalescence and phase inversion occurs in a drying emulsion film, through direct quantitative imaging. Our observations at different length scales are unified in a hydrodynamic model to arrive at a microscopic understanding of this complex macroscopic phenomenon.

In **Chapter 2** we observed two distinct modes of phase inversion in surfactant-stabilized o/w emulsions exposed to a unidirectional drying stress. Coalescence occurs either through a nucleation-and-growth mechanism, where coalesced pockets form and grow randomly throughout the sample, or through a coalescence front that propagates into the sample from the drying end. The way in which coalescence occurs is determined by a balance between the established pressure profile across the film and the local critical disjoining pressure in the emulsion. For very stable emulsions, narrow plateau borders can develop, leading to steep pressure gradients; the actual pressure only exceeds the critical pressure in a narrow zone around the drying front and front coalescence results. The opposite occurs for unstable emulsions; only shallow pressure profiles develop before coalescence commences throughout the bulk of the sample. Moreover, we find that surfactant concentration plays a significant role through its effect on the critical disjoining pressure at which coalescence occurs. This, to our knowledge, is the first observation and explanation of different modes of coalescence dynamics in dense emulsion films.

Although our observations can be explained by the measured pressure gradients, several new questions have arisen. The most significant one is the surfactant accumulation; it is obvious that the surfactant, which gets transported with the continuous phase, will accumulate at the drying front due to the unidirectional drying in our system. We can thus expect not only a pressure gradient but also a surfactant gradient in the drying films; in **Chapter 2** we purposefully assumed this effect to be negligible, due to a lack of experimental techniques to determine the hypothetical surfactant concentration gradient. However, from our measurements of the critical disjoining pressure, we know that this governing parameter is sensitive to the local surfactant concentration; moreover, a difference in surfactant concentration also leads to changes in local osmotic pressure. Hence, we could imagine that in fact surfactant accumulation could be important. To evaluate this, we need a method to measure surfactant concentrations locally; this could be achieved through a fluorescently-labelled surfactant, and quantitative intensity mapping

using fluorescence microscopy. Moreover, the coalescence events between interfaces may still be clearly visible if the fluorescent surfactant exhibits solvochromic emission, as the Nile Red dye, used in Chapter 2, does. This approach could give access to the relationship between the local rate of coalescence and the local surfactant concentration; from the image analysis, as shown in Figure 6.1, local coalescence rates can already be measured in our experimental set-up.

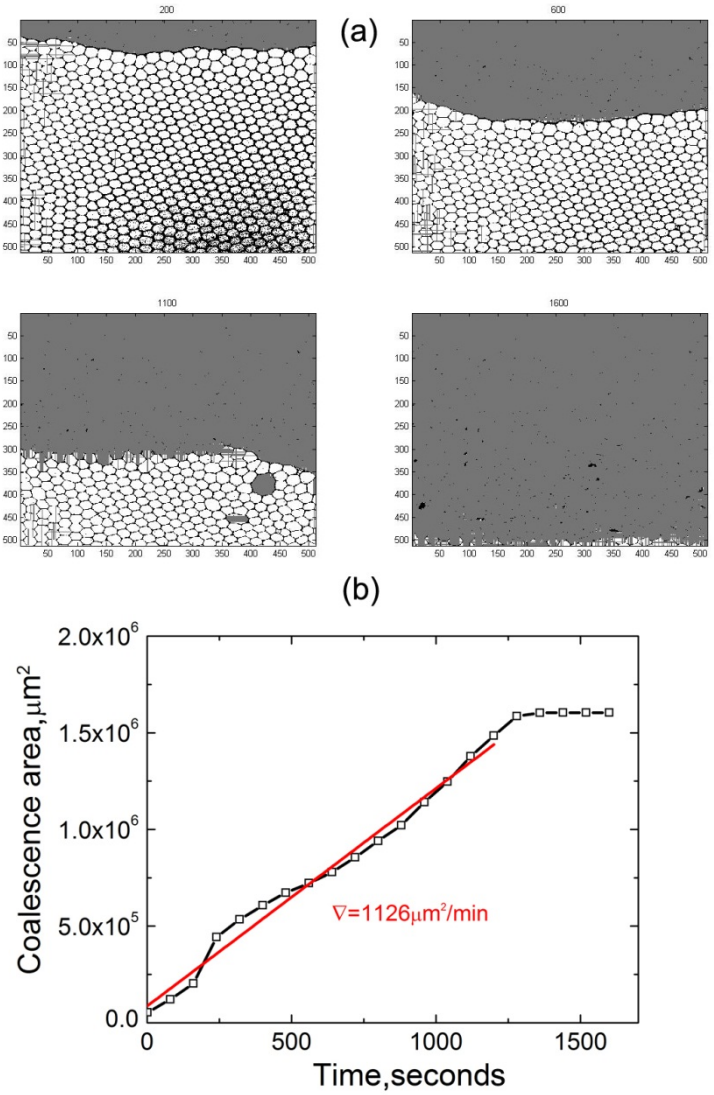

Figure 6.1 (a) Quantitative analysis of the raw confocal microscopy images showing a front-coalescence process. and (b) The local coalescence rate ∇ of the coalescence dynamics from a local field-of-interest.

Another crucial unanswered question is how the collective coalescence we study relates to the time of rupture of an individual film at a given disjoining pressure. This information could be obtained by studying the coalescence of a single, large droplet formed on a pressure-controlled droplet tensiometer (Sinterface PAT-1) with a macroscopically flat interface, as illustrated in Figure 6.2. This could provide crucial information on the relationship between the ratio of actual pressure and critical pressure, droplet size and film rupture frequency.

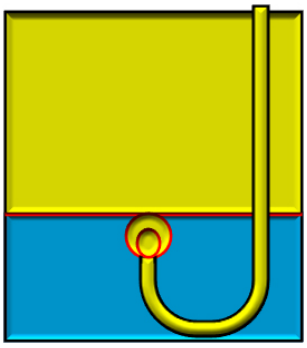

Figure 6.2 Schematic illustration of a set-up for studying single-film rupture.
Yellow presents oil and blue presents water.

In **Chapter 3** we develop a hydrodynamic model to explain the dynamics of film formation, and present detailed calculations. In this model we focus on the critical water volume fraction (ε_{cr}) which inversely proportional to critical disjoining pressure. We vary ε_{cr} over several decades to determine how the pressure gradients develop in time. We observe two trends; for relatively unstable emulsions, only shallow pressure gradients develop, while very stable emulsions result in very steep pressure profiles. From the slope of these pressure profiles we estimate the boundaries for the observed front and bulk coalescence modes. The predictions from this model agree well with our experimental observations, indicating that the critical disjoining pressure, a parameter largely overlooked until now, is the key factor in setting the coalescence dynamics. The model also showed the importance of the rate of water evaporation; slower evaporation, giving the system more time to equalize the pressure gradients, thus lead to more shallow profiles which trigger bulk coalescence. We can even imagine that the local pressure will be the constant throughout the film, leading to spontaneous coalescence everywhere in the film, if the rate of water evaporation approaches zero. Another, unexplored aspect relating to water evaporation is how the evaporation rate changes in time due to the oil layer that accumulates at the drying

end. As water needs to transport through this water layer to evaporate it becomes increasingly hindered when this layer grows. We can imagine that the emulsion film enters a sintered state due to this hindered evaporation, as predicted by other models, such as that of Routh and Russel[1]. This process could be experimentally manipulated through the use of oil with different water solubility, to investigate how relevant this is in reality.

Manipulating coalescence in dense emulsions

In **Chapter 4** we show the successful synthesis of well-defined thermoresponsive surfactants through Atom Transfer Radical Polymerisation (ATRP) using a alkyl-functional initiator. These surfactants can be used to stabilise emulsions for over four months at room temperature, below the collapse transition of the hydrophilic block of the surfactant, yet can be triggered to break the emulsion within minutes when the sample is heated to above 40 °C. This on-demand coalescence is mediated by desorption of the surfactants from parts of the surface, as evidenced by surface tension measurements and direct microscopic observations of the droplets surface. Our results suggest that these well-defined thermoresponsive surfactants form an interesting platform to study droplet coalescence and triggered phase inversion in emulsion systems. Moreover, the ability to break a very stable emulsion on demand has industrial relevance for several applications, such as in film formation of waterborne emulsion paints and the recovery of products during emulsion-based extraction and reaction processes.

An interesting observation during our study of the thermoresponsive surfactants is the surface-pinned phase separation of the surfactant from the aqueous solution upon heating the sample. During a fast quench, distinct droplets, of rather well-defined size, appear at the droplet surface; in time these droplets grow, as discussed in Chapter 4 and illustrated in Figure 6.3. This is reminiscent of a spinodal decomposition process, but confined to a 2-dimensional interface. When we make a slow quench, by adjusting the heating rate, no spinodal structures are observed but a homogeneous surface layer forms, which could be a sign of a slow nucleation and growth process (Figure 6.4). This system might thus be an interesting approach to study 2-dimensional demixing transitions, with temperature as a convenient quench parameter.

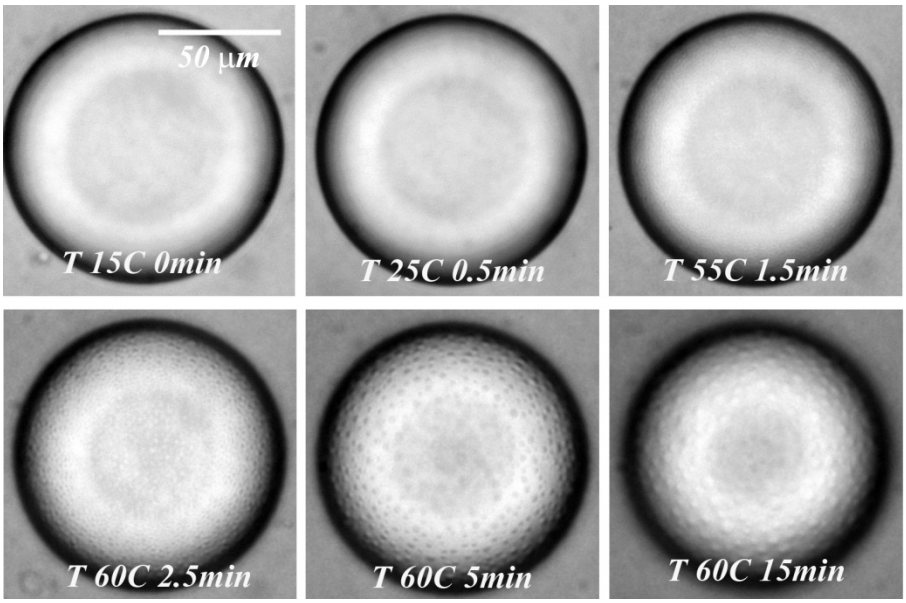

Figure 6.3 2D demixing of thermoresponsive surfactants during a fast quench (+20°C/min).

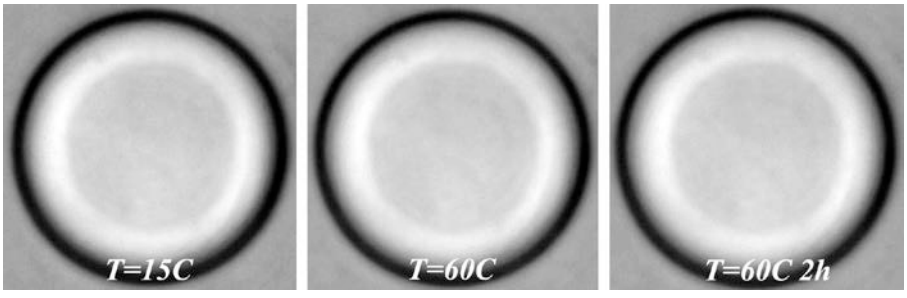

Figure 6.4 No signs of microscopic droplets during a slow quench of the same system (+1°C/min).

In our coalescence studies with thermal responsive surfactants, we noticed the important role of applied pressure on the coalescence kinetics. As illustrated in Figure 6.5, coalescence only occurs partially when heating a diluted sample concentrated by gravity alone. However, upon applying an external force (grey arrow) to densify the creamed emulsion layer, the demixing reaches completion.

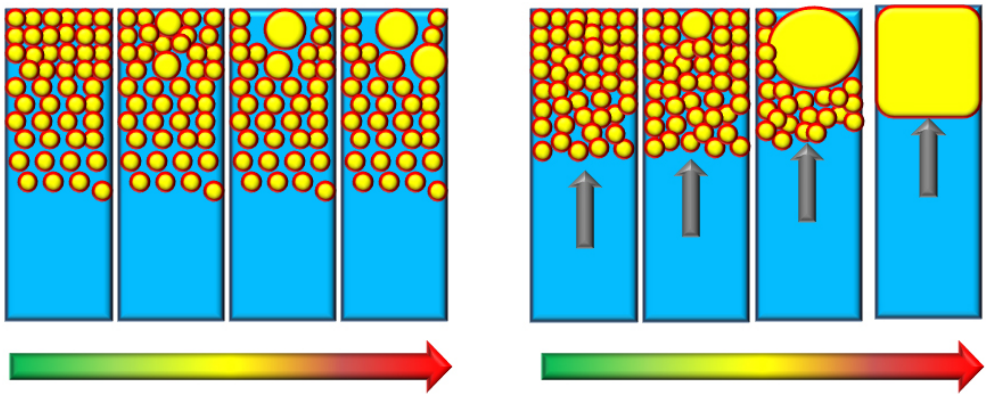

Figure 6.5 Schematic illustration of application of an external force to finalize coalescence. The grey arrow indicates the external force, lower arrow indicates an increasing temperature.

In **Chapter 5** we reported on a new approach to study coalescence in dense thermoresponsive emulsions using a microfluidic-based microcentrifugation method in which a constant external field can be applied. We have shown that both thermodynamic and kinetic properties can be measured through automated image analysis, and that the temperature-responsivity of the surfactants can be used to trigger different modes of coalescence on demand. These results form further proof that our conclusions in Chapters 3&4 regarding the nature of the transition from front to bulk coalescence are valid; also here we observe that changing the critical disjoining pressure, through changing the temperature, can induce a spontaneous switch in coalescence mode. This new approach forms a stepping stone for further investigations into the governing mechanisms that dominate phase inversion and film formation.

As mentioned above, the coalescence of individual films and the nature of the activated process that govern its kinetics, remain relatively unexplored, yet it may have significant influence on the whole film formation process. Using our thermoresponsive surfactant, preliminary data, shown in Figure 6.6, show that we can achieve local film rupture by heating a single film between emulsion droplets with a focussed high-intensity IR laser. This could offer precise control over the location and moment of the first coalescence event in a dense film); and in turn could drastically simplify these types of studies.

Future study could also focus on manipulating the distances and arrangements of individual or groups of droplets, for which optical tweezers are an ideal method.

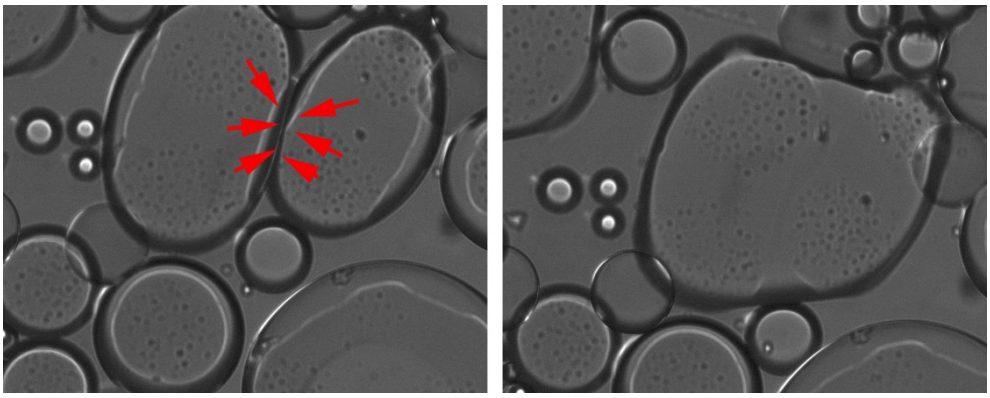

Figure 6.6 Individual film rupture under local heating; (left) before local heating, arrows indicate forcus position of the laser, (right) upon irradiation with focussed IR light, only the targeted film ruptures and the droplets coalesce.

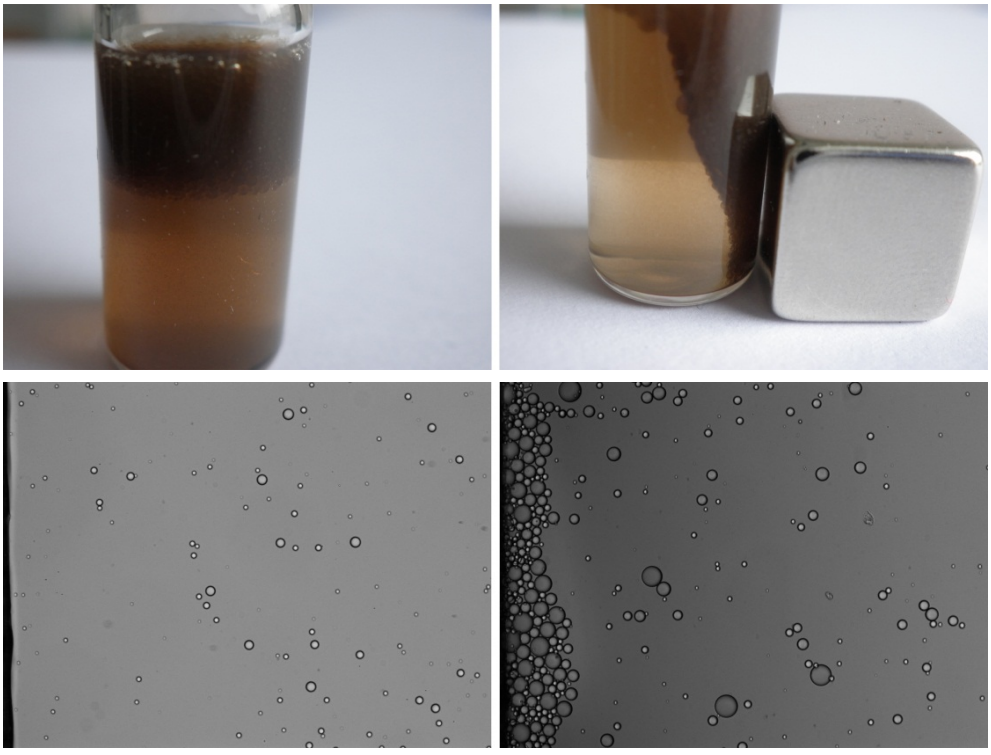

Figure 6.7 The magnetic tests of magnetic emulsion on macro and micro scales.

The constant external force applied by centrifugation in Chapter 5, could also be replaced by a magnetic driving force; the inclusion of magnetic nanoparticles in the oil can be used to apply forces to individual droplets. In this way, emulsions can be concentrated, with a well-defined pressure (as illustrated in Figure 6.7). The magnetic field can be calibrated

from the velocity of the droplets in dilute suspensions, which can be used to apply constant pressures quantitatively. This would avoid the cumbersome synchronisation between camera and spinning microfluidic device in the microcentrifugation experiments presented in Chapter 5.

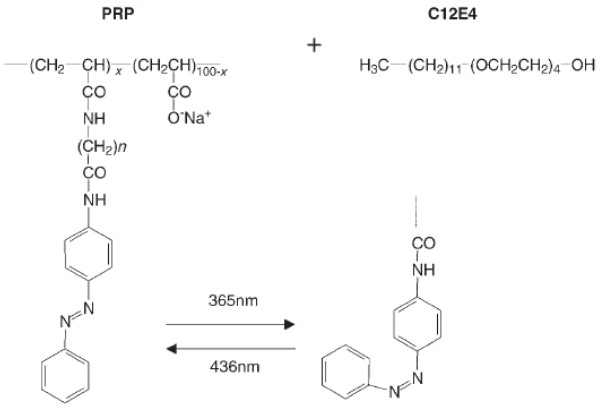

Figure 6.8 Molecular structure of light-responsive azobenzene-modified poly(sodium acrylate) and a non-ionic surfactant [2].

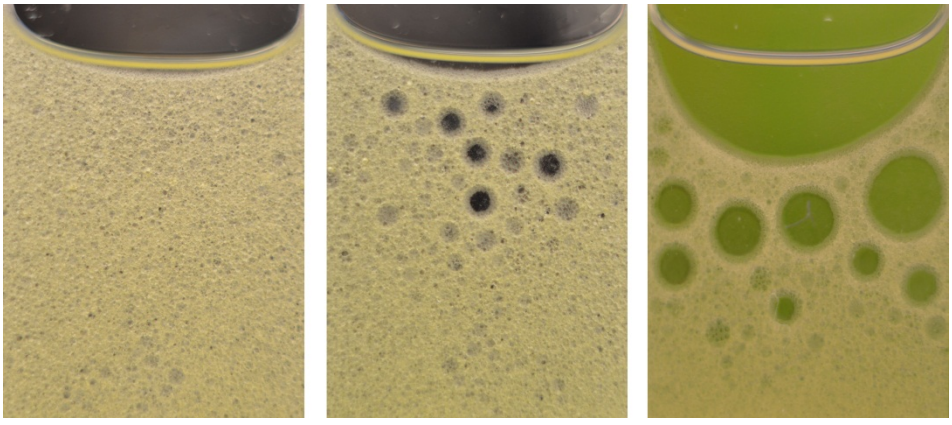

Figure 6.9 Light-triggered coalescence of a dense emulsion stabilised by a light-responsive polymer-surfactant complex.

We have also started to explore other means to trigger the coalescence of responsive emulsions. We focussed on a light responsive surfactant system, as it is, in practice, more easy to flood a painted wall with light than heating up the entire room. Secondly, earlier work on these light-responsive systems showed full reversibility. Moreover, there is no transfer gradient problem as in our thermoresponsive system. We used a azobenzene-modified polymer, as illustrated in Figure 6.8, which undergoes a light-induced cis-trans

isomery[3]. Combined with a non-ionic surfactant, the interfacial configuration can be altered significantly upon exposure to light. Figure 6.9 shows initial results how coalescence can be triggered upon illumination with UV light.

Using the knowledge and methods developed in this thesis, new avenues for studying film formation have been opened. While our work focussed on highly idealised emulsions, real coating systems exhibit some complicating factors, such as viscoelasticity of the latex droplets, and even chemical reactions between different species of droplets, interactions with several surface active species and solid pigment particles. Moreover, the length scales in real paints are a few orders of magnitude smaller, requiring the development of new methodologies suitable for these length scales. These topics will be subject for future study, and are required to fully understand and control the properties of water-based coatings.

Reference

1. A. F. Routh and W. B. Russel, Langmuir, 1999, 15, 7762-7773.
2. S. Khoukh, P. Perrin, F. B. de Berc and C. Tribet, Chemphyschem, 2005, 6, 2009-2012.
3. T. G. Shang, K. A. Smith and T. A. Hatton, Langmuir, 2003, 19, 10764-10773.

Samenvatting

In dit laatste hoofdstuk presenteren we een samenvatting van dit proefschrift; hierin belichten we de belangrijkste resultaten uit de verschillende hoofdstukken en de verbanden daartussen.

Coatings en verven spelen een belangrijke rol in ons dagelijks leven; ze vergroten de levensduur van materialen door bescherming te bieden tegen, bijvoorbeeld, corrosie, beschadiging door weersinvloeden, afzetting van vuil en ze brengen tevens letterlijk kleur in onze leefomgeving. In recente jaren hebben de effecten van deze verven en lakken op ons milieu en de gezondheid van de gebruikers, zowel professioneel als gewone consumenten zoals u en ik, veel in de aandacht gestaan en zijn onderhevig geworden aan steeds strengere landelijke en internationale regelgeving. In dit kader is er een sterke beweging ontstaan om de klassieke oplosmiddel-gebaseerde verven te vervangen door milieu- en gezondheidsvriendelijkere water-gebaseerde alternatieven; met als ultiem doel het volledig uitbannen van vluchtige organische verbindingen, ook wel VOCs genoemd (naar het engels: Volatile Organic Compounds) , uit verven. Een omslag van klassieke verven, die grotendeels uit deze vluchtige organische verbindingen bestaan, naar VOC-arme watergedragen verven heeft al grotendeels plaatsgevonden voor decoratieve verven voor de consumenten markt. Echter, voor meer veeleisende toepassingen in de industrie, is de weg naar het vervangen van VOCs door water er een vol met uitdagingen en obstakels. Dit komt met name doordat de meeste op water gebaseerde verven nog lang niet dezelfde kwaliteit en stabiliteit kunnen bieden als hun VOC-gebaseerde tegenhangers. Het verder verbeteren, en ontwikkelen van nieuwe, watergedragen verven speelt dus een cruciale rol bij het uitbannen van vluchtige organische verbindingen uit verfsystemen.

Hoewel watergedragen verven een veelbelovende kandidaat zijn ter vervanging van traditionele VOC-rijke verven, worden enkele cruciale eigenschappen, zowel tijdens opslag en applicatie, als tijdens hun leven als coating, nog maar slecht begrepen. Deze watergedragen verven zijn complexe systemen waarin een veelvoud aan moleculen en microscopisch kleine deeltjes zijn opgelost en gesuspendeerd in de waterfase. Na het aanbrengen, en tijdens het drogen, van de verf moet dit complexe mengsel een zogenaamde

fase-inversie ondergaan; microscopisch kleine polymeerdeeltjes die in de waterfase zijn gesuspendeerd moeten uiteindelijke zelf de matrix van de coating vormen. Het systeem moet dus inverteren van een suspensie van polymeerdeeltjes in water naar een polymeerlaag, het liefst zonder overgebleven waterdruppels. Het is deze eindtoestand die de uiteindelijke coating vormt en daarmee de eigenschappen, zoals de stabiliteit en resistentie tegen weersinvloeden of vervuiling, bepaalt. Echter, hoe belangrijk dit proces van fase-inversie ook is voor de eigenschappen van de watergedragen verven, het proces zelf blijft grotendeels een mysterie. Dit komt met name door de enorme complexiteit van het droogproces en de bijbehorende fase-inversie; een proces dat geregeerd wordt door een ogenschijnlijk oneindig aantal chemische en fysische parameters.

Om licht in de duisternis te werpen, hebben we in dit proefschrift gekozen voor een aanpak van simplificatie; door het aantal relevante parameters terug te brengen tot een minimum hebben we gepoogd een eerste diepte-inzicht te krijgen in het fase-inversie proces tijdens filmvorming. We zijn hiermee gestart door, met behulp van directe observatie, met zowel microscopische waarnemingen door middel van confocale fluorescentie microscopie, als macroscopische waarnemingen met een gewone huis-tuin-en-keuken camera, dit proces te bekijken. In plaats van het bestuderen van een echte verffilm, hebben we een film “nagebootst” door middel van zeer goed gedefinieerde druppels van een polymeer te maken. Op basis van deze directe observaties hebben we een mathematisch model ontwikkeld, dat een aantal van de belangrijkste parameters gedurende filmvorming beschrijft. Met dit model kunnen voorspellingen worden gedaan over filmvorming in complexere systemen. Tevens hebben we in dit proefschrift resultaten beschreven over hoe we, van buitenaf, in kunnen grijpen in het filmvormingsproces door het ontwerpen en synthetiseren van een nieuw type surfactanten die een specifieke gevoeligheid vertonen voor de omgevingstemperatuur. Met beide strategieën hebben we nieuw inzicht verkregen in het cruciale proces van filmvorming in watergedragen verven.

Het begrijpen van filmvorming in geconcentreerde emulsies

Het eerste deel van dit proefschrift is gericht op het ontwikkelen van inzicht en begrip in het complexe proces van druppelcoalescentie en fase-inversie in een drogende emulsiefilm. Door het combineren van directe observatie, zowel op micrometer- als centimeter-

lengteschalen, met mathematische modellering, hebben we een directe relatie kunnen leggen tussen de gebeurtenissen op de moleculaire en microscopische schaal en het uiteindelijke droogproces op de schaal van een hele verffilm. In **Hoofdstuk 2** hebben we laten zien dat fase-inversie in drogende emulsiefilms plaats kan vinden via twee, ogenschijnlijk, compleet verschillende routes. Het samenvloeien van druppels, dat tot de fase-inversie leidt, vindt ofwel overal in de film tegelijkertijd plaats, waarbij grotere druppels her en der ontstaan en zo verder groeien. De film onstaat zo op een onregelmatige, chaotische manier. In andere situaties observeerden we juist dat druppels enkel samenvloeien aan het droogoppervlak, waardoor de film ontstaat door een front dat langzaam door de film heen trekt. Dit hebben we verklaard door het opstellen van een model, waarin zowel de stroming van vloeistof door de film in de richting van het droge oppervlak wordt beschreven, alsmede de thermodynamische stabiliteit van de druppels expliciet wordt behandeld. Hieruit bleek dat met name de initiële stabiliteit van de emulsie een cruciale rol speelt in het bepalen van het type fase-inversie dat optreedt. Als de initiële emulsie instabiel is, begint het samenvloeien van de druppels snel na aanvang van het drogen, waardoor er weinig tijd is om een groot drukverschil op te bouwen tussen het droge en natte uiteinde van de film. Echter, bij erg stabiele emulsies, kunnen enorme drukverschillen ontstaan, die we ook direct gemeten hebben, waardoor alleen aan het drogende front voldoende druk op de druppels wordt uitgeoefend om ze te laten samenvloeien. Verder bleek dat de initiële stabiliteit van de emulsie eenvoudig gestuurd kan worden met behulp van de concentratie surfactant die aan het monster wordt toegevoegd. Voor zover bij ons bekend, is dit de eerste waarneming en verklaring van deze twee routes waarop fase-inversie kan plaatsvinden.

In **Hoofdstuk 3** presenteren we een uitgewerkte versie van het hydrodynamische model dat de stroming van vloeistof door een drogende, en zeer geconcentreerde, emulsie beschrijft. Water stroomt door de dunne films en kanalen tussen de dichtgepakte emulsiedruppels richting het droge uitende van de film; deze stroming wordt gedreven door capillaire drukverschillen die heersen over de dikte van de film. Ons model voorspelt, afhankelijk van initiële parameters, hoe deze drukprofielen zich ontwikkelen in de tijd. Door variatie van de, voor verfsystemen relevante, parameters, zoals droogsnelheid en initiële emulsiestabiliteit, kunnen we voorspellen wanneer welk type fase-inversie optreedt.

Het manipuleren van filmvorming in geconcentreerde emulsies

In **Hoofdstuk 4** beschrijven we de chemische synthese van een serie, goed-gedefinieerde, temperatuurgevoelige surfactanten door middel van een specifiek type polymerisatie reactie, Atom Transfer Radical Polymerisation (ATRP) genaamd, waarmee een hydrofobe alkaanstaart aan een temperatuurgevoelig polymeer gekoppeld kan worden. Emulsies die worden gestabiliseerd door deze surfactanten zijn zeer stabiel; zelfs na 4 maanden bij kamertemperatuur is geen significante verandering in de toestand van de emulsies waar te nemen. Echter, door de temperatuur van de emulsie enigszins te verhogen naar 40 °C, net boven de kritische temperatuur waarbij het polymeer van oplosbaar in water naar onoplosbaar verandert, wordt de emulsie binnen enkele minuten volkomen instabiel. Hiermee kan coalescentie tussen de druppels dus worden geprogrammeerd met een simpele externe stimulus. Onze experimenten laten zien dat dit gedrag veroorzaakt wordt door het verwijderen van surfactants van bepaalde gedeelten van het oppervlak. Met het verhogen van de temperatuur verandert het oppervlak van een emulsiedruppel van een homogene, moleculaire laag van surfactanten, naar een oppervlak met microscopisch waarneembare druppels van onoplosbaar geworden surfactanten, en kale plekken waar de olie en de waterfase in direct contact komen. Deze vinding, dat emulsies “on-demand” gevormd en gedestabiliseerd kunnen worden, kan in wetenschappelijk onderzoek gebruikt worden om het coalescentieproces, dat typisch op onvoorspelbare tijd en plaats optreedt, gemakkelijker en in meer detail te bestuderen. Maar ook in toepassingen zou het gebruik van een stimuli-responsieve surfactant van groot nut kunnen zijn, onder andere voor het controleren en sturen van filmvorming in watergedragen verven en in het terugwinnen van stoffen die doormiddel van een emulsiefase geëxtraheerd zijn.

Tot slot, hebben we in **Hoofdstuk 5** een nieuwe methode gepresenteerd om filmvorming en coalescentie in geconcentreerde emulsies te bestuderen. Bij deze methode wordt de coalescentie in een temperatuurgevoelige emulsie geïnduceerd door middel van een verandering van temperatuur; de drijvende kracht voor coalescentie en filmvorming wordt nauwkeurig aangepast door middel van een centrifugaalkracht. Deze kracht wordt opgelegd door een microcentrifuge, die gemonteerd is op een microscoop met een hoge-snelheidscamera. Op deze manier kunnen we in de tijd, en met hoge tijdsresolutie, onder precieze controle van alle relevante parameters, de coalescentiekinetiek volgen. We hebben

laten zien dat aan de hand van de zo verkregen data zowel thermodynamische parameters als kinetische eigenschappen nauwkeurig bepaald kunnen worden. Bovendien hebben we in dit laatste hoofdstuk verder bewijs geleverd dat het type fase-inversie dat optreedt gestuurd kan worden door het aanpassen van de initiële stabiliteit van de emulsie. Wij denken dat deze nieuwe microcentrifugatiemethode een opstap vormt naar het ontwikkelen van verder inzicht in het complexe fenomeen van fase-inversie in drogende films.

Het inzicht en de methodiek die tijdens dit project is ontwikkeld heeft een veelvoud aan nieuwe mogelijkheden blootgelegd voor het verder verkennen van filmvorming in complexe mengsels. Waar ons werk zich heeft gericht op gesimplificeerde, ge-idealiseerde, emulsies, blijven er verschillende uitdaging in het verschiet voor studies naar echte, complexe verfsystemen. Onderzoek naar echte verfsystemen wordt bemoeilijkt door onder andere de grote ondoorzichtigheid van de verf, chemische reacties die plaatsvinden tijdens het drogen, de veelvoud aan opgeloste en gesuspendeerde moleculen en deeltjes, en de veel kleinere lengteschalen van de deeltjes in verf ten opzichte van de hier gebruikte emulsies. Deze uitdagingen, die essentieel zijn voor het volledig begrip van filmvorming, en voor het ontwikkelen van nieuwe watergedragen verven met verbeterde eigenschappen, zullen op de agenda staan voor onderzoek in de komende jaren.

List of Publications

- **H. Feng**, J. Sprakel, D. Ershov, T. Krebs, M. A. C. Stuart and J. van der Gucht, Two modes of coalescence in a drying emulison, *Soft Matter*, **2013**, 9, 2810-2815
- **H. Feng**, N. A. L. Verstappen, A. J. C. Kuehne and J. Sprakel, Well-defined temperature-sensitive surfactants for controlled emulsion coalescence *Polymer Chemistry*, **2013**, 4, 1842-1847.
- **H. Feng**, J. Sprakel, D. Ershov, T. Krebs, K. Schroen, M. A. C. Stuart and J. van der Gucht; Switching between two modes of coalescence in dense thermoresponsive emulsions. Submitted
- **H. Feng**, J. Sprakel, M. A. C. Stuart and J. van der Gucht; hydrodynamic model for drying emulsion. In preparation.

Acknowledgement

There are plenty of stories about the work presented in this book during my PhD period. I hereby express my most sincere appreciation for all of you and would like to share the honor and glory with you!

I want to thank Jacques, Rina and Rosilie for offering me this opportunity for to experience studying abroad. After I arrived in the Netherlands you still took care of me and it is a great pleasure to be here and to work with you.

Martien, my promoter, I would like to thank you first. Thank you so much for choosing me as a researcher for this project! It is an honor to be your PhD student and to be a member of Fysko. Despite your extremely busy schedule you always took care of me and my project as much as possible and I really appreciated that. Although the project got on track slightly later than we expected, you did not blame me or anyone else, but always encouraged me with warm words and offered me lots of good ideas to conquer the problems. This is the spirit I have learned from you. 'Never give up! Just try harder and harder and see how good you could be in your career!' I will remember the essentials of this lesson for the rest of my life.

Jasper, my co-promoter, I would like to thank you a lot for supervising me, guiding me, helping me and even comforting me during my PhD period. It is also a great pleasure to be one of your students! You helped me out with the irregular coalescence videos by using ImageJ plugin Kymograph and then established a model and taught me how to use it in Matlab. You even accompanied me to many places, Eindhoven, Amsterdam, and even to Sofia (Bulgaria) for progress reports, support and cooperation etc. Your kindness, patience and integration abilities gave me faith and supported me in every aspect so that I could complete this project.

Joris, my volunteered daily supervisor, my gratitude to you is already beyond words, but I still want to say thank so much for everything you did for me. My appreciation only expresses 1% of what I feel. As I mentioned at beginning of this paragraph, you volunteered to become my supervisor when I was doing a lot of Confocal Microscopy experiments but little progress was obtained. You just looked at me and then asked me why I didn't try using those UV curing glue chambers for experiments and, after that, the experiments became reproducible and reliable. Then you became deeper and deeper

involved and told Martien and Jasper that you were willing to supervise me, which turned out to be a very critical moment in my research life. Some people may call it coincidence. I would call it my fortunate destiny. My project accelerated by having your much experienced practical instructions. Your presence in our regular discussions also catalyzed my exploration process for this project. You are so willing to help students, no matter when and what. I know I can go to you when I have questions or problems, and you always help me solve them, and then redefine them as challenges. I have learnt so much from you about how to deal with study, work and life. I sincerely appreciate having a chance to work with and for you and hope that our cooperation will be even more fruitful in the near future because I will still be working for you in the coming years. I promise you that I will do my very best!

Frans and Renko, thank you for the Chinese spring festival interview at my home. It is an unforgettable memory for me and it was the start of my career at Fysko. Your courses and regular discussions were a lot of help.

I would like to thank the whole Fysko group for supporting and helping me in all sorts of ways. I would like to thank Josie for helping me with all the documents and taking care of me during these four years. I can talk with you on any topic and about everyone. You have always been a considerate person for me, and sometimes even for my wife. I really appreciate your kindness and warm attention. Mara thank you for all of your help in arranging my working conditions and materials. Sometimes you even brought the chemicals to my office which made it easy for me to work. I also want to thank Anita for all the help in filling out all the financial forms and making a good choice in Optare. Bert thank you for always helping me reimburse my tickets with patience, no matter how many times I asked for help. I would like to thank Remco for helping me and instructing me with all the various devices. Sometimes I even occupied too much of your time for data analyzing. I would like to thank Ronald for helping me solve many computer problems in the past four years.

Thanks to the Fysko 2009-2013 batch for helping, supporting and being there during my PhD period. It is a great pleasure to work with you guys! I will start with my office roommates, Thao and Liyakat. We shared and talked so much that I know almost everything about you! Thank you so much for being there with me! I would like to thank to Dmitry, the smart and generous guy who is willing to help others. I couldn’t have done this

project so easily and quickly without your help in programming data analysis! The discussions with you are also very inspiring and helpful. You convinced me to become a starter of Matlab with 0 level. I would like to thank Yuan and Junyou for your help and taking care of me with Chinese support in Fysko. Thank you Soumi for your understanding and encouragement when I was not in the configuration. I would like to thank Jeroen for helping me in so many ways with synthesis and many details of working in the cellar. Christian, thanks for your help and involvement in all aspects of work. You are such a nice guy. I would also like to thank all the rest of you guys: Yunus, Armando, Lennart, Sabine, Monika, Evan, Marc, Gosia', Gosia'', Juan, Helene, Hande, Hanne, Inge, Jacob, Harke, Johan, Merve, Natalia, Celine, Nadia, Katarzyna, Kamuran, Wolf and Antsje. It was a great pleasure working with all of you and we had a lot of fun together!

During my four year PhD period, I had a chance to meet and cooperate with many brilliant scientists from various fields and backgrounds. I would like to thank Karin and Thomas for their help in preparing the Microfluidic device. I am looking forward to further cooperation. I also want to thank Nikolai and Elka for their hospitality when we worked together in Sofia, measuring critical disjoining pressure. I also thank the four outstanding gentlemen in my jury: Professors Velders, Keddie, Geurink and Snoeijer for being part of this special day.

Thank you Xifeng Lu and Aichun Shu for helping me in the Netherlands for the last four years.

I would like to thank my parents Yonghe Feng, Lizhi Qian, my parents-in-law Faguan Zheng and Ningying Fang and my sister Yixi Feng. Thank you for your total support and understanding concerning my studying abroad! Leaving you for four years is very long and difficult, although we do have our video-talks through internet quite often. I am hoping that in the near future I will be able to spend more time with you in person in either the Netherlands or China.

I especially would like to thank my beloved wife Tingting Zheng and my sweet dog Wei. You do not just support, understand and accompany me but you work together with me in building our future! I am not able to express my appreciation in words of any language. No matter how long it is or how tough it is, you are always there for me and with me! We have conquered 3000 kilometers to meet in Beijing and then conquered 8000 kilometer to continue in the Netherlands and thus conquered almost 150000 kilometers to be together in the Netherlands for the past four years! The number and lists could go on to infinity if

necessary! I just want to say that I am very grateful to have you as my wife in my life. You are the biggest fortune in my whole life now and forever. For the rest of my life I will take care of you just as you take care of me. I cherish this bonding between us!

致亲爱的父母：冯永和、钱丽芝、岳父岳母：郑法观、方宁英和小妹冯怡溪。谢谢你们四年来对我出国留学的支持和理解！四年来，我们虽然不在你们的身边，但是我们时时刻刻都能感觉到你们对我们的支持和关心！爸爸妈妈们都学会了使用 QQ 和 Gtalk 来给我们留言提醒，天冷了 QQ 上提醒加衣保暖的留言让我倍感温馨；起风了 Gtalk 上询问天气情况的话语让我觉得父母就在身边；周末的视频语音时刻是我每周最开心的时刻：一家人围桌而坐，尽管相聚 8000 公里，仍然能够感觉到彼此的喜怒哀乐！希望在不远的未来我能够面对面地陪伴爸爸妈妈们更多一些时间，让爸爸妈妈们享受儿女膝下承欢的天伦之乐！

致心爱的老婆郑婷婷和威仔：可爱的老婆，我们的关系已经超越了相互陪伴相互支持相互守望，我们是一起为了美好的未来而奋斗的彼此！我们就是彼此！我们的血脉我们的思想我们的灵魂早已在这个奋斗的过程当中渗透和缝入了彼此，也许这就是缔结连理的含义吧！大学时我们跨越了 3000 公里来相会；出国时我们一起飞越了 8000 公里来荷兰继续奋斗；在荷兰我们奔驰了 150000 公里来建造我们未来！一起经历了这么多，我深深地感激生活让我遇上了你成为了你的老公，拥有你是我这一生最大的福气！让我们珍视彼此相守一生一世！

Huanhuan Feng
Leiden
2013-11-1

About the Author

Huanhuan Feng was born on 22th February 1984 in Tonghai County, Yunnan Province, China. He finished his senior high school period in Yuxi city. He entered College of Chemistry, Beijing Normal University with an outstanding college entrance examination score. He got the bachelor degree of science in 2006 and then continued his study in Polymer Chemistry and Physics in same university and got the master degree in 2009. During his study in Beijing, he married with Tingting Zheng. Later he moved to Netherlands to continue his academic career. He started his Ph.D. project sponsored by Dutch Polymer Institute (DPI) at the lab of Physical chemistry and Colloid Science of Wageningen University under the supervision of Prof. dr. Martien Cohen Stuart, Prof. dr. Jasper van der Gucht and Dr. Joris Sprakel. The results are included in this thesis.

Overview of completed training activities (VLAG)

Courses

Polymer Physics	2009
Colloid Science	2010
Han-Sur-lesse Winterschool	2010
Advance Soft Matter	2011
Statistical thermodynamics	2012

Conference & Colloquia

Lab Group meeting and colloquia	2009-2013
Dutch Polymer Institute Meeting	2009-2013
Dutch Soft Matter Day	2010-2013
Ph.D. excursion	2010&2013
DPI Annual meeting	2009-2013
FOM Physics Days	2013&2014
Europe Coating Show	2010